Technical University of Lodz
The Faculty of Electrical, Electronics, Computer and Control Engineering
Department of Microelectronics and Computer Science

Paweł Pawlik, MSc

Accelerating electric field strength amplitude and phase calibration based on particle beam induced electric field strength transient detection in linear particle accelerators

Kalibracja amplitudy i fazy natężenia przyspieszającego pola elektrycznego w liniowych akceleratorach cząstek w oparciu o detekcję zmian natężenia pola elektrycznego wywołanych wiązką cząstek

PhD Dissertation

Thesis supervisor: Prof. Andrzej Napieralski

Łódź 2007

For my parents

Acknowledgement

I would like to thank to my thesis supervisor prof. Andrzej Napieralski for his guidance that helped me in the preparation of this dissertation. I want to give a special thanks to dr Mariusz Grecki for his comments and support. Moreover I want to thank to dr Stefan Simrock for his encouragement and support. I also want to thank Henning Wedding for his help and support.

I acknowledge the support of the European Community-Research Infrastructure Activity under the FP6 "Structuring the European Research Area" program (CARE, contract number RII3-CT-2003-506395), and Polish National Science Council Grant "138/E-370/SPB/6.PR UE/DIE 354/2004-2007".

Abstract

This work presents a single bunch induced transient detection system developed for detecting changes of a 1.3 GHz electric field strength in superconducting cavities of the FLASH accelerator (DESY in Hamburg). Amplitudes of the changes are 3000 to 10000 times smaller then electric field strength amplitudes in the cavities itself. The purpose of the system is to measure a phase of the relativistic particle beam with respect to an electric field strength phase in the cavity and an amplitude of the electric field strength change. Developed hardware, software and algorithms are presented. Tests of the system are also included.

Acronyms

ADC	-	**A**nalog to **D**igital **C**onverter
CARE	-	**C**oordinated **A**ccelerator **R**esearch in **E**urope
COM	-	**C**omponent **O**bject **M**odel
DAC	-	**D**igital to **A**nalog **C**onverter
ddd	-	**D**OOCS **D**ata **D**isplay
DESY	-	**D**eutsches **E**lektronen-**SY**nchrotron
digital IO	-	digital **I**nput **O**utput
DOOCS	-	**D**istributed **O**bject **O**riented **C**ontrol **S**ystem
EF	-	**E**lectric **F**ield
EFS	-	**E**lectric **F**ield **S**trength
ENS	-	**E**quipment **N**ame **S**erver
FLASH	-	**F**ree Electron **LAS**er in **H**amburg
HASYLAB	-	**Ha**mburg **Sy**nchrotron Radiation **Lab**oratory
HERA	-	**H**adron **E**lectron **R**ing **A**ccelerator
IN	-	**I**nphase **N**egative
IP	-	**I**nphase **P**ositive
IQ modulator	-	**I**nphase **Q**uadrature modulator
LI	-	**L**ine **I**nphase
LLRF	-	**L**ow **L**evel **R**adio **F**requency
LO	-	**L**ocal **O**scillator
LQ	-	**L**ine **Q**uadrature
NF	-	**N**oise **F**igure
ONC RPC	-	**O**pen **N**etwork **C**omputing **R**emote **P**rocedure **C**all
QN	-	**Q**uadrature **N**egative
QP	-	**Q**uadrature **P**ositive

RF	-	**R**adio **F**requency
SPDT	-	**S**ingle **P**ole **D**ouble **T**hrow
TESLA	-	**T**eV-**E**nergy **S**uperconducting **L**inear **A**ccelerator
TTF	-	**T**esla **T**est **F**acility
VME bus	-	**V**ersa**M**odule **E**urocard bus
VUV-FEL	-	**V**acuum **U**ltra-**V**iolet **F**ree **E**lectron **L**aser
X-FEL	-	**X**-Ray **F**ree **E**lectron **L**aser

CONTENTS

LIST OF FIGURES

LIST OF TABLES

CHAPTER 1

Introduction

Physicists, who try to understand behavior of matter have made a great progress in the past thirty years. The limits of accelerators, experiments and theory have been increased. The goal of particle physics is to explain building blocks of matter and the fundamental forces acting between them. Today we know that matter is made of a few fundamental building blocks, called quarks and leptons.

Unfortunately the theory of Standard Model is incomplete. A gauge principle which is the basis for the theory requires all field quanta to be mass-less. In contrast W and Z bosons, the field quanta are 80-90 times heavier than proton. The way to give the particles a mass and preserve the gauge principle is a Higgs mechanism. The currently known theory of particle physics which explains all of experiments and the Higgs mechanism is called "The Standard Model". The theory has been tested and validated with high precision in a diversity of experiments. Only the Higgs particle has not been observed so far.

One of the biggest challenges of particle physics currently, is to establish the Higgs mechanism, to discover the Higgs particle and examine its properties, or to find a different theory for the particle masses. The measurements made at electron-positron colliders found the upper limit for the mass of the Higgs particle to be less

than 200 GeV in the Standard Model. To generate the Higgs particle directly and study its properties precisely accelerators with higher energy than those available today are required.

One of the projects with an aim to achieve the goal is TESLA [10, 28] (**T**eV-**E**nergy **S**uperconducting **L**inear **A**ccelerator). It is an international scientific project set to create a high-energy e+e- superconducting linear collider with center-of-mass energy reaching up to 1 TeV. It will become an indispensable tool for physicists in studding the Higgs particle. The accelerator was planned to be built near Hamburg and to be 33 km long. Unfortunately Germany had an economic crisis and the German government, the main sponsor for the project, decided to support only small commercial part of the accelerator, XFEL [28, 26, 16], [1] (**X**-Ray **F**ree **E**lectron **L**aser).

The X-ray laser is a tool for performing research in the field of structural and electronic properties of matter on atomic scale about molecules, large biomolecular complexes and condensed matter. The lasers have certain features especially useful in this kind of study. Their wavelengths are similar to the distances between atoms. They have an ability to penetrate matter and show its true behavior.

The science of the X-ray lasers and its applications have made an enormous progress over the last thirty years. Unfortunately the dream of an X-ray laser in one Angstrom (0.1 nanometer) wavelength range has not been achieved yet.

A new type of an X-ray laser, XFEL is planned to be built till 2015 near Hamburg. It will have exceptional features unreachable by other currently available X-ray laser sources. It will give coherent polarized X-rays with the peak brilliance more than 100 million times higher than what is available today (Figure 1.1). It will have several times better time resolution than other lasers [28]. The single pulse duration is expected to be shorter than 100 fs. Moreover radiation of XFEL can be changed over a wide range of wavelengths.

One of applications of the XFEL laser is making photos of a nanometer scale molecule and recognition of their structure with atomic resolution. It will be possible to perform structural and functional analysis of large molecular complexes that are very important in functioning of cells and are very difficult to study with currently available techniques.

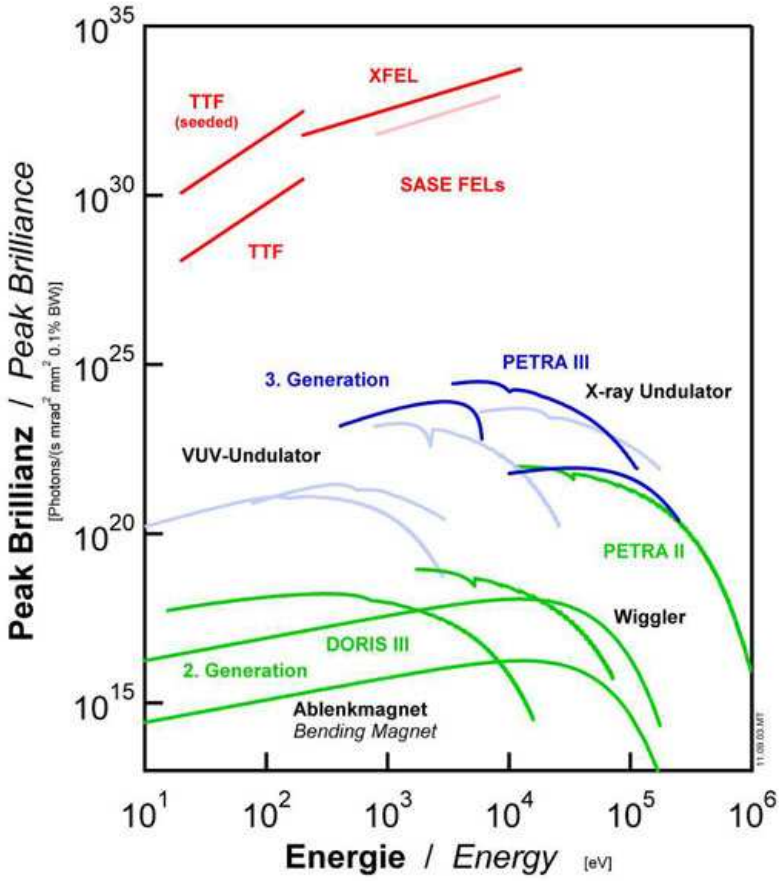

Figure 1.1: Brilliance in comparison (Source: DESY in Hamburg).

The laser can also be used in condensed matter physics, which goal is to determine electronic states of matter and its geometric structure on the atomic scale to study the fundamental interactions in matter and relation between microscopic and macroscopic properties of materials. Traditional techniques used to study novel materials face their limits, especially when trying to understand ultra-fast process on the nanometer length scale.

Currently available X-ray and neutron sources can be used to study equilibrium states of matter. X-rays from the free-electron laser at TESLA will give possibility to study dynamic states of matter and very fast transitions between different states of matter.

The TESLA technology planned to be used in XFEL is being developed in the FLASH [18] (**F**ree Electron **LAS**er in **H**amburg) accelerator (Figure 1.2) at DESY [12] (**D**eutsches **E**lektronen-**SY**nchrotron) in Hamburg. It is the 260 m linear accelerator

with an integrated X-Ray free-electron laser. An international scientific collaboration is working on development and tests of the TESLA technology in this facility. At the same time it is used for experiments with matter.

Figure 1.2: FLASH accelerator tunnel (self-made photo).

The development of the TESLA technology is carried at DESY (Figure 1.3), one of the leading scientific centers for research on particle accelerators in the world. It is a member of Helmholtz Association. DESY is a publicly founded national research center and has two locations: in Hamburg and in Zeuthen. DESY makes research in a field of natural sciences especially on:

- development and operation of accelerators
- particle physics (study of fundamental laws of matter and forces)
- research with photons (study in natural science with light generated by accelerators).

Research conducted at accelerators is made in a wide range of scientific fields - from particle physics to materials science and molecular biology. The scientific work is

Figure 1.3: DESY in Hamburg (Source: DESY in Hamburg).

performed in an international collaboration where 2750 scientists from 33 countries visit DESY every year to conduct research. 950 of them are working at HERA [20] (**H**adron **E**lectron **R**ing **A**ccelerator) in a field of particle physics. 1800 guests use HASYLAB [19] (**Ha**mburg **Sy**nchrotron Radiation **Lab**oratory). 1600 people are employed by DESY, 200 of them are working in Zeuthen.

The TESLA technology is developed at DESY by people working in different fields: mechanics, electronics, chemistry, physics and computer science. FLASH at DESY formerly known as VUV-FEL [18] (**V**acuum **U**ltra-**V**iolet **F**ree **E**lectron **L**aser) is used as a place for the development and test of this new technology. Group known as LLRF (**L**ow **L**evel **R**adio **F**requency) is working on development of the low power electronics used for the accelerator control. The work shown in this dissertation done in LLRF group presents a new method for accelerating EFS (**E**lectric **F**ield **S**trength) amplitude and phase calibration. It was developed for the TESLA technology and is an essential task during an accelerator startup and operation. It measures a correct EFS phase for the highest beam acceleration and scaling factors of ADC's (**A**nalog to **D**igital **C**onverter), which downconvert probe signals from cavities.

1.1 Accelerator operation

A particle beam in FLASH is accelerated by a 1.3 GHz EF (**E**lectric **F**ield) standing waves in 9 cell superconducting cavities [52]. The EF is operated in a pulsed mode with a 5 Hz to 10 Hz pulse repetition rate. Every pulse is composed of three parts: a filling, a flattop and a decay. During the first 500 μs (the filling) the EFS amplitude increases up to an operating level. The second 800 μs (the flattop) is used for the beam acceleration. During this period the EFS amplitude and phase is stabilized by an EFS control. The decay starts at the end of the flattop - whereas an EF source (a klystron) is switched off and the EFS in the cavities decays with their time constants.

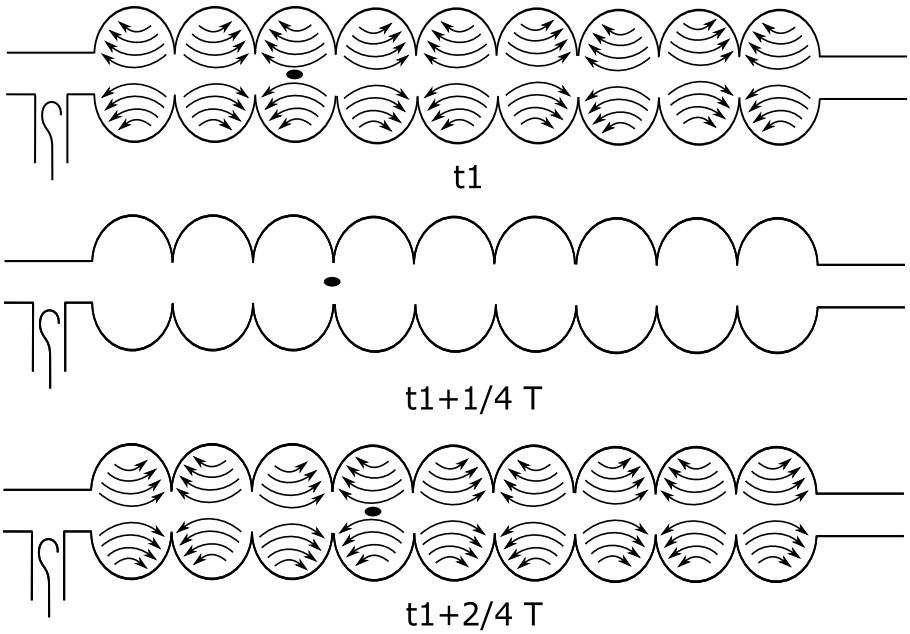

Figure 1.4: Accelerating EFS in a 9-cell TESLA cavity: t1 - a starting time; $T \approx 0.8\ ns$ - 1.3 GHz RF EFS period.

The beam is composed of series of electron bunches with a charge of a single bunch in a range between 0.5 nC to 2 nC. The electron bunches are sent with a 1 MHz repetition rate. All bunches move every 1 μs one after the other. In the final version of FLASH, 800 bunches will be accelerated during the single RF EF pulse.

The beam is accelerated by an RF EF standing wave in a cavity (Figure 1.4). Every half of a 1.3 GHz period, the EFS vector changes its direction to the opposite in every cell of the cavity. The bunch in the center of the single cell of the cavity has

the maximum acceleration when the EFS is maximal and has the opposite direction to the bunch movement. The bunch injected in the cavity in an incorrect time will not have the maximum acceleration instead it might even be decelerated.

$$V_{acc}(t_b) = V_c \cdot \cos\varphi = V_c \cdot \cos(\omega t_b) \tag{1.1}$$

Where:
V_{acc} - accelerating voltage
t_b - beam injection time
V_c - accelerating voltage for on-crest acceleration
φ - a beam injection phase with respect to the RF EFS phase
ω - an EFS angular frequency

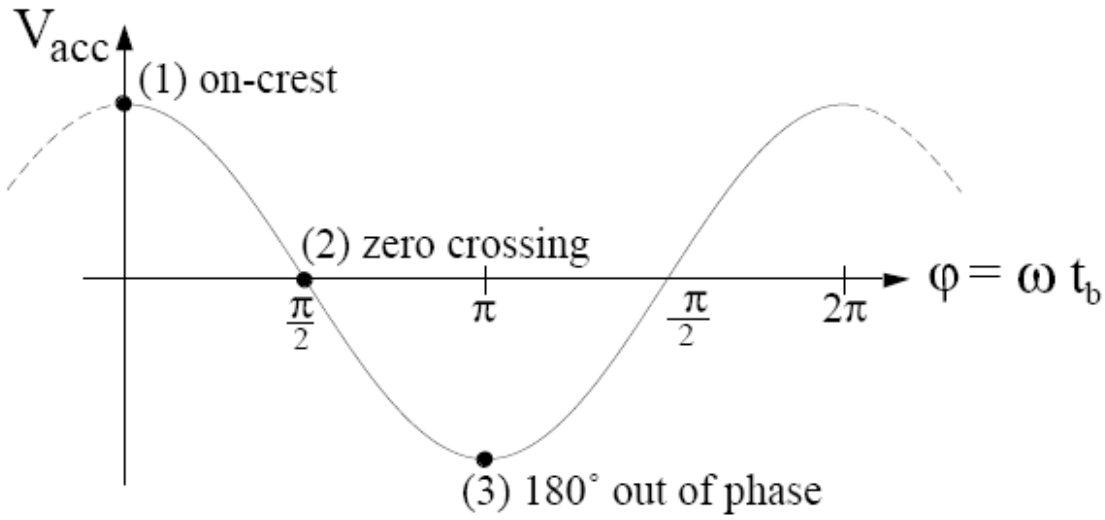

Figure 1.5: Dependence of accelerating voltage on a beam injection phase φ (Source [52]): $\omega = 2\pi \cdot 1.3\ G\frac{rad}{s}$ - EFS angular frequency; $\varphi = \omega \cdot t_b$ - beam injection phase; t_b - beam injection time.

The beam acceleration depends on the RF EFS amplitude and phase measured with respect to the beam injection time. The accelerating voltage of the beam is a cosine function of the phase between the EFS and the beam (1.1) [52] (Figure 1.5). The beam phase for the accelerating cavities is required to be set at a 0° (called on-crest[1]). An exception is the first module in the tunnel responsible for bunch compression,

[1]on-crest acceleration is when the beam phase is set for the maximum acceleration

where it is required to have a -10° off-crest[2]. For this phase, the particles in front of the bunch gain lower energy and the particles at the end of the bunch receive higher energy thus reducing the length of the bunch.

1.2 Accelerating EFS amplitude and phase calibration

Beam accelerating voltage depends on the phase between the beam and the RF EFS. For a proper accelerator operation, the RF EFS phase has to be set correctly [29]. The procedure for setting a correct RF EFS phase is called phase calibration.

The EFS in cavities is driven by a klystron. For economical reasons one klystron is a power source for one module composed of at least 8 cavities. The RF EFS in every cavity are coupled by probes. Signals from the probes are downconverted and multiplied by scaling vectors. The vectors set a correct amplitude of measured signals in MV/m units. They give correct signal power relation between the cavities. They also set phases of downconverted RF EFS from all cavities in the single module to the same value for on-crest acceleration [29]. Setting a correct amplitude of scaling vectors is called amplitude calibration.

1.3 Methods for accelerating EFS amplitude and phase calibration

Methods for accelerating EFS amplitude and phase calibration can be divided into two categories: based on a beam energy measurement and based on a beam induced transient measurement [56, 29, 58, 38, 36, 31, 53, 40, 59].

One of methods which is currently used for the calibration in FLASH uses high charge RF EFS transients [29]. A phase of these transients measured with respect to an absolute RF EFS gives information about a beam phase. On-crest acceleration is when the beam induced transient has 180° phase with respect to an absolute EFS

[2] off-crest acceleration is when the beam is not on-crest

(an RF EFS is maximally reduced, the maximum energy is taken by the bunched beam from a cavity). A relative amplitude of the transient gives information about relation between a transient amplitude and an EFS amplitude in the cavity. When a beam charge is known, an absolute EFS amplitude in the cavity can be calculated on the basis of a transient amplitude and a beam charge.

The transient induced by a single bunch is very small. It is around 3000 times smaller than an absolute RF EFS for a 12 MV/m EFS amplitude and a 1 nC single bunch charge. It is around 10000 times smaller then an RF EFS for a 21 MV/m amplitude and a 0.5 nC single bunch charge. These transients are too small to be detectable by currently used ADC's for a signals downconversion. The ADC's have 14 bit resolution with 13 bits for an amplitude measurement (real and imaginary parts of the EFS vector are downconverted by a single ADC at a 250 kHz intermediate frequency [52]). Taking into account measurement noise, their resolution reduces to 11 bits. To measure the transients, 3000 times lower then an absolute EFS amplitude with 1 bit resolution, it would be required to have an ADC with 11.5 bit resolution. As a conclusion, the transients induced by single bunches are 0.5 bit below measurement noise of the currently used ADC's. Moreover the transients are very fast. Therefore it would be necessary to have higher sampling rate ADC's then the currently used 1 MS/s in order to detect them.

To measure the beam induced transients it is necessary to generate high charge transients induced by many bunches. In order to generate them, a single bunch charge is increased to the maximum value, which is around 4 nC. The number of bunches has to be set at least to 30. RF EFS feedback has to be turned off. With an RF EFS feedback on, the transients would be suppressed and they would not be visible for a detection. The transients induced by around a 120 nC charge are detectable (30 bunches with around a 4 nC charge, give a 120 nC transient). In addition to increase accuracy, the measurement is repeated a number of times and the results are averaged.

The currently used method has several drawbacks. The main limitation is the fact that this measurement can not be done continuously during a normal accelerator operation. It is necessary to stop a normal accelerator operation and initiate a special conditions for the calibration. For this reason this procedure is performed very rarely. Phase drifts in the accelerator make this calibration incorrect after several days. After a week, the calibrated phase can differ from the required one

by up to 10°. Different conditions during the calibration and normal accelerator operation cause that the measured phase can be different in these two cases which makes the situation even worse.

The method has also other disadvantages. During an accelerator startup, the beam phase is unknown and can be even 180° off-crest. For the case the measurement with the high charge transients is unsafe. When the beam phase is completely wrong the accelerator does not have a correct beam transmission. The beam in this case can collide with an equipment installed in the tunnel and when the beam charge is high it can brake this equipment.

Another method for the beam phase calibration is based on a beam energy measurement. At the end of a module a special screen inside a bunch compressor is installed. The screen is observed by a camera. The bunch compressor is a device composed of four magnets, which bend the beam in such a way that the particles with higher energy have a longer way and the particles with lower energy have a shorter way. The beam visible on the screen changes the position depending on the beam energy. The Energy is measured by adjusting currents of the magnets to get the beam at the center position on the screen. The beam energy is calculated from the magnets current.

This method can be used to calibrate the beam phase by changing the RF EFS phase and looking for the highest energy. The beam phase equal to 0° for the RF EFS phase for which the beam has the highest energy. A disadvantage of the method is a requirement to change the RF EFS phase at least several times and measure the energy, this in turn destabilizes normal accelerator operation. The method is also destructive to the beam and cannot be used during normal operation.

1.4 Work motivation and aim

It is required to have a correct beam phase with respect to the RF EFS, all the time during normal accelerator operation. Therefore it is necessary to develop a new method able to perform the calibration during normal accelerator operation.

The method which could calibrate the accelerating RF EFS in cavities during normal accelerator operation can be based on a single bunch induced transient detection [2, 9, 3, 5, 4, 6, 7, 8]. This method would have several advantages over currently used methods [56, 29, 58, 38, 36, 31, 53, 40, 59]. The main advantage is an ability to perform the calibration continuously during normal accelerator operation thus any master oscillator distribution drifts could be compensated. This measurement can be done with the same conditions as during normal accelerator operation. Therefore it would reduce measurement errors.

The method would be especially useful during an accelerator startup when the beam phase is random and unknown. Measuring the beam phase using only a single 1 nC bunch would reduce a risk of braking the equipment installed in the accelerator tunnel when the beam does not have correct transmission and could collide with the equipment installed in the tunnel. Measuring the beam phase with the high charge transients (at least 120 nC) is much more risky.

1.5 Theses

In this work three main theses are proven:

Thesis 1 *It is possible to calibrate accelerating RF electric field strength amplitude and phase in linear particle accelerators during normal accelerator operation.*

Thesis 2 *An RF electric field strength transient induced by a single bunch can be used for amplitude and phase calibration in linear particle accelerators.*

Thesis 3 *An RF feedforward comb filter can be used for attenuation of a carrier signal while passing through the single bunch induced transients*

1.6 Transients induced by a beam

A particle beam consists of particle bunches. Each bunch moving through a cavity, induces an RF EFS change. The change is very small around 3000 times smaller then the EFS for a 12 MV/m amplitude and a 1 nC single bunch charge (Figure 1.6). For a 21 MV/m EFS and a 0.5 nC single bunch charge it is 10000 smaller then an absolute EFS. A single bunch moving through the cavity changes the EFS in around 3 ns. For the EFS in the cavity controlled without a feedback it changes back to its original state in the period that equals a cavity time constant. For FLASH it is around 765 μs. For a few microseconds this transient can be modeled as a step function.

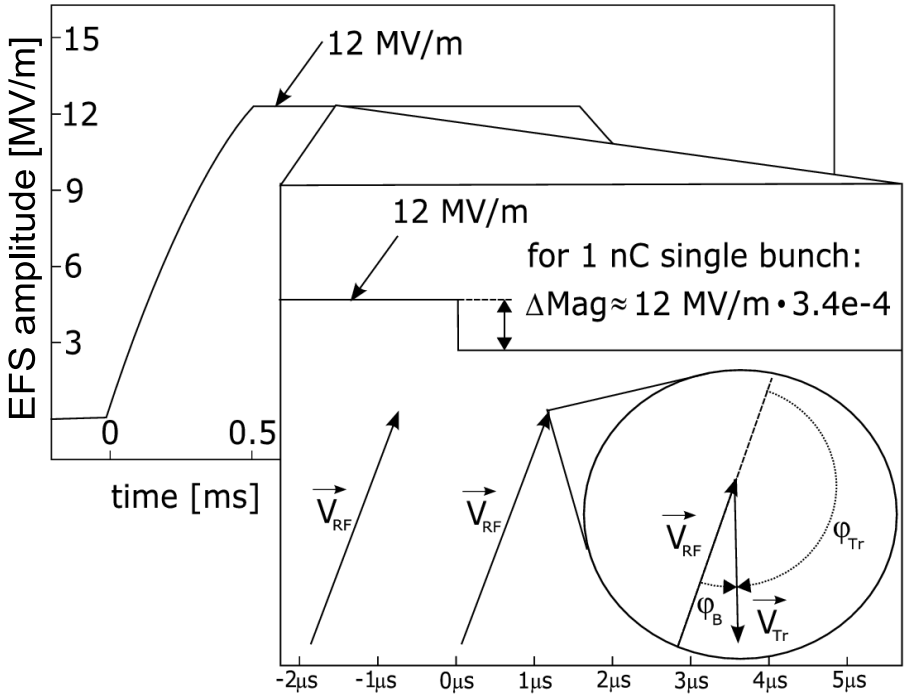

Figure 1.6: An EFS transient induced by a single bunch: $\vec{V}_{RF}$ - EFS vector without a transient; $\vec{V}_{tr}$ - transient vector; φ_{tr} - transient vector phase; φ_b - beam phase ($\phi_b = \varphi_{Tr} - 180°$).

An amplitude and a phase of the beam induced transient can be calculated using a model presented in [52]. The model is a first order differential equation for an envelope (1.2). For the FLASH cavity: $\left(\frac{r}{Q}\right) = 1040\ \Omega$ - normalized shunt impedance, $Q_L \approx 3 \cdot 10^6$ loaded quality factor, $R_L = 1.56\ G\Omega$, $\omega_{1/2} = 2\pi \cdot 208\ \frac{rad}{s}$.

$$\frac{d}{dt}\begin{bmatrix} V_r \\ V_i \end{bmatrix} = \begin{bmatrix} -\omega_{1/2} & -\Delta\omega \\ \Delta\omega & -\omega_{1/2} \end{bmatrix} \cdot \begin{bmatrix} V_r \\ V_i \end{bmatrix} + \begin{bmatrix} R_L\omega_{1/2} & 0 \\ 0 & R_L\omega_{1/2} \end{bmatrix} \cdot \begin{bmatrix} I_r \\ I_i \end{bmatrix} \tag{1.2}$$

Where:
V_r, V_i - real and imaginary parts of an absolute EFS in the cavity
I_r, I_i - real and imaginary parts of the cavity input power
$\omega_{1/2}$ - half cavity bandwidth
$\Delta\omega$ - cavity detuning
R_L - loaded shunt impedance
$R_L = \frac{1}{2} \cdot R_{sh} = \frac{1}{2} \cdot \left(\frac{r}{Q}\right) \cdot Q_L$

For short bunches, a fourier component at an operating 1.3 GHz frequency of a single bunch current is two times larger then the current calculated from the bunch charge $I_b = 2I_{b0}$ [52]. The current calculated from the bunch charge (q_b - single bunch charge, t_b - period during which bunch is inside the cavity) equals $I_{b0} = \frac{q_b}{t_b}$. The single bunch can be modeled as a current pulse with an amplitude I_b and a pulse width t_b. For a simplification cavity detuning equals $\Delta\omega = 0\ \frac{rad}{s}$. A transient vector calculated using the cavity model (1.2) and mentioned assumptions equals:

$$\begin{bmatrix} V_{tr} \\ V_{ti} \end{bmatrix} = 2 \cdot \omega_{1/2} \cdot q_b \cdot R_L \begin{bmatrix} \cos(\varphi_b) \\ \sin(\varphi_b) \end{bmatrix} \tag{1.3}$$

Where:
V_{tr}, V_{ti} - real and imaginary parts of a transient vector
q_b - single bunch charge
φ_b - single bunch current phase

The transient vector for $\omega_{1/2} = 2\pi \cdot 208\ \frac{rad}{s}$, $q_b = 1\ nC$, $R_L = 1.56\ G\Omega$ equals:

$$\begin{bmatrix} V_{tr} \\ V_{ti} \end{bmatrix} \approx 4075V \begin{bmatrix} \cos(\varphi_b) \\ \sin(\varphi_b) \end{bmatrix} \tag{1.4}$$

A relative transient amplitude and phase is calculated by dividing the transient vector presented above by 12 MV (EFS of the cavity multiplied by a 1 m length of the cavity):

$$\frac{\vec{V}_{tran}}{\vec{V}_{field}} \approx 3.4 \cdot 10^{-4}\ V/V \cdot e^{i\left(\varphi_b - \varphi_{field}\right)} \tag{1.5}$$

Where:
$\vec{V}_{tran}$ - transient vector
$\vec{V}_{field}$ - RF EFS vector
φ_{field} - RF EFS phase

1.7 A concept for the beam induced transient detection

The transients induced by particle bunches are very small in comparison to an absolute value of RF EFS in the cavity. They are 3000 times smaller then the absolute EFS for a 1 nC bunch charge and a 12 MV/m EFS amplitude. In the case of a 0.5 nC single bunch charge and a 21 MV/m EFS amplitude they are 10000 times smaller then the absolute EFS in the cavity. To detect them with required accuracy it is necessary to use special hardware. The hardware has to filter a signal - attenuate a 1.3 GHz carrier and leave the transients unattenuated. The carrier has to be attenuated by around 100 dB to be smaller then the RF EFS changes induced by bunches.

RF EFS in the cavity with the transient can be modeled as a step function (Figure 1.7). EFS can be modeled as constant before the bunch comes into the cavity. When the bunch gets into the cavity it changes the RF EFS and the EFS becomes a sum of the absolute RF EFS vector and the transient vector. The vectors can be assumed to be constant for periods much smaller then the cavity time constant ($765\mu s$).

Commercially available filters are not sufficient for the carrier filtering. The transition from a stopband to a passband is not sharp enough to filter the carrier while leaving the transients. These filters would filter both the carrier and the transients.

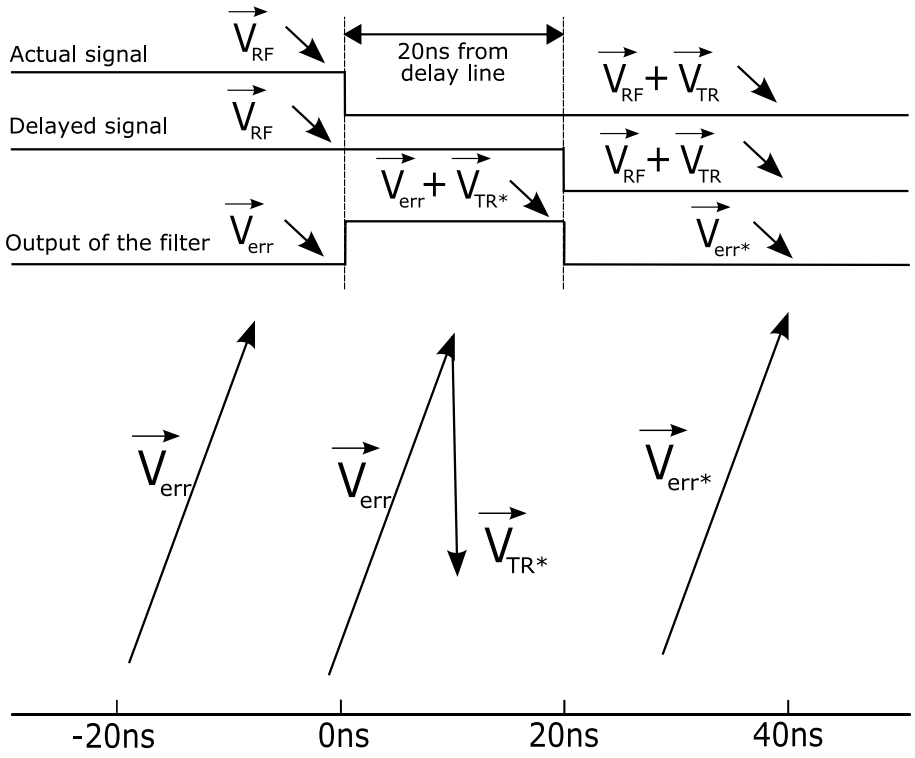

Figure 1.7: Vector analysis of the transient detection concept: $\vec{V}_{RF}$ - absolute EFS vector; $\vec{V}_{TR}$ and $\vec{V}_{TR*}$ - EFS transient vectors; $\vec{V}_{err}$ and $\vec{V}_{err*}$ - RF feedforward comb filter adjustment error vectors.

A concept for filtering can be based on subtraction of two the same 1.3 GHz signals, where the one is delayed with respect to the second one (Figure 1.7). This operation for the RF EFS signal with the transients gives as an output a filter adjustment error vector summed with pulses. The pulses carry information about the transient vectors.

An amplified result of the subtraction can be used later for the transient vector measurement. The presented concept can be implemented as a microwave circuit as presented in Figure 1.8. The subtraction is done as a sum of two 1.3 GHz signals with 180° phase difference and with the same amplitudes. In reality a perfect adjustment of the phase to 180° and amplitudes to be the same is not possible. Therefore the output of the filter always has the filter adjustment error vector instead of zero.

The filter is made of a splitter, a combiner, a delay line, a variable phase shifter and a variable attenuator. The variable phase shifter is used to adjust a phase of one of the signals in the filter to get 180° phase difference between them. The variable attenuator is used to adjust an amplitude to achieve the same amplitudes

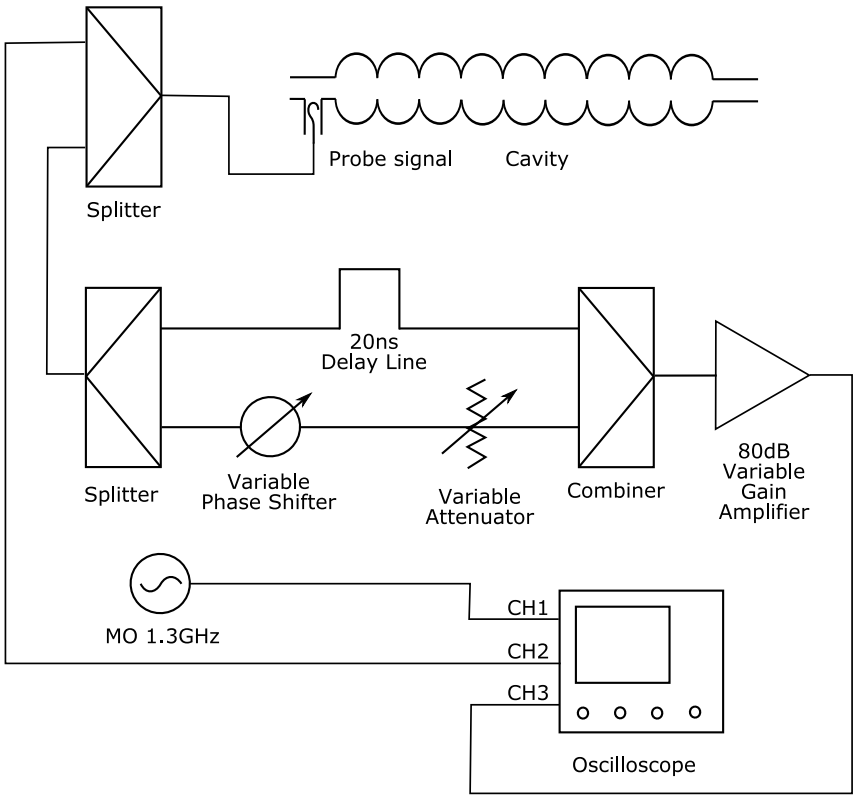

Figure 1.8: The transient detection concept.

in both signals. The output of the filter is amplified by around 80 dB and later downconverted by an oscilloscope.

The single bunch induced transient detection requires a comparison of two vectors, the absolute RF EFS vector with the transient vector. For this reason the oscilloscope digitizes two signals, the output of the filter that carries information about the transients and the absolute RF EFS from the cavity.

1.8 Conclusions

Accelerators are important tools for research in the field of particle theory of matter. Currently the biggest challenge of the theory is to validate the Higgs particle. TESLA is an international project with an aim to create a high-energy e+e- superconducting linear collider with center-of-mass energy reaching up to 1 TeV, which would be able to verify the Higgs particle. Currently only a commercial part of the project, the XFEL X-ray laser source will be built. With the laser it will be possible to perform a deeper analysis of large molecular complexes. Development of the TESLA technology for XFEL is being made at DESY in Hamburg in the Tesla Test Facility called FLASH.

A particle beam in FLASH is accelerated by a 1.3 GHz RF (**R**adio **F**requency) alternating electric field in 9-cell superconducting cavities. The beam acceleration strongly depends on the phase difference between beam injection time and an alternating EFS phase in the cavity. Correct accelerator operation requires setting a correct phase between the beam and the EFS in all accelerating cavities and also correct scaling vectors for downconverters. This procedure is called an amplitude and a phase calibration.

Currently used methods for the amplitude and the phase calibration have disadvantages. They can only perform the calibration by modifying accelerator settings. The method used at DESY requires setting special accelerator conditions. These conditions require stopping normal accelerator operation. Therefore this measurement can be performed only rarely.

The aim of the dissertation was to develop a new method for the accelerating EFS amplitude and phase calibration, which does not have disadvantages of the old methods. Concept for the new method is based on detecting accelerating RF EFS changes in the cavity induced by the beam bunches. The method allows calibration of the accelerating EFS during normal accelerator operation. The changes called transients are 3000 to 10000 times smaller then the EFS itself and are available during normal accelerator operation. The main part in the system for detecting the transients is an RF filter that attenuates a 1.3 GHz carrier signal and leaves the changes unattenuated. The concept for filtering is based on subtracting two 1.3 GHz signals - an actual and a delayed. The output of the filter consists of pulses. The pulses carry information about the single bunch induced transients.

CHAPTER 2

System for transient detection

The system for single bunch induced transient detection (Figure 2.1, Figure 2.3) consists of microwave parts, a control system and an oscilloscope. The microwave parts are responsible for signal conditioning. The control system directly controls the microwave parts and stores the data in the DOOCS (**D**istributed **O**bject **O**riented **C**ontrol **S**ystem) servers [13] for the transient measurement and control. The oscilloscope's duty is a signal downconversion, calculations and control of the whole system.

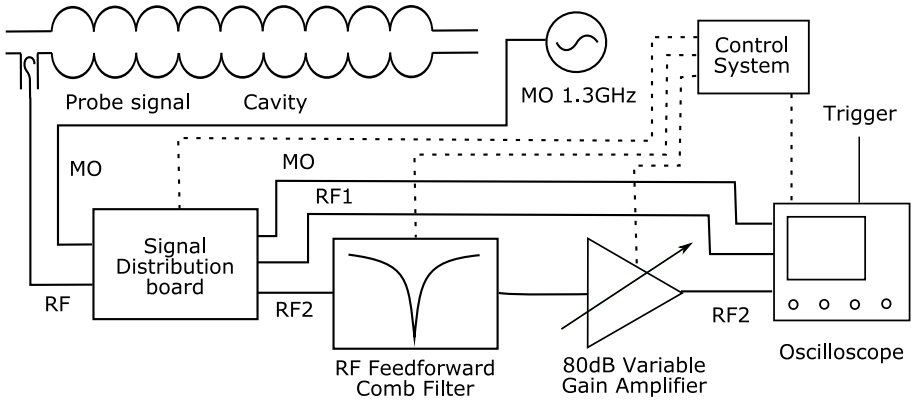

Figure 2.1: The system for single bunch induced transient detection version number 3.

The microwave parts consist of: a signal distribution board, an RF feedforward comb filter and an 80 dB variable gain amplifier board. The transient detection and measurement operates by comparing the RF EFS vector from the cavity with the transient vector. Therefore it is necessary to downconvert both of them. The signal distribution board splits the signal from a cavity into two. RF1 is used to measure the absolute RF EFS vector from the cavity probe. The oscilloscope directly digitizes it. The second signal RF2 is used for the transient vector measurement. This signal is conditioned with the RF feedforward comb filter and with the variable gain amplifier. The conditioned RF2, which carries information about the transient vector, is downconverted by the oscilloscope.

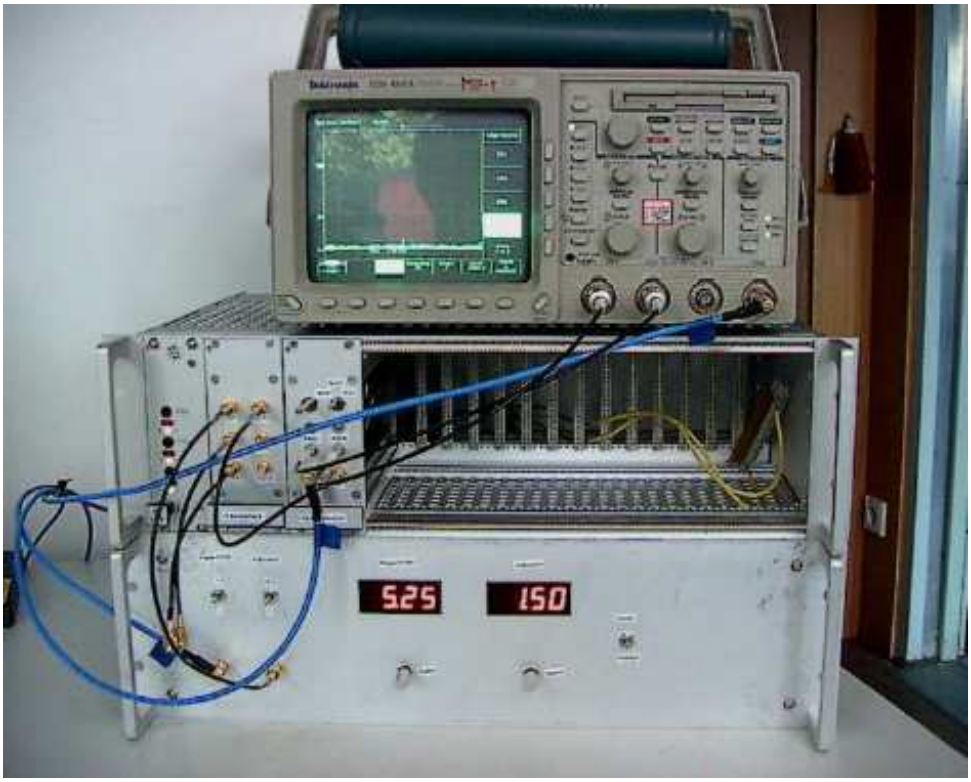

Figure 2.2: Single bunch induced transient detection system version number 1.

The control system comprises: a computer VME board and an Industry Pack VME carrier board with three modules. The VME computer has a SPARC processor and Solaris operating system. The second mentioned board, has three modules: 8 channel ADC, 8 channel DAC and a digital IO module. The VME computer controls modules, which regulate the signal conditioning system.

The oscilloscope is the LeCroy WaveRunner 6100A. It has 1 GHz bandwidth, 10 GS/s

maximum sampling rate and Windows 2000 operating system. The Matlab [24] script is running on it. The script, takes data, calculates the transient vectors, stores results in the DOOCS server installed in the VME computer and controls the signal conditioning system using the control system.

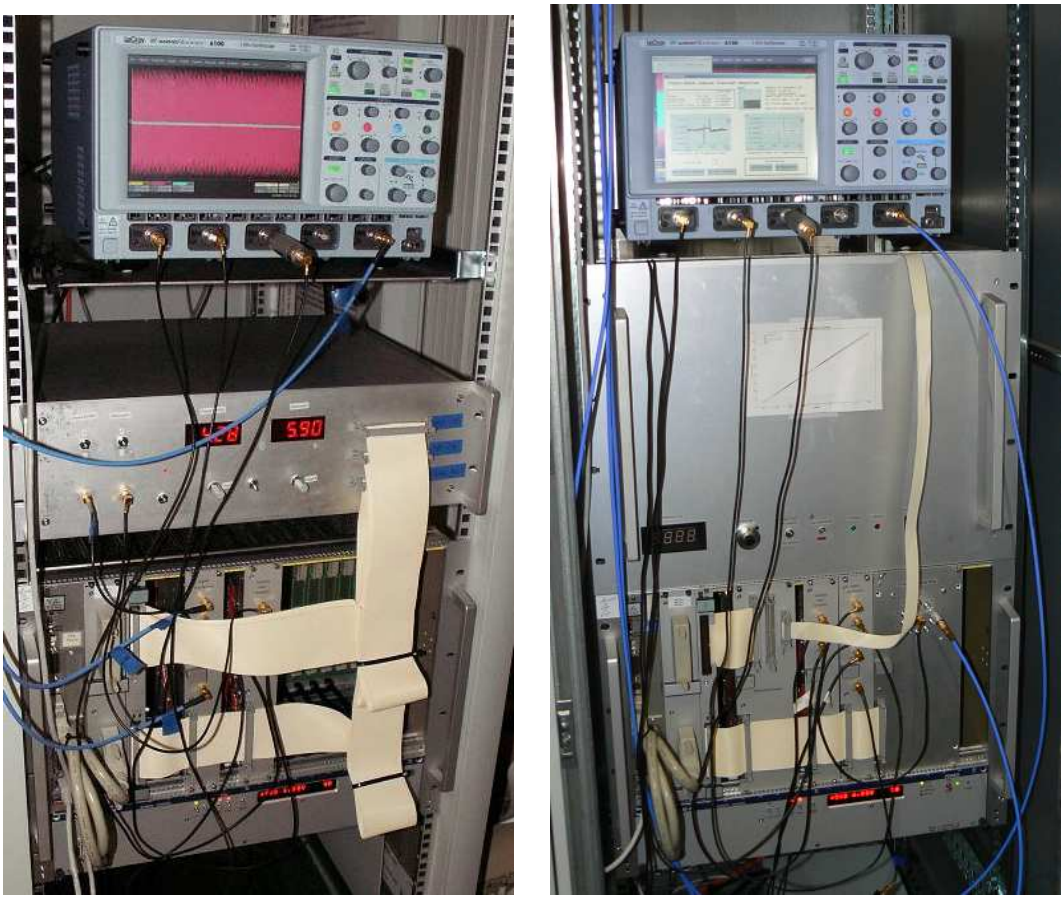

Figure 2.3: Single bunch induced transient detection system (version number 2 - left picture, 3 - right picture).

The transient detection system works in two modes: normal operation and calibration. The normal operation is used for the transient measurement. The calibration is done rarely to measure the scaling factors which tell how the data captured by the oscilloscope from RF1 and RF2 relate one to the other.

2.1 Signal distribution board

The signal distribution board (Figure 2.4) delivers signals to the RF feedforward comb filter and to the oscilloscope. It splits the signal from a cavity probe 'RF inp.' into two 'RF out1' and 'RF out2' during normal operation and a 1.3 GHz "LO inp." local oscillator during calibration. It also delivers a 1.3 GHz local oscillator signal to the oscilloscope.

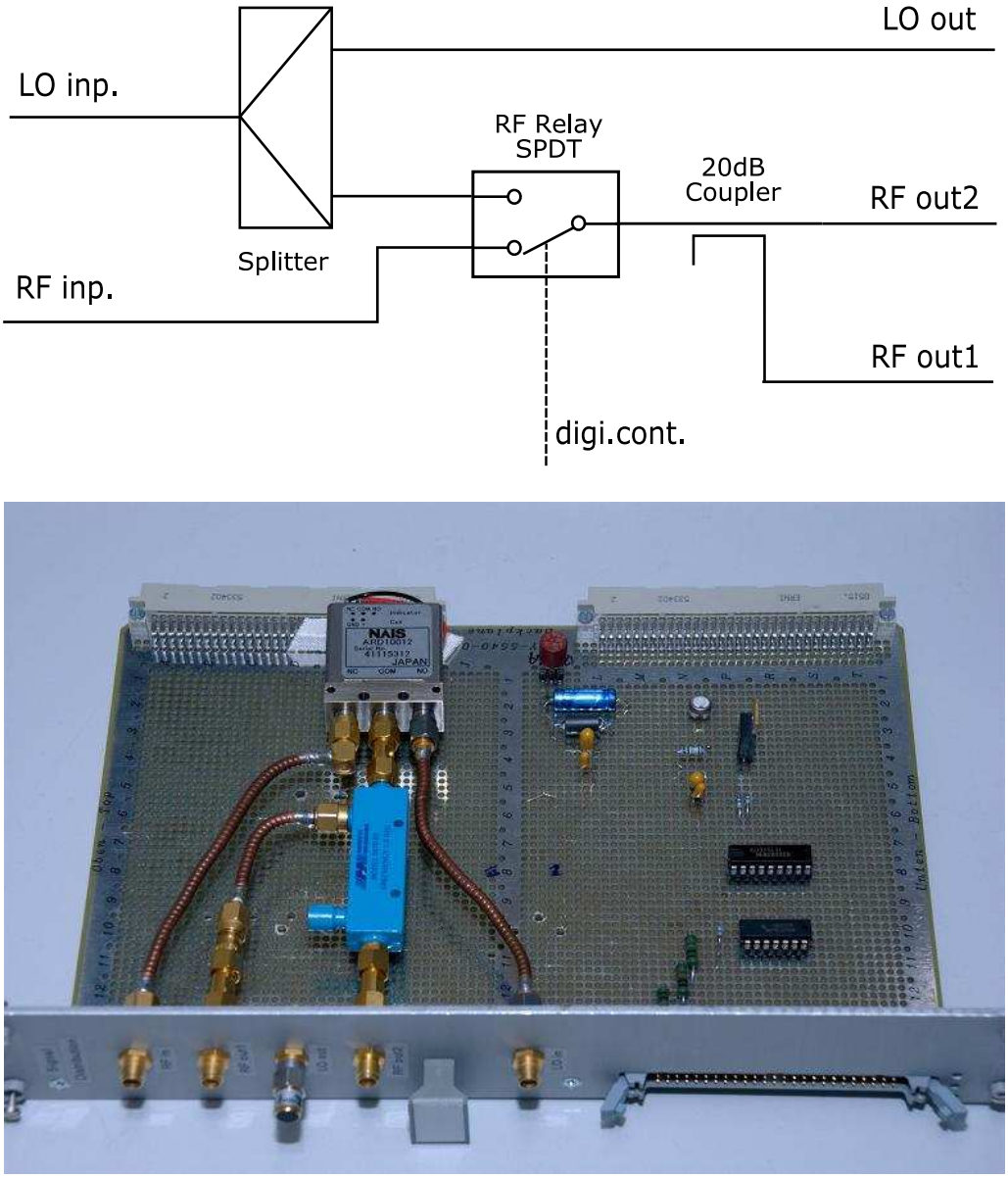

Figure 2.4: Signal distribution board.

2.2 RF feedforward comb filter

The most critical part of the transient detection system is the RF feedforward comb filter. Its purpose is to attenuate a carrier by around 100 dB while leaving the small transients unattenuated. It is a passive microwave circuit working at a 1.3 GHz frequency.

2.2.1 Filter model

Ideal model

To understand how the RF feedforward comb filter works, a frequency response of an ideal model was calculated (Figure 2.5). This model consists of an ideal splitter, a combiner and cables that only delay a signal. It does not take into account the cable attenuation. The calculations have been made with some assumptions. The outputs of the splitter at the filter input are two identical signals. They have the same phases and amplitudes. The amplitudes are $\sqrt{2}$ times smaller then the input X(f) signal. The branch 1 and 2 are modeled as delays without an attenuation. The delay in the branch 1 is higher than in the branch 2. The output signal Y(f) of the combiner at the output of the filter is a sum of its input signals from the branch 1 and 2 attenuated by $\sqrt{2}$.

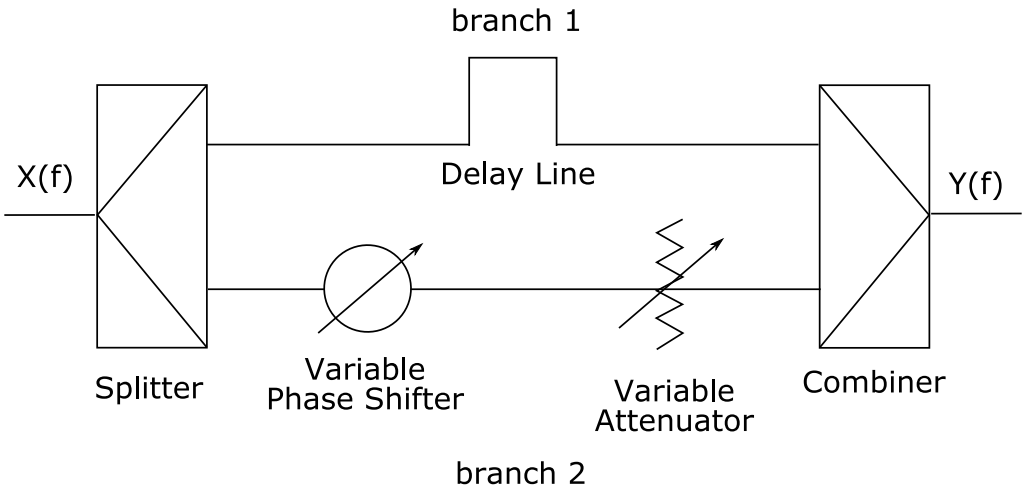

Figure 2.5: RF feedforward comb filter.

The calculated transfer function of the ideal filter model equals:

$$T(f) = \frac{Y(f)}{X(f)} = M_T(f)\, e^{i\varphi_T(f)} \tag{2.1}$$

$$M_T(f) = |\cos \pi f (t_{d2} - t_{d1})| \tag{2.2}$$

$$\varphi_T(f) = angle\{sign[\cos \pi f (t_{d2} - t_{d1})]\, e^{i-\pi f(t_{d1}+t_{d2})}\} \tag{2.3}$$

Where:
t_{d1} - delay of line in branch 1
t_{d2} - delay of the line in the branch 2
sign() - signum function
angle()- returns the phase of complex number in radians

The M_T and φ_T are respectively an amplitude and a phase of the transfer function of the RF feedforward comb filter. The output amplitude depends only on the difference between delays in the two branches. The angle depends on the sum of these delays and also on their difference. The amplitude equals zero when the phase of a cosine equals $\varphi_T(f) = \frac{\pi}{2} + \pi k$ for k=0,1,2... . The difference between two frequencies with amplitudes of transfer function equaling zero is:

$$\Delta f = \frac{1}{t_{d1} - t_{d2}} \tag{2.4}$$

Rule for filtering a frequency f_a

The application of this filter is to attenuate a certain frequency f_a. To achieve this goal difference between the delays of two branches has to fulfill a certain condition. This condition can be calculated by comparing an amplitude of the transfer function M_T (2.2) to zero:

$$(t_{d1} - t_{d2}) = \frac{1 + 2k}{2f_a} \tag{2.5}$$

$$t_{d1} = \frac{1+2k}{2f_a} + t_{d2} \tag{2.6}$$

Where:
k = 0,1,2,...
f_a - attenuated frequency

The minimum gain is when an odd number of half-periods of the frequency f_a fit in the difference between delays. An example for t_{d1} calculated for $k = 5$ and $t_{d2} = 5\ ns$ is presented in Figure 2.6.

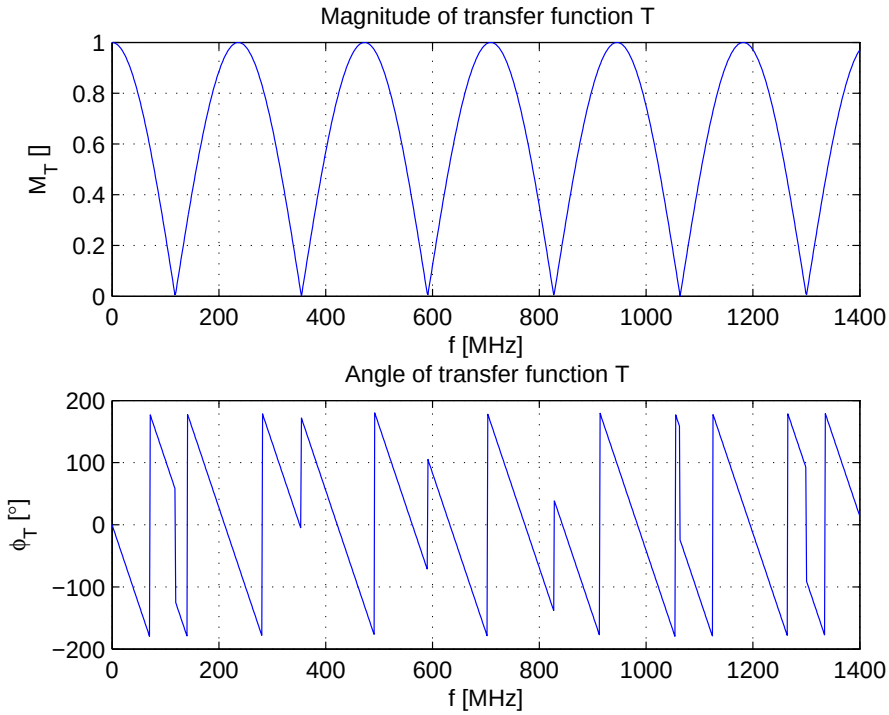

Figure 2.6: Frequency response for k=5.

When the difference between the delays of two branches is measured, it is possible to calculate k value of the model (2.7). It is also possible to do it when the difference between two neighboring frequencies with the maximum attenuations are measured (2.8).

$$k = round\left[\frac{1}{2} + f_a\left(t_{d1} - t_{d2}\right)\right] \tag{2.7}$$

$$k = round\left[\frac{1}{2} + \frac{f_a}{\Delta f}\right] \tag{2.8}$$

Where:
round() - function for changing a real number into the nearest integer

After replacing the t_{d1} in (2.1) with the (2.6), the amplitude and the phase of the transfer function becomes:

$$M_T(f) = \left|\cos\left(-\pi f \frac{1+2k}{2f_a}\right)\right| \tag{2.9}$$

$$\varphi_T(f) = angle\{sign\left[\cos\left(-\pi f \frac{1+2k}{2f_a}\right)\right] e^{i-\pi f\left(\frac{1+2k}{2f_a}+2t_{d2}\right)}\} \tag{2.10}$$

The measurements of a real circuit with an attenuation are presented in Figure 2.7 for $t_{d2} \approx 5.5\ ns$, $t_{d1} \approx 94.6\ ns$:

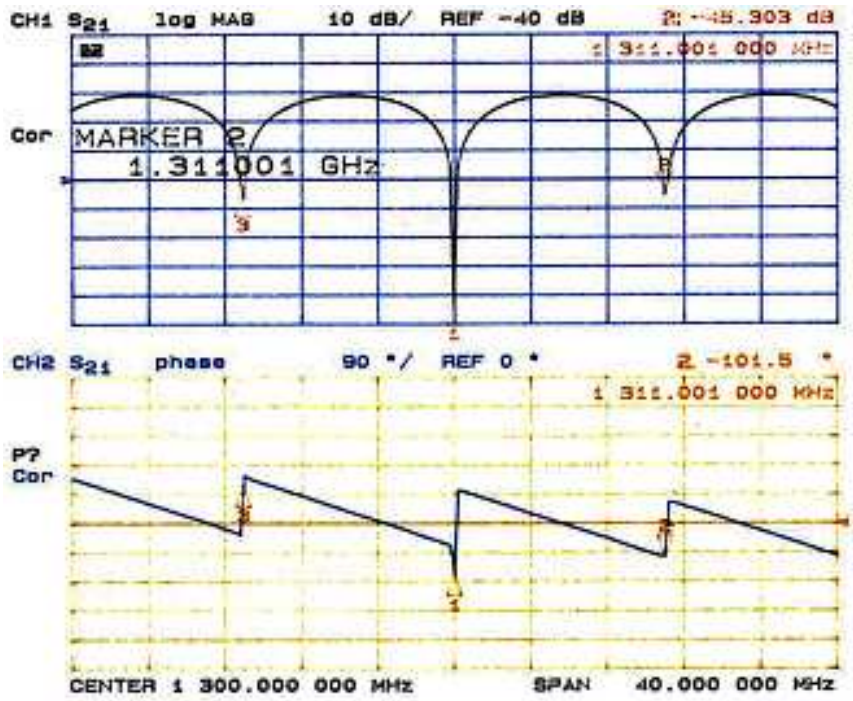

Figure 2.7: Measured frequency response (scanned plotting).

The measurements were performed at DESY in Hamburg with the Hewlett Packard 8753A Network Analyzer for a center frequency 1.3 GHz and a span 40 MHz. The amplitude of the transfer function was plotted with 10 dB per div, with reference

point at -40 dB. The phase of the transfer function is presented with 90° per div, with 0° reference point. In Figure 2.7 we can also see a marker for the nearest point with the minimum gain at a 1311.001 MHz frequency. An amplitude in that point is a -48.3 dB and an angle $-101.5°$. At this frequency, attenuation is lower than at a 1.3 GHz, which is caused by a limited resolution of the network analyzer in the frequency axis. Changing the center frequency to 1311.001 MHz altered the attenuation at this frequency to a similar value as before for the 1.3 GHz and for the 1.3 GHz attenuation changed to the value previously seen at 1311.001 MHz. It proves that every point with the minimum gain has a very similar attenuation and the differences seen on the network analyzer were caused by the limited accuracy of the equipment in the frequency axis. To compare these results with an ideal model, -80 dB was added to the calculated amplitude of the transfer function of this model, otherwise minus infinity would have been seen in the frequencies with zero gain (logarithm of 0 equals minus infinity). The modeled response for similar delays as for the measurements: $t_{d2} = 5.3\ ns$, $k = 115$ which is for $t_{d1} = 94.2\ ns$ and a frequency resolution of 200 points is presented in Figure 2.8.

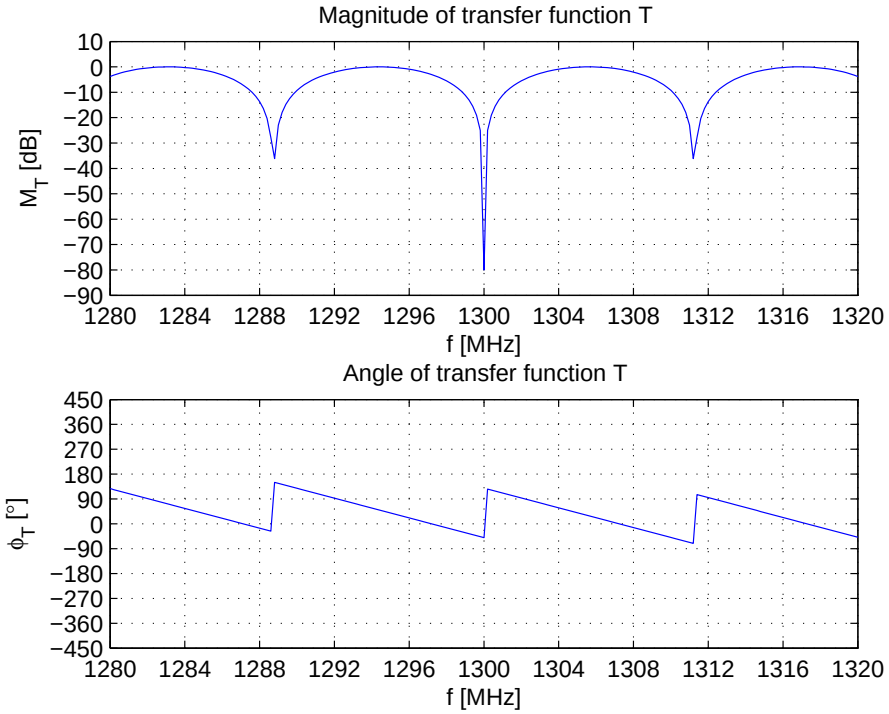

Figure 2.8: Modeled frequency response.

The obtained frequency response is very similar to the measured one. The only

clearly visible difference is that the minimum attenuation in the ideal model is 0 dB while in the measured response it is around -10 dB. This is because the modeled frequency response does not take into account an attenuation of the delay line. The attenuation of the delay lines is taken into account later.

The influence of the amplitude and phase adjustment errors on the frequency response

In a real circuit it is not possible to set a variable attenuator and a phase shifter to perfectly attenuate an output signal at the frequency f_a. There will always be some filter amplitude adjustment error ΔM_{err} and a phase adjustment error $\Delta\varphi_{err}$. In the real filter operation it is necessary to understand how the filter behaves with the filter phase and amplitude adjustment errors. For this purpose, formulas for an amplitude and a phase of the transfer function for the different amplitude adjustment errors ΔM_{err} and the phase adjustment errors $\Delta\varphi_{err}$ were calculated:

$$M_T(f) = \sqrt{\frac{1}{4}\left(\frac{\Delta M_{err}}{M_X}\right)^2 + \left(1+\frac{\Delta M_{err}}{M_X}\right)\cos^2\left(-\pi f\frac{1+2k}{2f_a} - \frac{\Delta\varphi_{err}}{2}\frac{f}{f_a}\right)} \quad (2.11)$$

$$\begin{aligned}\varphi_T(f) = angle\Bigg\{&\cos\left[-2\pi f\left(\frac{1+2k}{2f_a}+t_{d2}\right)\right] + \left(1+\frac{\Delta M_{err}}{M_X}\right)\cos\left(\Delta\varphi_{err}\frac{f}{f_a} - 2\pi f t_{d2}\right)\\ &i\sin\left[-2\pi f\left(\frac{1+2k}{2f_a}+t_{d2}\right)\right] + i\left(1+\frac{\Delta M_{err}}{M_X}\right)\sin\left(\Delta\varphi_{err}\frac{f}{f_a} - 2\pi f t_{d2}\right)\Bigg\}\end{aligned} \quad (2.12)$$

Where:

ΔM_{err} - difference between the optimal amplitude for the frequency f_a suppression in the branch 2 with an actual

M_X - the amplitude of the input signal X(f)

$\Delta\varphi_{err}$ - difference between the optimal phase for the frequency f_a suppression in the branch 2 with an actual

k - the same as in formula (2.5) and (2.6)

For the ΔM_{err} and the $\Delta\varphi_{err}$ set zero the above amplitude and phase of the transfer function equals (2.9) (2.10). To compare this response with the real measurements, the measured frequency response for the $t_{d2} \approx 5.5\ ns$, $t_{d1} \approx 105.9\ ns$ is presented in Figure 2.9.

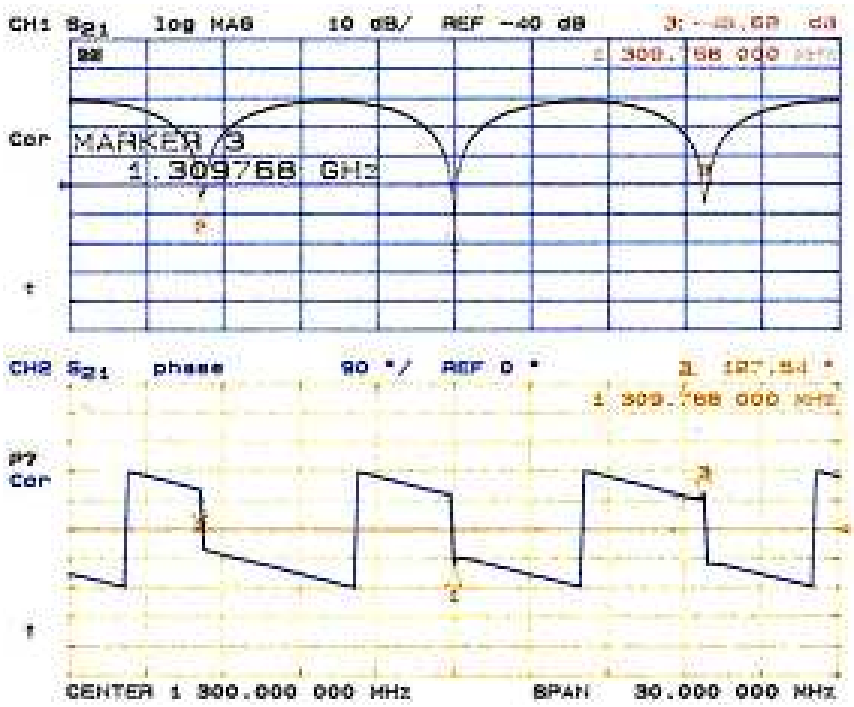

Figure 2.9: Measured frequency response (scanned plotting).

Figure 2.10 presents the modeled frequency response for $t_{d2} = 4.97\ ns$, $k = 130$ which is for $f_a = 1.3\ GHz$, $\Delta M_{err} = 60\ \mu V$, $M_X = 100\ mV$, $\Delta\varphi_{err} = 0.226°$ and the frequency resolution of 200 points.

The influence of the $\Delta\varphi_{err}$ and the ΔM_{err} on the frequency with the minimum gain and on the value of the minimum gain

For an attenuation of one frequency it is useful to know how the frequency f_a and the minimum gain change with $\Delta\varphi_{err}$ and ΔM_{err}. Assuming that the $\Delta M_{err} = 0$, it can be found how the frequency with the minimum gain will differ from the f_a with the $\Delta\varphi_{err}$, this new frequency will be named f_{a2}:

$$f_{a2} = \frac{1}{1 + \frac{\Delta\varphi_{err}}{\pi(1+2k)}} f_a \tag{2.13}$$

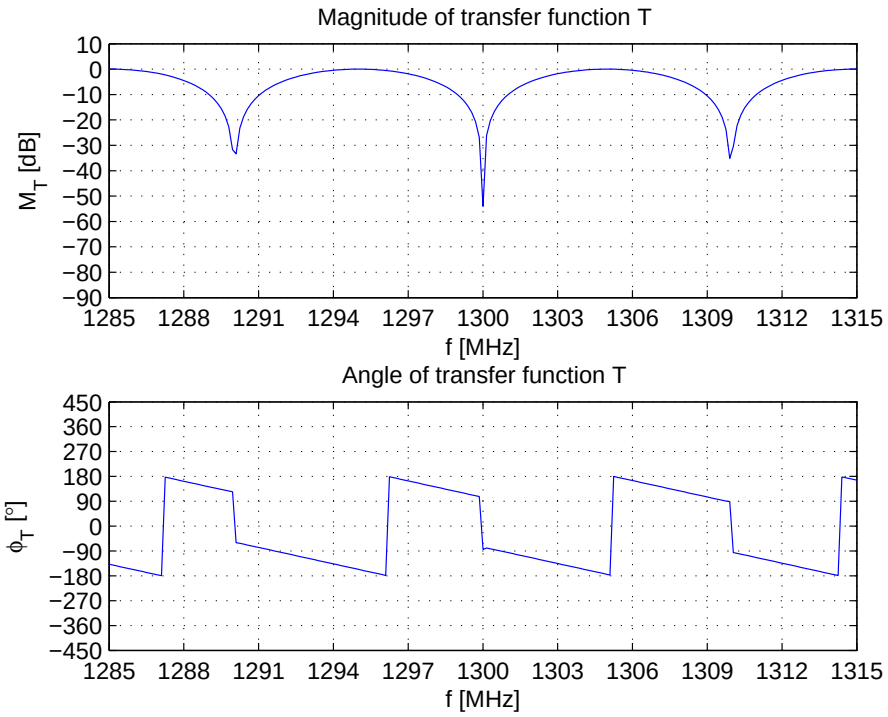

Figure 2.10: Modeled frequency response.

The minimum gain can be found by replacing a cosine in (2.11) with zero:

$$min\left[M_T\left(f\right)\right] = \frac{\Delta M_{err}}{2M_X} \tag{2.14}$$

From the above equations it can be seen that the frequency with the minimum gain changes as a function of the filter phase adjustment error $\Delta\varphi_{err}$. From (2.13) it can also be found how the phase in the branch 2 should be changed to get the minimum gain at f_a. The minimum gain is only a function of the filter amplitude adjustment error ΔM_{err}. From (2.14) it can be found how the amplitude in the branch 2 should be changed to have a desired attenuation, that in the case of the beam induced transient detection equals to $\approx 10^{-5}$.

The phenomenon described by the equations (2.13) and (2.14) was observed during measurements. The phase changes of the variable phase shifter in the branch 2 altered the frequencies with minimum gains. The attenuation changes in the same branch with the variable attenuator modified the values of minimum gains.

Simplified model with cable attenuation

The main difference between the measurements and the calculated frequency response is a lack of cable attenuation in the calculated response. Next step for the RF feedforward comb filter modelling is to add the attenuation of the cable. An attenuation of cables in a function of a frequency is linear in logarithmic scale. A linear function in a logarithmic scale can be expressed as a function:

$$A = f^a \cdot 10^b \tag{2.15}$$

Where:
A - attenuation in [dB/100ft]
f - frequency
a, b - formula factors, that can be calculated from datasheet

Adding (2.15) to formula (2.11) we get model with attenuation:

$$M_{T(dB)}(f) = 20 \cdot \log_{10} \sqrt{\frac{1}{4}\left(\frac{\Delta M_{err}}{M_X}\right)^2 + \left(1 + \frac{\Delta M_{err}}{M_X}\right)\cos^2\left(-\pi f \frac{1+2k}{2f_a} - \frac{\Delta\varphi_{err}}{2}\frac{f}{f_a}\right)} \cdot dB - f^a \cdot 10^b \frac{dB}{Hz \cdot 100ft} \cdot mf \cdot vp \cdot c \cdot \left(\frac{1+2k}{2f_a} + t_{d2}\right) \tag{2.16}$$

Where:
vp - cable velocity of propagation [%]
c - speed of the light in [m/s]
mf - meter to feet conversion factor ($3.28\frac{foot}{m}$)

Or formula with the delays in the two filter brunches t_{d1} and t_{d2}:

$$M_{T(dB)}(f) = 20 \cdot \log_{10} \sqrt{\frac{1}{4}\left(\frac{\Delta M_{err}}{M_X}\right)^2 + \left(1 + \frac{\Delta M_{err}}{M_X}\right)\cos^2\left(\pi f\left(t_{d2} - t_{d1}\right)\right)} \cdot dB - f^a \cdot 10^b \frac{dB}{Hz \cdot 100ft} \cdot vp \cdot c \cdot t_{d1} \tag{2.17}$$

The measurements were performed on the filter built using SS402 cable from Harbour Industries. The "a" and "b" factors can be calculated using the values for an attenuation of SS402 at $f_1 = 400\ MHz$ and $f_2 = 3\ GHz$ from its datasheet [39]:

$$\begin{aligned} \log_{10} f_1 &= 8.60 \\ \log_{10} A_1 &= 0.85 \\ \log_{10} f_2 &= 9.47 \\ \log_{10} A_2 &= 1.32 \end{aligned} \tag{2.18}$$

Calculated factors a and b equal:

$$\begin{aligned} a &= 0.53 \\ b &= -3.77 \end{aligned} \tag{2.19}$$

Figure 2.11 presents the modeled frequency response for $t_{d2} = 4.97\ ns$, k=130, $f_a = 1.3\ GHz$, $\Delta M_{err} = 60\ \mu V$, $M_X = 100\ mV$, $\Delta\varphi_{err} = 0.226°$, $a = 0.53$, $b = -3.77$, $vp = 70\%$ and the frequency resolution of 200 points.

It is visible that this model conforms the measurements presented in Figure 2.9. There is additional attenuation of around 10 dB (in the presented frequency range), which was absent in the modeled frequency response without attenuation shown in Figure 2.10.

Rule for achieving L attenuation, at an f_a frequency

In order to attenuate an explicit frequency f_a by L it is required to adjust an amplitude and a phase of the signal in the branch 2 with certain accuracy. The calculated maximum ΔM_{err} and $\Delta\varphi_{err}$ gives information if it is possible to achieve a given attenuation, and also gives information about required accuracy of the phase shifter and the variable attenuator. To estimate this precision, comparison of an amplitude and an attenuation can be used:

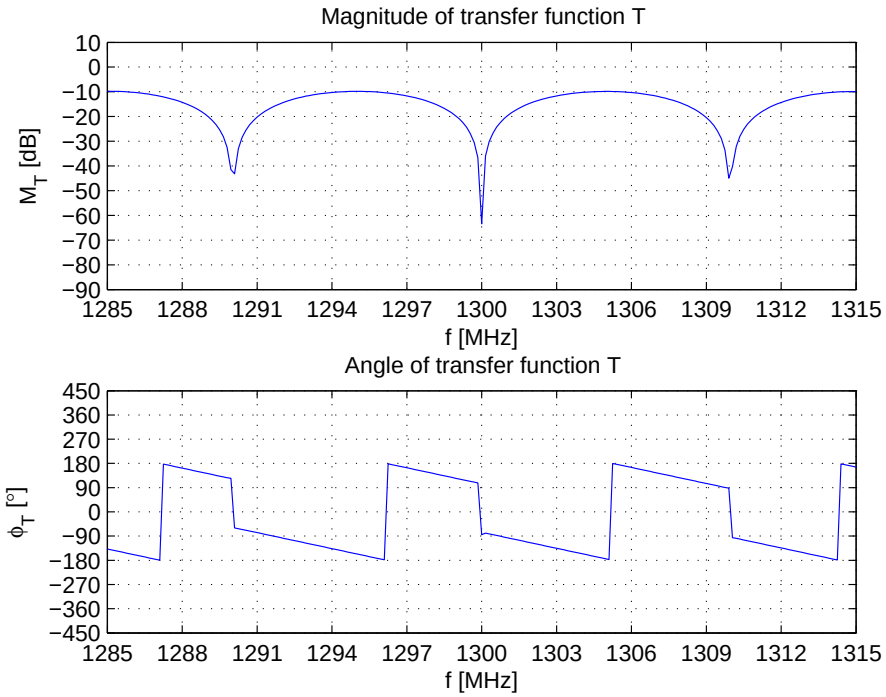

Figure 2.11: Modeled frequency response.

$$M_T(f) = \sqrt{\frac{1}{4}\left(\frac{\Delta M_{err}}{M_X}\right)^2 + \left(1+\frac{\Delta M_{err}}{M_X}\right)\cos^2\left(-\pi f\frac{1+2k}{2f_a} - \frac{\Delta\varphi_{err}}{2}\frac{f}{f_a}\right)} \leq \frac{1}{L} \tag{2.20}$$

Solution to this comparison is:

$$\arccos\left[\frac{\frac{2}{L^2}-\frac{1}{2}\left(\frac{\Delta M_{err}}{M_X}\right)^2}{\left(1+\frac{\Delta M_{err}}{M_X}\right)}-1\right]-\pi \leq \Delta\varphi_{err} \leq -\arccos\left[\frac{\frac{2}{L^2}-\frac{1}{2}\left(\frac{\Delta M_{err}}{M_X}\right)^2}{\left(1+\frac{\Delta M_{err}}{M_X}\right)}-1\right]+\pi \tag{2.21}$$

For:

$$-\frac{2}{L} \leq \frac{\Delta M_{err}}{M_X} \leq \frac{2}{L} \tag{2.22}$$

For the $L = 10^5$ which is 100 dB.

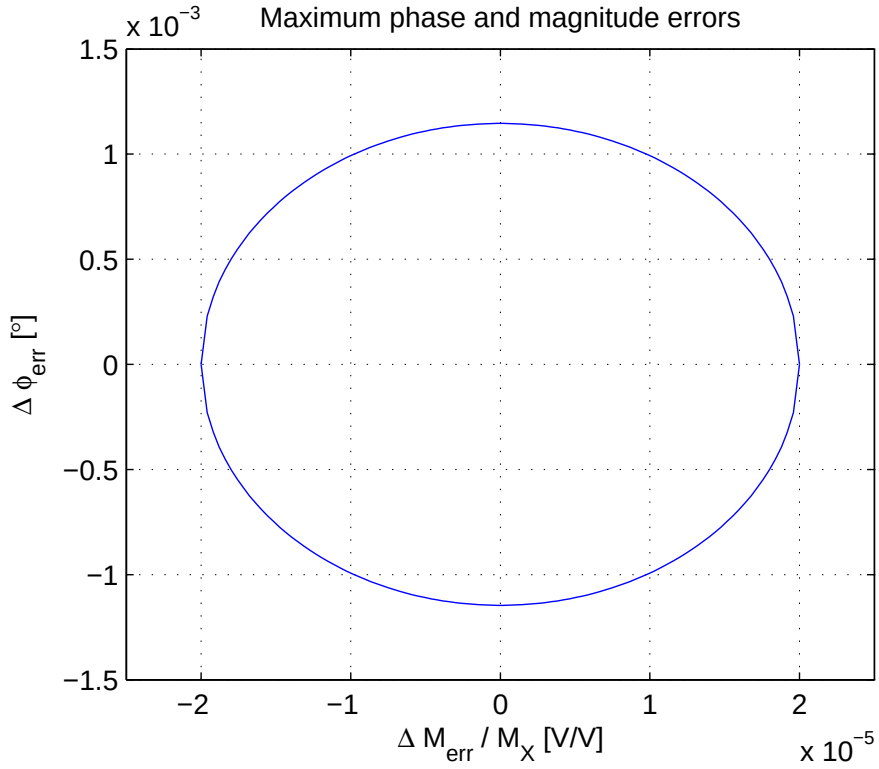

Figure 2.12: Maximum filter phase and amplitude adjustment errors.

In order to have 100 dB attenuation, the filter amplitude adjustment error $\Delta M_{err}/M_X$ and the phase adjustment error $\Delta\varphi_{err}$ should be inside the circle in Figure 2.12. The formula (2.21) can be used to estimate the maximum filter amplitude and phase adjustment errors in the branch 2 in order to achieve the required attenuation L.

$$\max\left[\Delta\varphi_{err}\right] = -\arccos\left[\frac{2}{L^2} - 1\right] + \pi \tag{2.23}$$

$$\max\left[\frac{\Delta M_{err}}{M_X}\right] = \frac{2}{L} \tag{2.24}$$

For 100 dB attenuation, the maximum filter phase and amplitude adjustment errors equal:

$$\max\left[\Delta\varphi_{err}\right] = -\arccos\left[\frac{2}{(10^5)^2} - 1\right] + \pi \approx 0.001^\circ \tag{2.25}$$

$$\max\left[\frac{\Delta M_{err}}{M_X}\right] = \frac{2}{10^5} \approx 10^{-5} \tag{2.26}$$

During the measurements the maximum attenuation of around 100 dB at 1.3 GHz presented in Figure 2.13 was observed. An effective attenuation was lower as the minimum attenuation for the maximum gain near this frequency was -11.1 dB, which was the attenuation of the combiner, the splitter and the cable. Therefore the effective attenuation is a difference of these two values and equals 88.8 dB.

Another problem during the measurements was a noise limit. It was not possible to see a better attenuation then 100 dB because of the noise that can be seen in Figure 2.13 (for the attenuations higher then 90 dB, the measured phase is jumping by around 180°). The presented measurements were performed for 25 dBm signal power. In the measurements for 0 dBm signal power, the maximum attenuation was around 25 dB smaller then for 25 dBm. It could be evidence that it was not possible to see the maximum attenuation because of the noise limit. With a higher signal power better results could have been probably obtained.

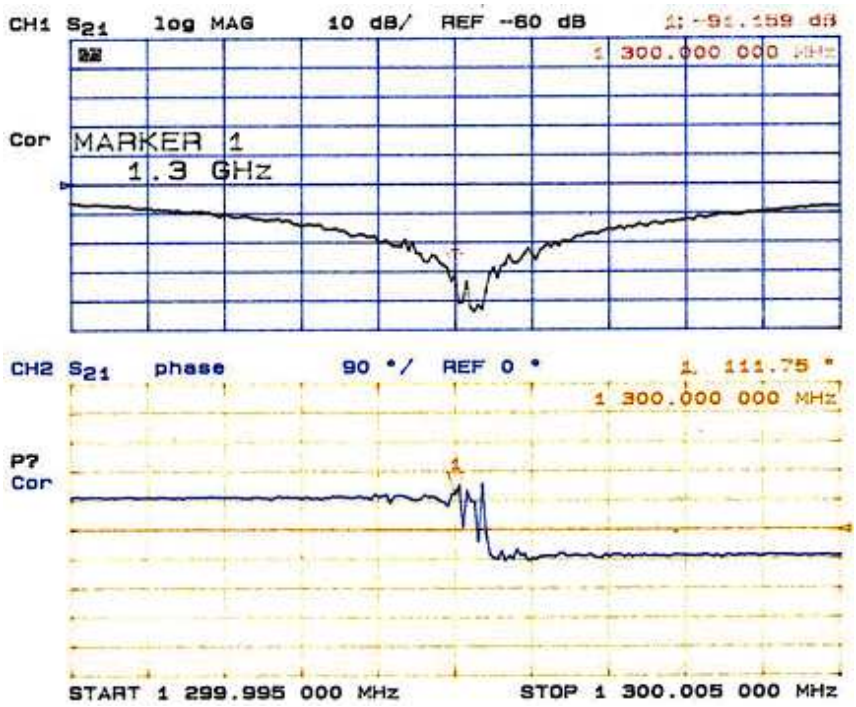

Figure 2.13: Maximum attenuation during measurements (scanned plotting).

By rearranging the formula (2.13) it is possible to find the filter phase adjustment error $\Delta\varphi_{err}$ from the actual frequency with the maximum attenuation and required:

$$\Delta\varphi_{err} = \pi\,(1+2k)\left(\frac{f_a}{f_{a2}} - 1\right) \tag{2.27}$$

Where:
f_a - a desired frequency with maximum attenuation
f_{a2} - an actual frequency with maximum attenuation

For an $f_a = 1.3\ GHz$, $f_{a2} = 1.3\ GHz + 250\ Hz$ and k=130 it equals:

$$\Delta\varphi_{err} = -9 \cdot 10^{-3}\ ^{\circ} \tag{2.28}$$

It is also possible to find the filter amplitude adjustment error ΔM_{err} from Figure 2.13 by rearranging the formula (2.14):

$$\frac{\Delta M_{err}}{M_X} = 2\min\left(M_T\right) \tag{2.29}$$

For a $M_X = 3.97\ V$ (25 dBm input signal and 50 Ω load) $\Delta M_{err} = 142\ \mu V$ ($L_{eff} = 100\ dB - 11.1\ dB = 88.9\ dB$, 100 dB - full attenuation, 88.9 dB - effective attenuation, $\Delta M_{err} = \frac{M_X}{L_{eff}}$). The modeled frequency response for $t_{d2} = 4.9\ ns$, k=130 ($t_{d1} = 105.3\ ns$), $f_a = 1.3\ GHz$, $\Delta M_{err} = 142\ \mu V$, $M_X = 3.97\ V$, $\Delta\varphi_{err} = -9e-3$, $a = 0.53$, $b = -3.77$, $vp = 70\ \%$ and 200 points is presented in Figure 2.14.

By comparing Figure 2.13 with Figure 2.14 it is evident that the frequency response is very similar with one visible difference, the measured frequency response has noise which is absent in the modeled response.

Conclusions

The model presented in this chapter conforms to the measured frequency response of the filter, it is especially visible when Figure 2.9 is compared to Figure 2.11 and Figure 2.13 with Figure 2.14. Therefore It can be concluded that the model of the RF feedforward comb filter is correct and can be used for simulations and calculations in a frequency domain.

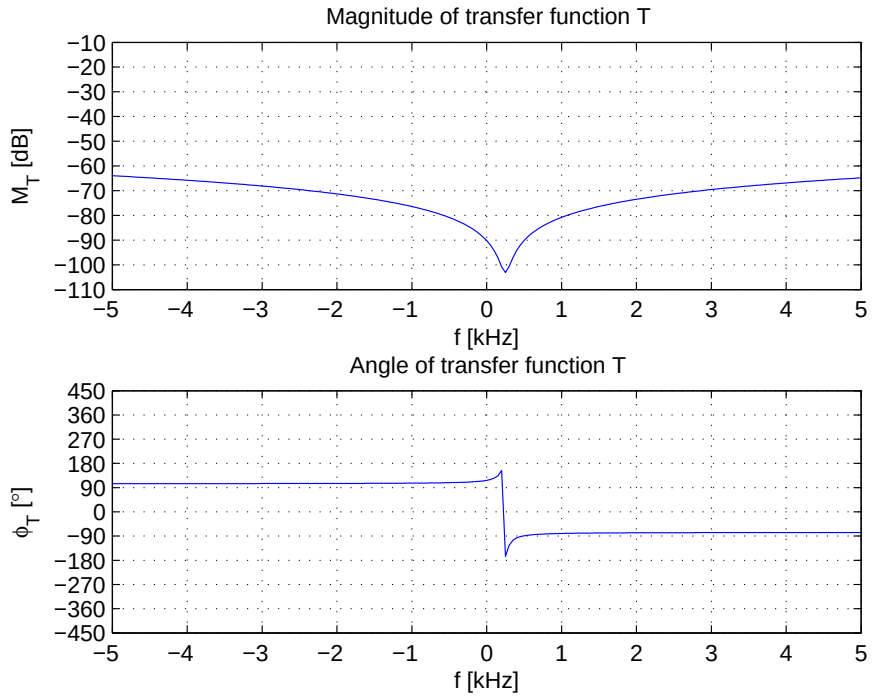

Figure 2.14: Modeled frequency response for 1.3 GHz center frequency.

2.2.2 Temperature stabilization

Thermal sensitivity

The requirement on the filter amplitude and phase adjustment accuracy in the branch 2 with respect to the branch 1 (Figure 2.5) are very high, $2 \cdot 10^{-5}$ in an amplitude and 0.001° in a phase. The delay line in the branch 1 is made of a cable. Its phase shift and attenuation depend on temperature. Any temperature fluctuations induce the cable attenuation and phase shift changes [57]. When it happens the signal amplitude and phase in the branch 1 also changes. The branch 2 amplitude and phase must be readjusted to compensate the changes or the temperature has to be kept stable.

In order to find out what is the required temperature stability, the cable temperature sensitivity was measured. The measurement was performed on 21 m M-54 type cable with the CTS C-40/600 climatic test chamber using following devices: ZN2PD-20 (the splitter), AD8302 (the amplitude and phase detector), the R&S Signal Generator SML 3, the Agilent 34970A Data Acquisition Switch Unit and K-type

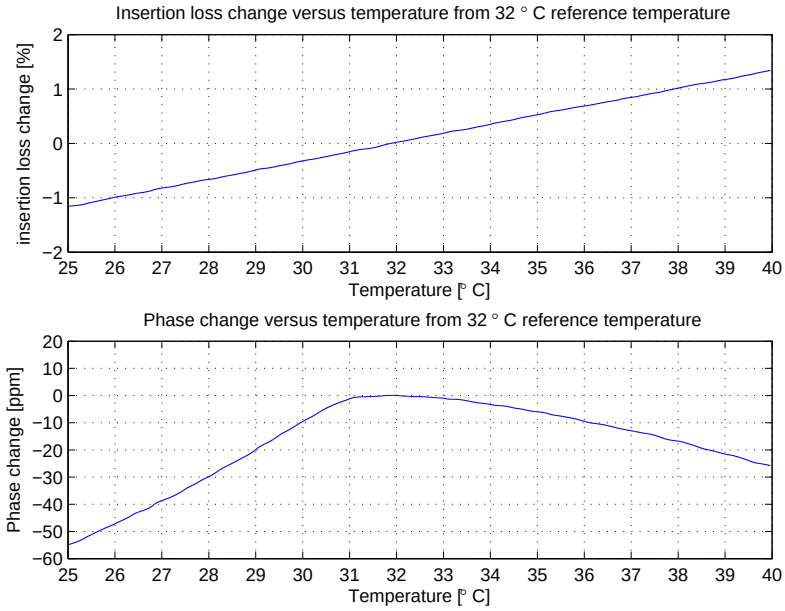

Figure 2.15: Insertion loss and phase change of the M-54 type cable from Midwest Microwave versus temperature from 32 $°C$ reference temperature.

temperature sensors. The result is presented in Figure 2.15.

The system uses 5 m M-54 type Midwest Microwave delay line cable. 1.3 GHz signal thermal amplitude and phase sensitivity in the cable was calculated on a basis of the measurement and the data from manufacturer's catalog [48] ($L_{foot} = 0.08\ \frac{dB}{foot}|_{1\ GHz}$ - cable insertion loss, $vp = 76.5\ \%$ - velocity of propagation). The calculations results are presented in Figure 2.16.

Temperature stabilization

The data presented in Figure 2.16 was processed by an algorithm to find the required temperature stability. Two cases where taken into account. The first was the delay line with a special circuit for compensation of the amplitude and phase changes in the range: $3.2 \cdot 10^{-4}\ V/V$ in an amplitude and 0.0018 ° in a phase. The second was the delay line without the compensation. Therefore the required amplitude and phase stabilities in both cases were different:

- $3.2 \cdot 10^{-4}\ V/V$ in an amplitude and 0.0018 ° in a phase for the cable with compensation,

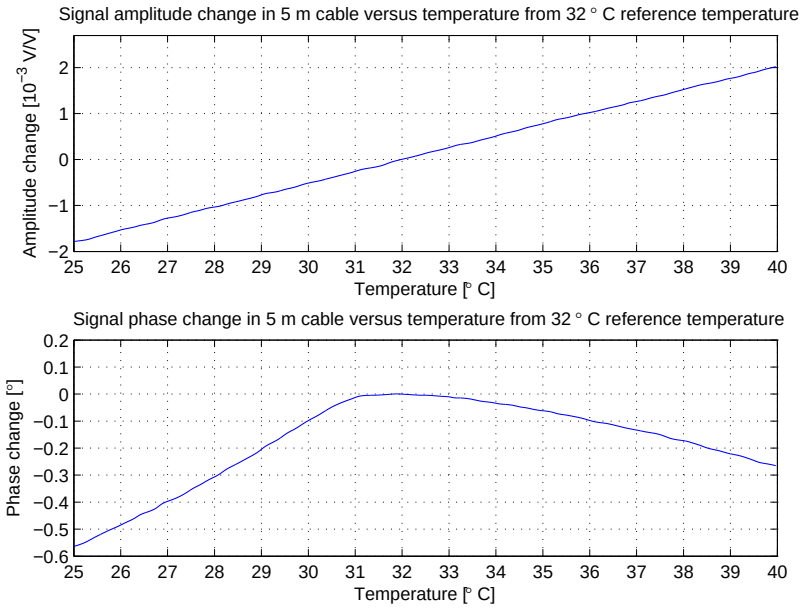

Figure 2.16: Signal amplitude and phase change of 5 m M-54 type cable from Midwest Microwave versus temperature from 32 $°C$ reference temperature.

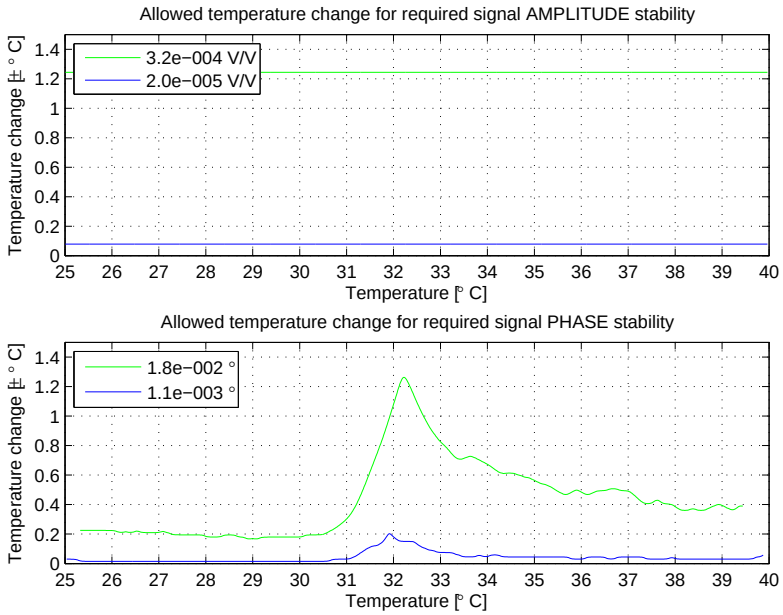

Figure 2.17: Allowed temperature change for the given signal amplitude and phase stability. — with compensation in a range $3.2 \cdot 10^{-4}\ V/V$, — without compensation.

- $2 \cdot 10^{-5}$ in an amplitude and 0.001° in a phase for the cable without compensation

Figure 2.17 presents the calculated required temperature stability separately for an amplitude and phase. Figure 2.18 presents the calculated required stability for both amplitude and phase. The mandatory temperature stableness depends on the value of an absolute temperature. For the $\approx 32°C$, the temperature can be changed by the highest value while keeping the amplitude and phase changes below the demanded level. The temperature changes at $32°C$ must be kept below $\pm 0.1\ °C$ for the delay line without the compensation circuitry. In case of the cable with the compensation circuit the temperature changes at $32°C$ must be kept below $\pm 1.2\ °C$, which is much easier then in the former case.

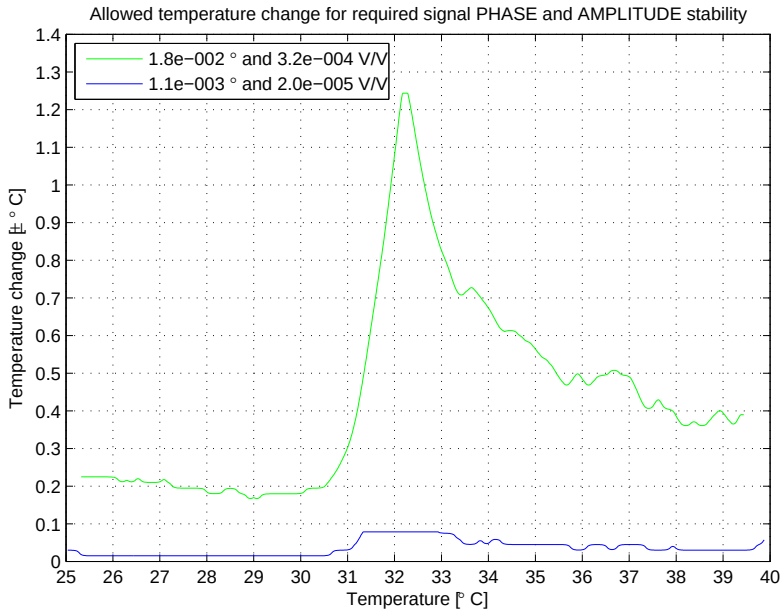

Figure 2.18: Allowed temperature change for the given signal phase and amplitude stability. — with compensation in a range $3.2 \cdot 10^{-4}\ V/V$, — without compensation.

The presented analysis shows that the delay line cable must be stabilized thermally. The temperature stabilization is done with the temperature controlled oven built at DESY by Krzysztof Czuba [35]. It has sufficient performance to stabilize the temperature of the delay line cable with the compensation circuit in order to keep the signal amplitude and phase changes below the demanded level. The delay line cable also needs a special circuit for the amplitude and phase changes compensation

in a range: $3.2 \cdot 10^{-4}$ V/V in an amplitude and 0.0018 ° in a phase. The temperature stabilization of the delay line without compensation circuitry might be very difficult and expensive. Therefore the hybrid solution of temperature stabilization and compensation of the signal changes is used in order to keep the signal amplitude and phase changes below $2 \cdot 10^{-5}$ in an amplitude and 0.001° in a phase.

2.2.3 Filter implementations

The RF feedforward comb filter had several implementations. The filter implementation version number 1 is the simplest. It is very similar to the version number 2 (Figure 2.19), the only difference between them is that in the version number 1 the variable attenuator and the phase shifter were controlled manually and that there were no relays for disconnecting the delay line.

An amplitude and a phase in the filter implementation version number 2 is adjusted with the mechanical motorized variable phase shifter and attenuator. Mechanical devices for a phase and an amplitude adjustments were chosen because they have a very good stability. In comparison the stability of a voltage controlled phase shifter and attenuator would not be sufficient for the high precision adjustments, 0.001° in a phase and $2 \cdot 10^{-5}$ in an amplitude.

The motorized devices are controlled by an ADC, DAC and digital IO modules installed in an Industry Pack VME carrier board. In addition two relays responsible for connecting and disconnecting the delay line are controlled by the digital IO module. The delay line is connected during a normal filter operation when the transients are measured. The relays disconnect the delay line during a filter calibration. In this stage the transient detection system measures the transfer function of the filter that influences transients amplitude and phase.

During the development, the first choice for the delay of the filter delay line was to 100 ns. The beam bunches are sent with 1 MHz repetition rate. Therefore the first harmonic of the single bunch induced transients is at 1 MHz sideband of 1.3 GHz carrier. With 100 ns delay, the filter has 10 dB attenuation at 1 MHz sideband and can have 100 dB attenuation at 1.3 GHz. As a result the filter would attenuate the carrier signal with 90 dB higher attenuation than the first harmonic of the transients.

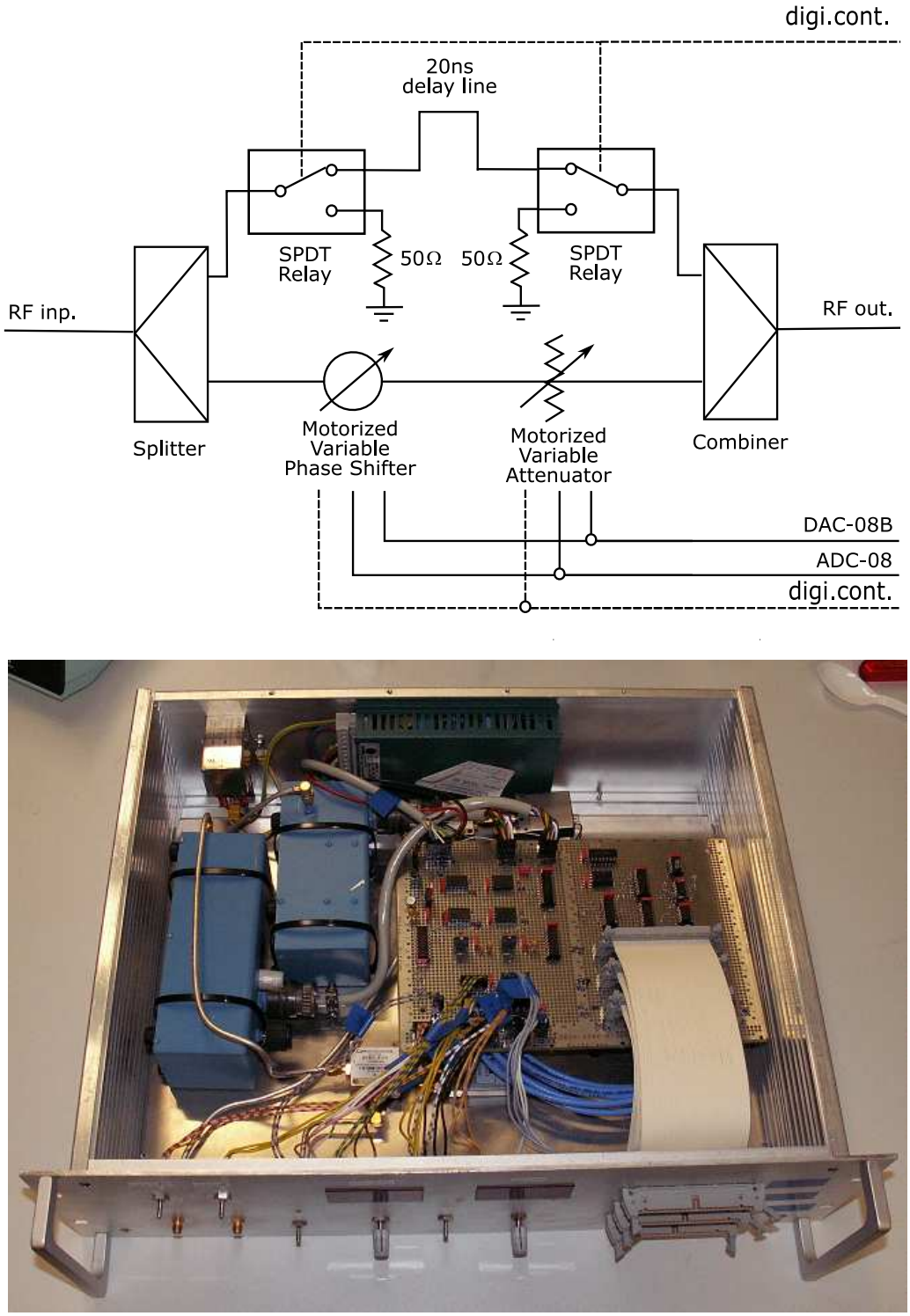

Figure 2.19: Feedforward comb filter version number 2.

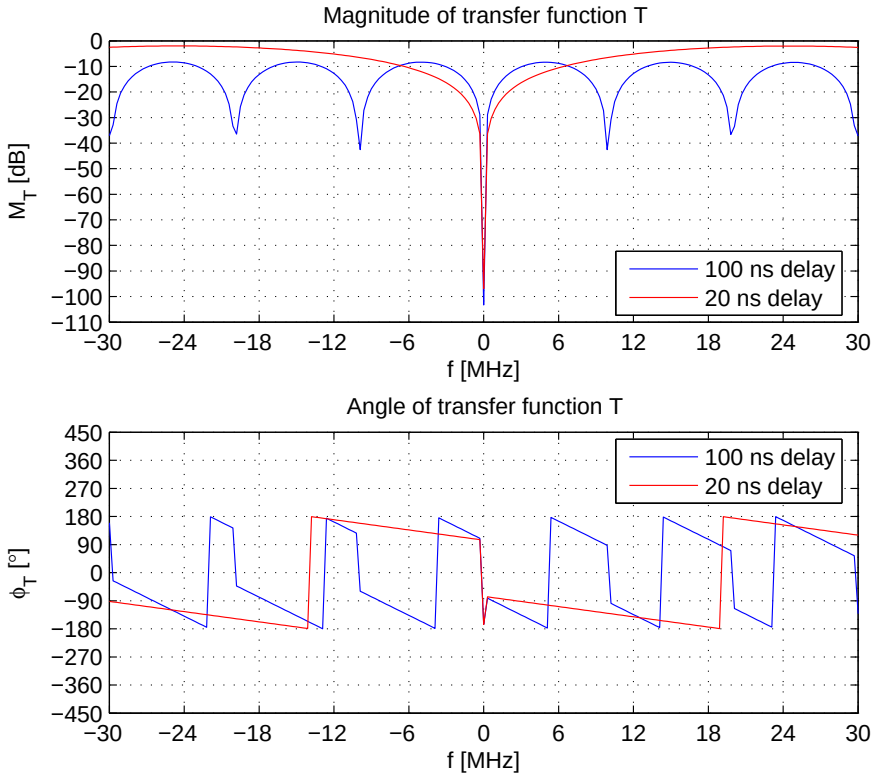

Figure 2.20: Comparison of the filter frequency response for two delays, 100 ns and 20 ns (model from Section 2.2.1).

After the tests in the module ACC1 in FLASH the delay was changed to 20 ns, for two reasons. The filter delay reduction lowers the attenuation of the delay line cable from 8.3 dB to 2 dB (Figure 2.20). The frequency response of the filter depends on the delay of the delay line. For shorter delays it has a higher attenuation for the frequencies that are close to 1.3 GHz carrier by around 8 dB (Figure 2.20). The signal from a cavity probe at an output of the filter with 100 ns delay during tests had some signals at the frequencies close to the carrier (frequencies at passband modes of the TESLA cavity - 1300.091 MHz, 1299.260 MHz, 1296.861 MHz, 1293.345 MHz, 1289.022 MHz, 1284.409 MHz [52]) even with an accurate filter adjustment (Figure 2.21). The signals can be reduced using shorter delay. In the case the filter delay is changed from 100 ns to 20 ns, a signal to noise ratio should increase by around 14.3 dB (Figure 2.20, 6.3 dB - reduced cable attenuation, 8 dB higher attenuation of the signals at frequencies close to the carrier 1.3 GHz).

The filter is required to have 100 dB attenuation at 1.3 GHz frequency. This can

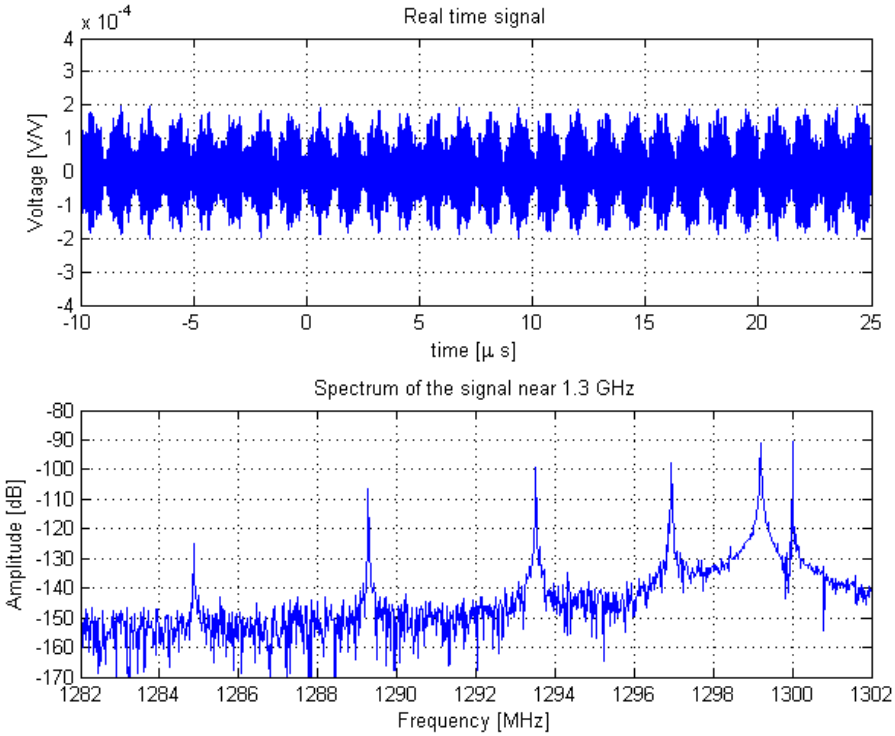

Figure 2.21: The signal at the output of the feedforward comb filter without transients.

only be achieved by adjusting a phase and an amplitude with the resolution of $0.001°$ in a phase and $2 \cdot 10^{-5}$ in an amplitude. In order to relax the requirements on the adjustment accuracy concept for fine-tuning was developed (Figure 2.22). The principle is to use a sum of two vectors for the adjustment. The one large vector for a rough adjustment $\vec{V}_{RFfield}$ and the second much smaller for fine-tuning $\vec{V}_{fine-tuning}$.

Implementation of this concept is presented in Figure 2.23. The splitter divides signal into two. The one of them is delayed with the delay line $\vec{V}_{RFdelayed}$ (Figure 2.22). The second is adjusted by the mechanical variable attenuator and the phase shifter. This part is responsible for the rough filter adjustment $\vec{V}_{RFfield}$. This signal is splitted into two by the 20 dB directional coupler. The signal coupled by 20 dB is adjusted by the mechanical variable attenuator and the phase shifter. In addition the signal is attenuated by 30 dB. The result is responsible for fine-tuning of the filter $\vec{V}_{fine-tuning}$. The $\vec{V}_{fine-tuning}$ signal is 50 dB smaller then the $\vec{V}_{RFfield}$ roughly adjusted signal. Both of them are summed by the combiner. The result is added to the $\vec{V}_{RFdelayed}$ signal by the combiner to get the filter output which is the

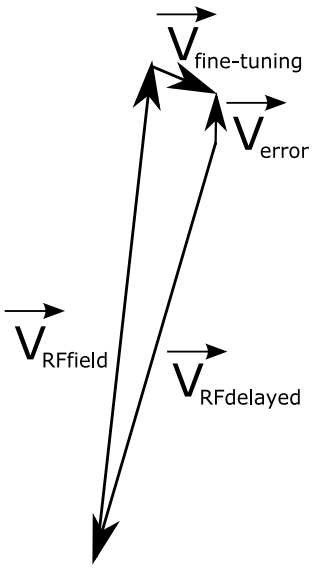

Figure 2.22: Concept for fine-tuning of the RF feedforward comb filter. $\vec{V}_{RFfield}$ - signal vector used for a rough filter adjustment; $\vec{V}_{fine-tuning}$ - signal vector used for filter fine-tuning; $\vec{V}_{RFdelayed}$ - delayed signal vector; $\vec{V}_{error}$ - filter adjustment error vector.

$\vec{V}_{error}$ filter adjustment error vector.

This idea makes it easy to adjust the phase with higher precision then required. This solves the problem with the filter adjustment, however it does not solve the difficulties caused by temperature changes. Temperature fluctuations cause the attenuation and the phase shift changes of the delay line, which requires the continuous filter adjustment. The mechanical motorized attenuator and phase shifter can not change its positions all the time, because it can brake them. In addition it is a difficult task to control these motorized components. Therefore it is required to find a different way to compensate temperature changes. The one solution could be a temperature stabilization of the filter.

In the case the phase stability at 0.001° is required, the temperature stabilization might not be possible. Another idea would be to compensate the phase and attenuation changes caused by temperature changes. It could be done by using a vector modulator for the fine-tuning instead of the motorized variable phase shifter and attenuator (Figure 2.24).

The stability of vector modulators is not sufficient to use them as the devices for a rough adjustment. Moreover the output of them is noisy in comparison to the output

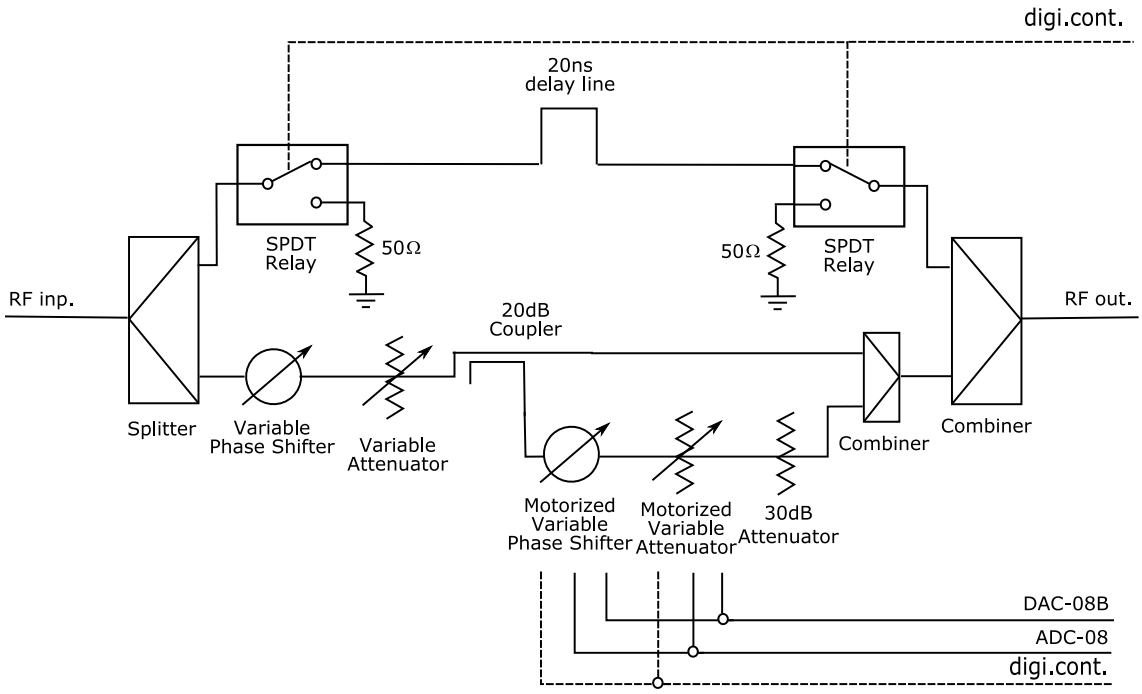

Figure 2.23: Feedforward comb filter version number 3b.

of the passive mechanical attenuator and phase shifter. As a result IQ modulator can only be used for the fine-tuning and its output is 70 dB smaller then the signal from the rough adjustment (40 dB from the couplers and 30 dB from the attenuators, Figure 2.24).

The mentioned idea works very well when the output of the filter is used as an error vector for a feedback algorithm, which controls the vector modulator. In this case IQ modulator compensates slow temperature changes and keeps the phase adjustment error below 0.001° in a phase and $2 \cdot 10^{-5}$ in an amplitude (Figure 2.25, Figure 2.26). Unfortunately this concept works only for limited periods of the time, like several days. When a temperature change is too large, the error vector goes out of the working range of the vector modulator and the filter becomes detuned. The one solution would be to increase the working range of the vector modulator by reducing the attenuation at its output. Unfortunately in this case the output of the filter becomes too noisy. Therefore it is required to stabilize the temperature roughly to keep the error vector in the working range of the vector modulator. Solution used in the developed system comprises the temperature stabilization and the fine-tuning done with the IQ modulator.

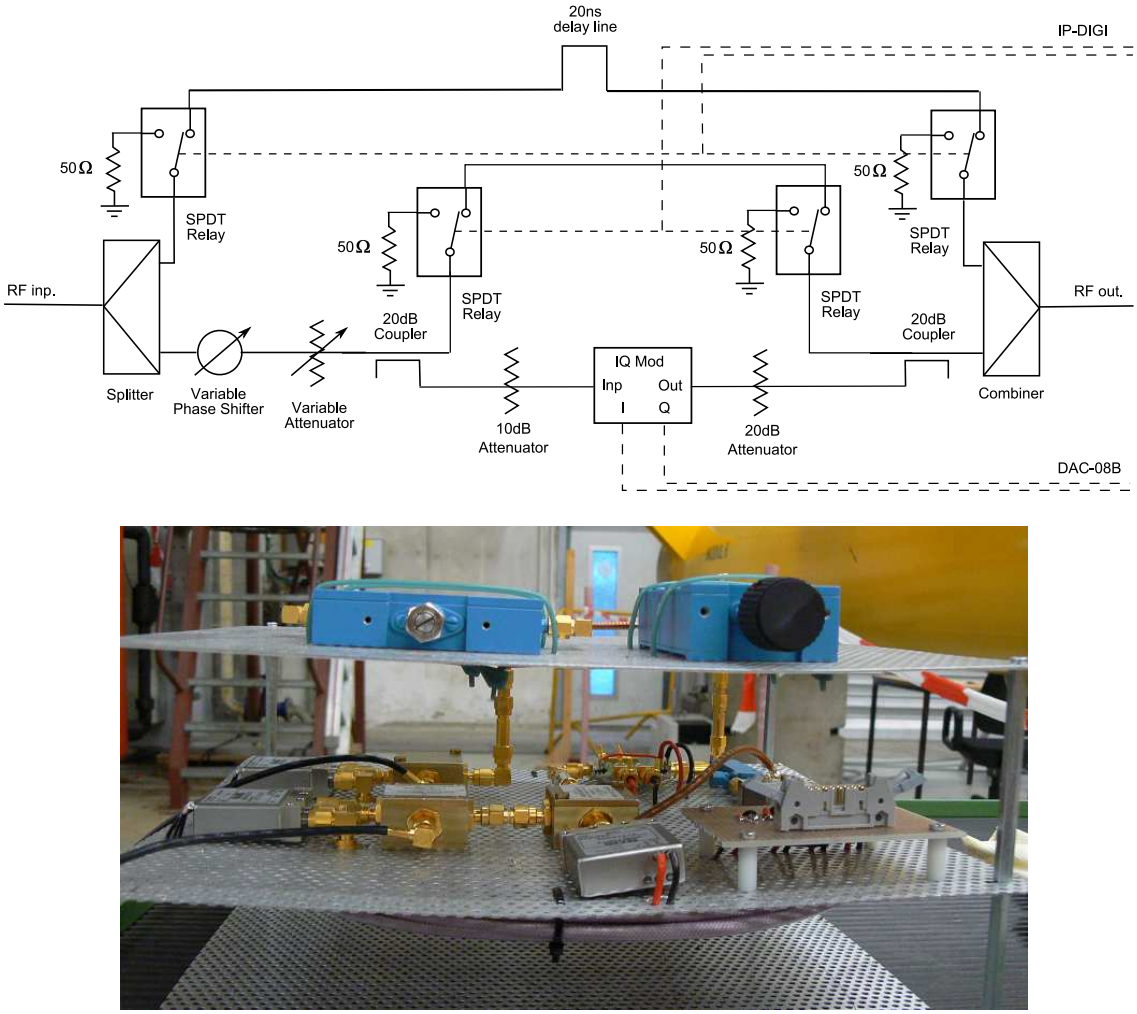

Figure 2.24: Feedforward comb filter version number 3.

2.2.4 Filter adjustment - basic principle

The basic principle of the filter adjustment is to reduce the vector output of the filter at 1.3 GHz frequency to zero. This output can be analyzed as a vector (Figure 2.27). The filter adjustment error vector $\vec{V}_{error}$ equals a sum of the two vectors $\vec{V}_{RFdelayed} + \vec{V}_{RFfield}$. The M_{error} and the φ_{error} are respectively the amplitude adjustment error and the phase adjustment error. The adjustment procedure starts with changing the amplitude of the $\vec{V}_{RFfield}$ vector with the variable attenuator to minimize the filter amplitude error. The easiest way to do it is by looking on a complex value at an output of the filter $\vec{V}_{error}$ vector. Small amplitude and phase changes of the $\vec{V}_{RFfield}$ vector for the preadjusted filter are linear in a complex space. Therefore it is easy to find the amplitude and phase adjustment errors minima. While the filter amplitude

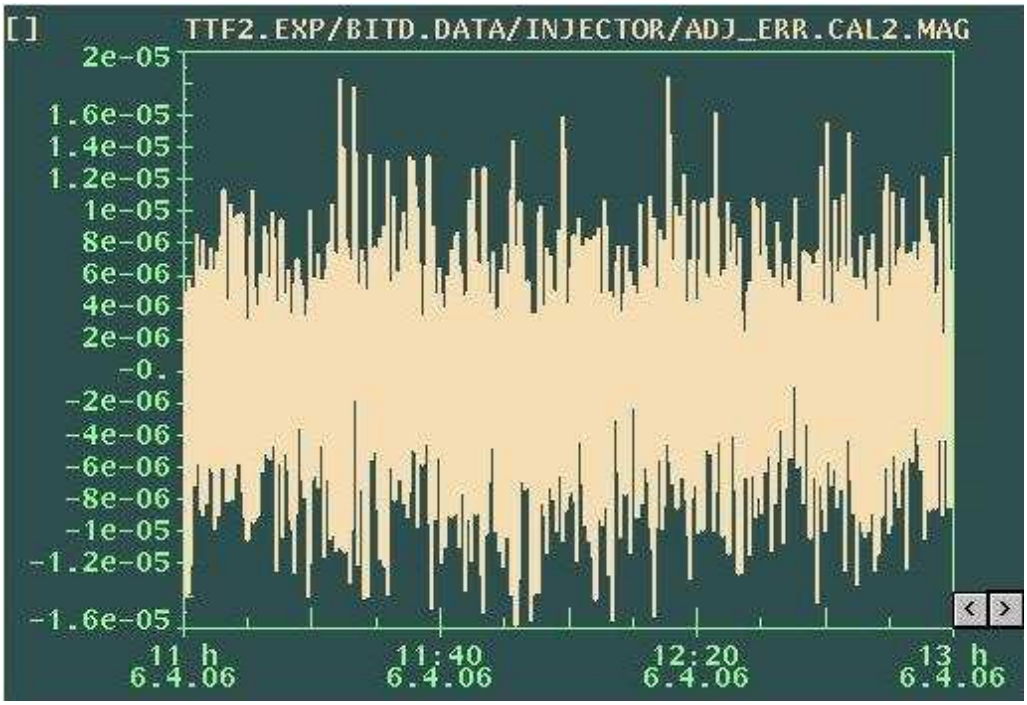

Figure 2.25: Amplitude adjustment error [V/V].

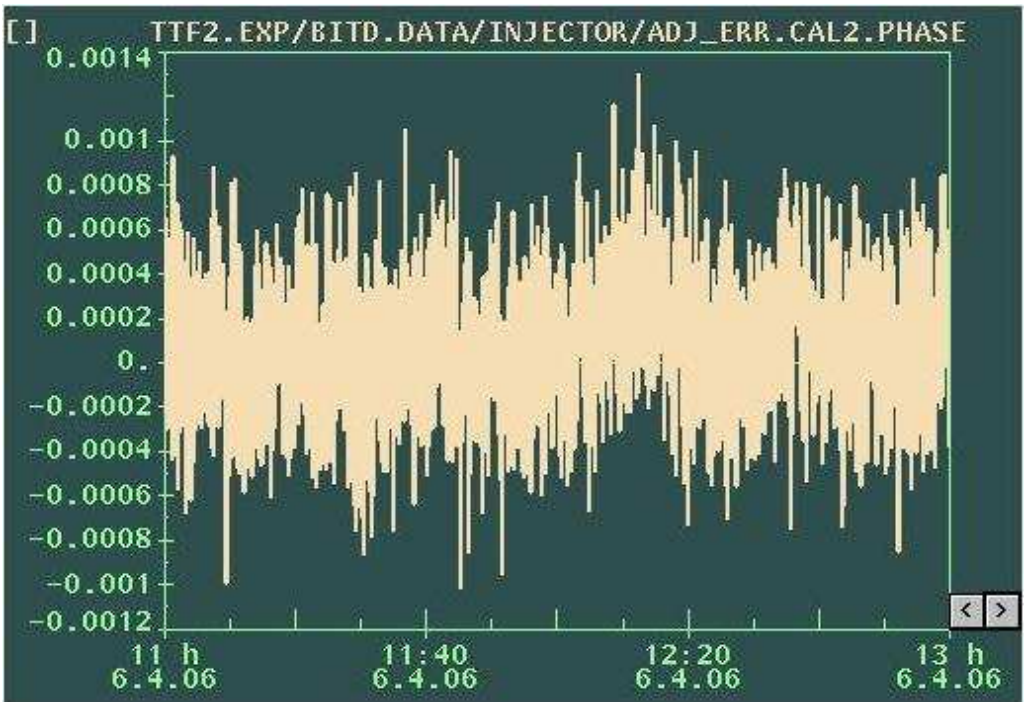

Figure 2.26: Phase adjustment error [°].

error is minimized, the filter phase error is minimized with the variable phase shifter. These two steps are repeated until the filter adjustment error vector equals zero. At this point gain of the amplifier is raised to increase the filter adjustment precision. The procedure is repeated until the amplifier achieves the maximum gain and the $\vec{V}_{error}$ vector equals zero. When it happens the procedure is finished.

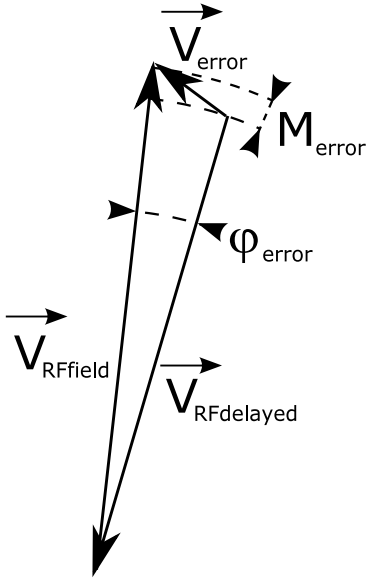

Figure 2.27: The adjustment error vector of the RF feedforward comb filter. $\vec{V}_{RFfield}$ - signal vector used for the filter adjustment; $\vec{V}_{RFdelayed}$ - delayed signal vector; $\vec{V}_{error}$ - filter adjustment error vector; φ_{error} - filter adjustment phase error; M_{error} - filter adjustment amplitude error.

2.3 Variable gain amplifier

The filtered signal from the RF feedforward comb filter has to be amplified. The power output of the filter depends on the mode of the transient detection system operation and on the filter adjustment accuracy. The signal is large when the filter is not adjusted and small when it is precisely adjusted. Therefore the amplifier must have a regulated gain. The signal that is amplified is very small. As a result it is necessary to have a low noise amplifier to keep a good signal to noise ratio. The implementation of the low noise variable gain amplifier used in the system is presented in Figure 2.28.

The gain is regulated by connecting or disconnecting the amplifiers to the main

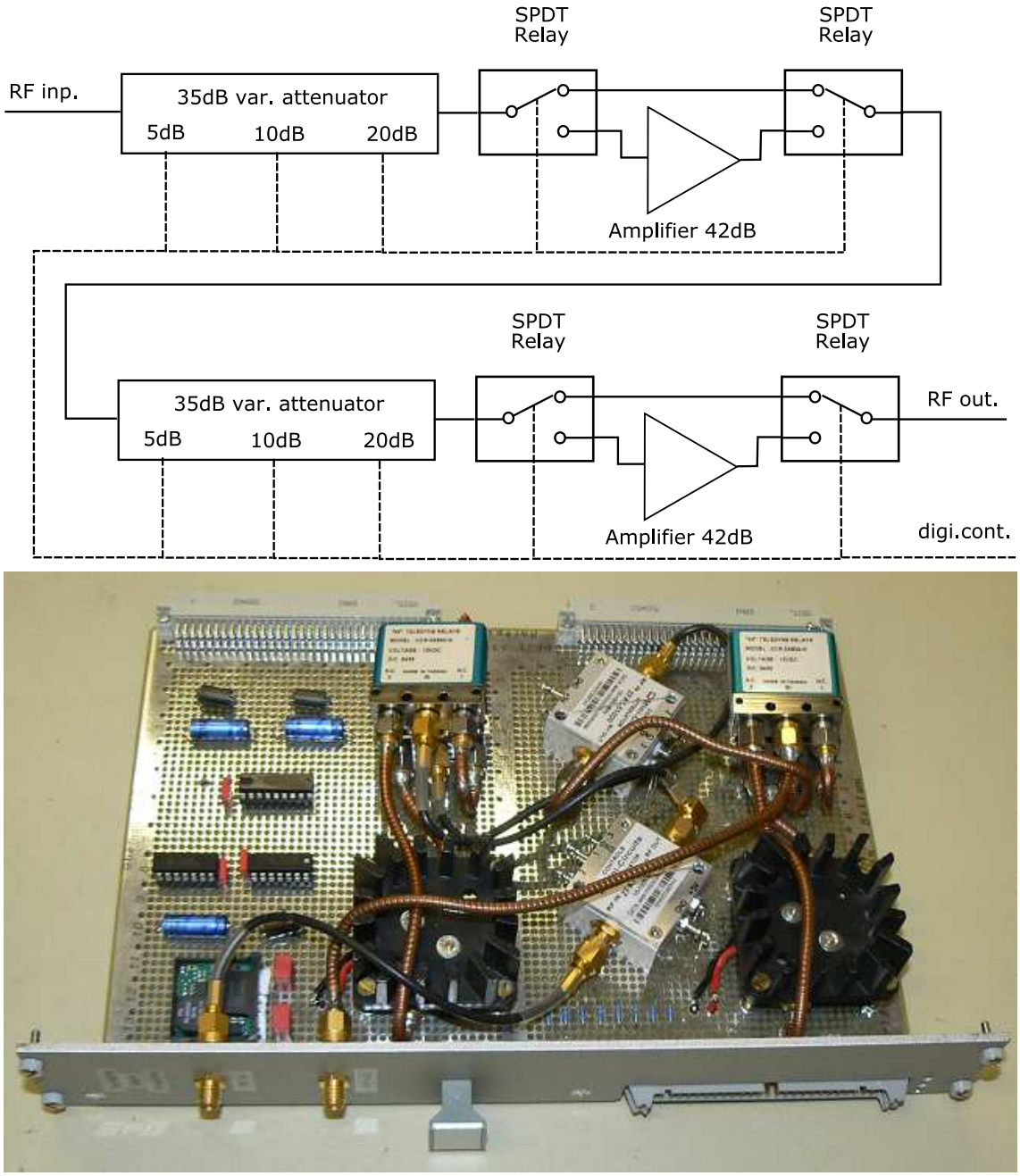

Figure 2.28: Variable gain amplifier.

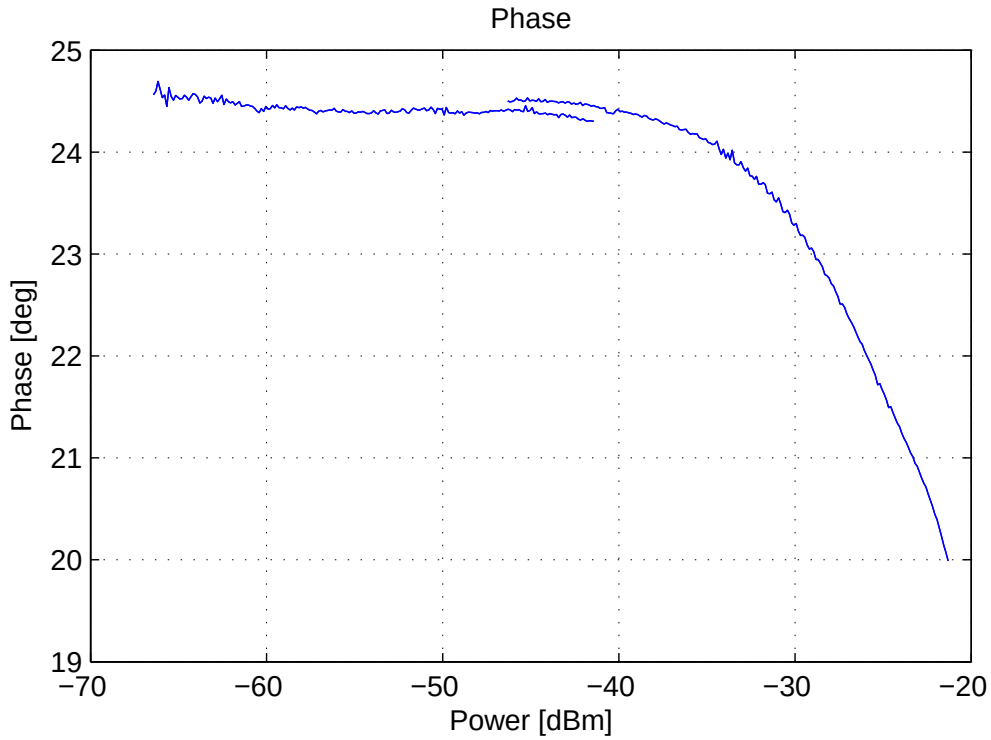

Figure 2.29: Phase shift of the amplifier in the function of the input power.

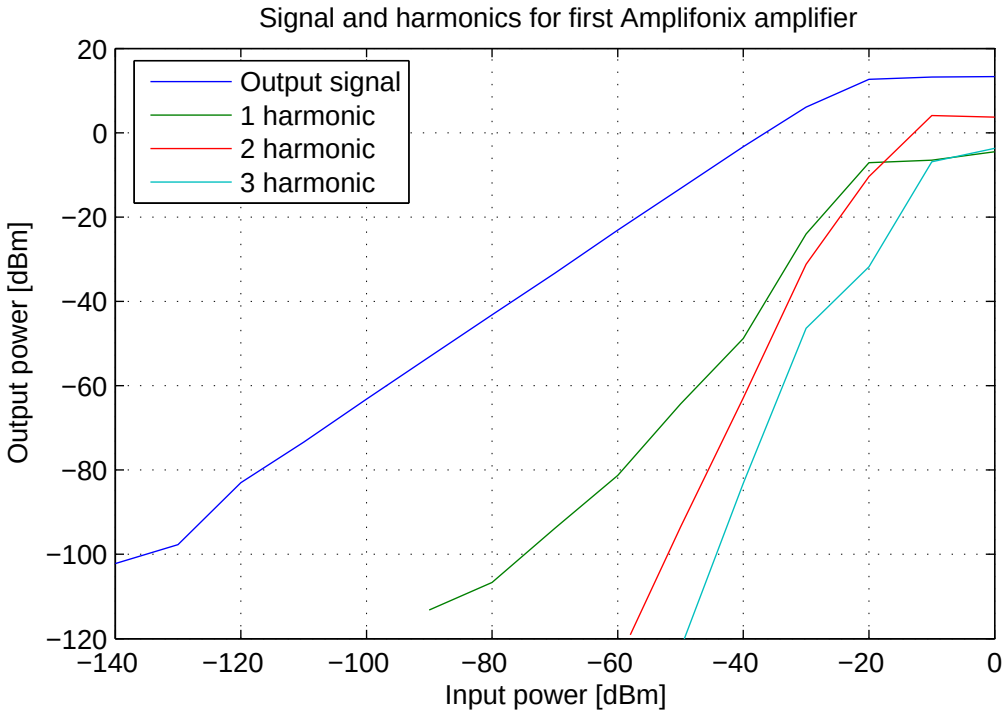

Figure 2.30: Harmonics of the amplifier.

transmission line with the digitally controlled relays. In addition to get smaller gain steps, the variable attenuators are installed in front of the amplifiers. These attenuators are digitally controlled with 5 dB minimum step and 35 dB maximum attenuation. Therefore the gain can be controlled from 0 dB to 80 dB with 5 dB step. In order to have the low noise amplifier, the amplifiers with $NF = 0.24\ dB$ [50](**N**oise **F**igure) are used in the presented circuit.

The reason to install the attenuators in front of the amplifiers is to keep a power level of the input signals out of the amplifiers saturation range. The maximum input power of the amplifiers can be found on a basis of the amplifiers measurement presented in Figure 2.29. This power equals -40 dBm, for the higher input powers, the amplifiers phase shifts are changing due to amplitude to phase modulation. In order to keep these phase shifts fixed, the input power should not exceed -40 dBm.

The two attenuators are used instead of the one in front of the first amplifier to get a better signal to noise ratio. A single attenuator installed in front of the first amplifier would reduce the input signal power too much. Therefore it is better to use a second attenuator which attenuates an already amplified signal by the first amplifier. In this case the attenuated signal has higher power then in the case where only the one attenuator is used. As a result the signal that has the higher power is larger then the noise and has a better signal to noise ratio.

The amplifiers have harmonics presented in Figure 2.30. In order to reduce the influence of the harmonics it is necessary to use a bandpass filter. In addition, a bandpass filter reduces also the noise in the measured signal and works as an antialiazing filter in front of an oscilloscope. The bandwidth of this filter was chosen to 780 MHz, because it was the highest bandwidth of the bandpass filter at 1.3 GHz center frequency available commercially from RLC electronics company. The filter with this bandwidth removes the amplifier output harmonics, increases a signal noise level and also works as an antialiazing filter.

2.4 Downconversion techniques

An output signal from the filter and the cavity is an RF signal with a carrier frequency at 1.3 GHz. These signals have to be downconverted before the measurement and comparison. The new emerging technology in the downconversion is a digital downconversion - the signal with a carrier is digitized by an ADC and later digitally downconverted. This is in the contrary to an analog method where already downconverted signal by an analog components is digitized. The single bunch induced transient detection system uses the method with the digital downconversion.

In addition a new low noise downconversion method was tested during the development of the single bunch induced transient detection system. This method is based on the "Law of cosines" [47, 23].

2.4.1 RF signal vector detector based on the "Law of cosines"

The first tests with the single bunch induced transient detection were unsuccessful. Only noise was detectable at the output of the system. During these tests an analog IQ demodulator was used as a device for downconverting 1.3 GHz signal. To reduce the noise level, the low noise method for a phase and an amplitude detection was developed. This method is based on the "Law of cosines" [47, 23].

The concept is based on measuring the amplitudes of four signals: the $\vec{V}_{LO'}$, $\vec{V}_{RF'}$, $\vec{V}_{SQ}$, $\vec{V}_{SI}$ (Figure 2.31). The signals $\vec{V}_{SQ}$ (2.30) and $\vec{V}_{SI}$ (2.31) are sums of the LO and RF signals. The sum operation is performed in a microwave circuit with combiners. The amplitude detection is made with amplitude detectors based on the Schottky diode. It is possible to calculate a real and an imaginary parts of the $\vec{V}_{RF}$ vector (2.32)(2.33) from the amplitudes of the four mentioned earlier signals on the basis of the "Law of cosines".

Output sum vectors:

$$\vec{V}_{SQ} = \vec{V}_{LO} \cdot e^{i\frac{\pi}{2}} + \vec{V}_{RF} \tag{2.30}$$

$$\vec{V}_{SI} = \vec{V}_{LO} + \vec{V}_{RF} \tag{2.31}$$

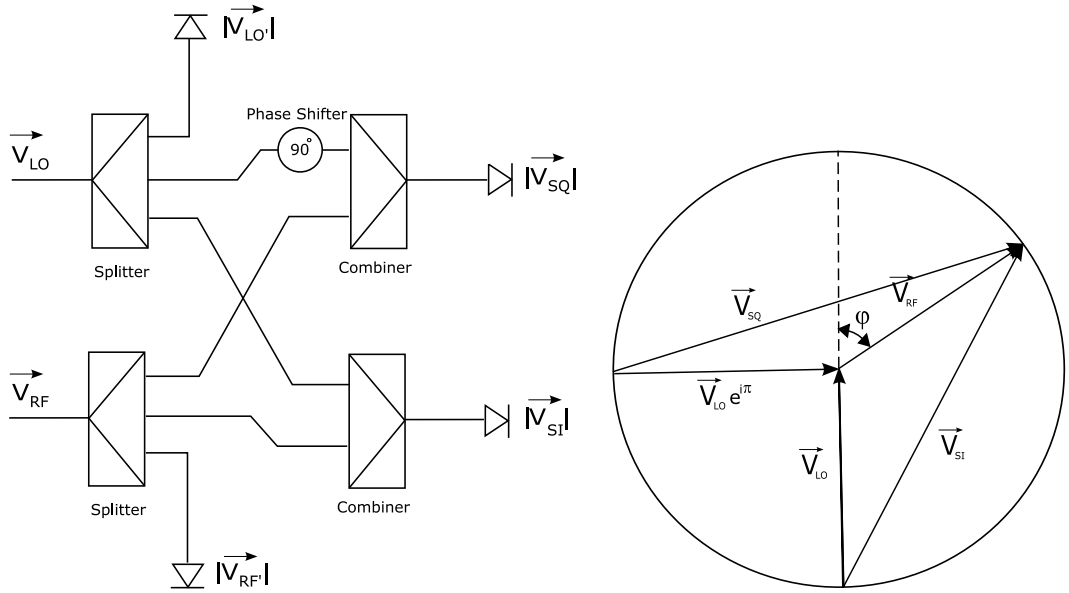

Figure 2.31: Phase detector based on the "Law of cosines": $\vec{V}_{LO}$ - 1.3GHz local oscillator signal; $\vec{V}_{RF}$ - 1.3GHz RF signal; $\left|\vec{V}_{LO'}\right|$ - amplitude of the LO signal; $\left|\vec{V}_{RF'}\right|$ - amplitude of RF signal; $\left|\vec{V}_{SQ}\right|$ - amplitude of sum quadrature; $\left|\vec{V}_{SI}\right|$ - amplitude of sum inphase.

Real and imaginary parts of $\vec{V}_{RF}$ vector:

$$Im\left(\vec{V}_{RF}\right) = \left|\vec{V}_{RF}\right| \sin(\varphi) = \frac{\left|\vec{V}_{SQ}\right|^2 - \left|\vec{V}_{LO}\right|^2 - \left|\vec{V}_{RF}\right|^2}{2\left|\vec{V}_{LO}\right|} \tag{2.32}$$

$$Re\left(\vec{V}_{RF}\right) = \left|\vec{V}_{RF}\right| \cos(\varphi) = \frac{\left|\vec{V}_{SI}\right|^2 - \left|\vec{V}_{LO}\right|^2 - \left|\vec{V}_{RF}\right|^2}{2\left|\vec{V}_{LO}\right|} \tag{2.33}$$

The presented method was tested and used during the first successful measurement of the single bunch induced transients on 17th of January 2005 (Section 4.1). It was the first time that the transients were visible and that they were larger then noise. The measured beam phase during this test was correct.

Unfortunately this phase detector has some disadvantages. It has high phase nonlinearities (Figure 2.32). Moreover it is required to use four ADC's or four oscilloscope channels to measure a real and an imaginary parts of the single signal. Because of

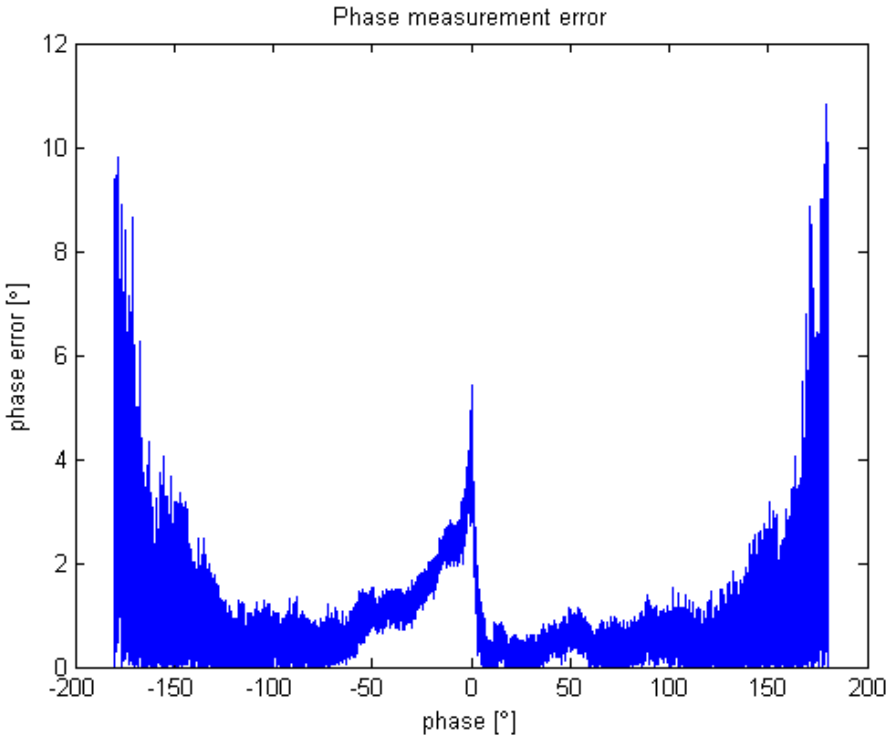

Figure 2.32: Phase measurement error.

these reasons, the phase detector based on the "Law of cosines" is not used in the transient detection system.

2.4.2 Digital downconversion

A digital downconversion is an alternative to the analog downconversion [25, 21, 32, 33, 44]. The digital downconversion, samples directly the RF signal with a carrier or a signal with an intermediate frequency. The samples are digitally multiplied by a complex oscillator and filtered by a digital low pass filter. The results of these operations are a real and an imaginary parts of the input signal. This method is currently extensively used in the wireless and wireline communication systems. The advantages of it over the analog IQ demodulation are:

- The downconversion errors are smaller. Digitizing the RF signals directly, reduces analog components installed in front of ADC. As a result, errors caused by analog parts are reduced.

- Digital processing does not change with temperature and time. Whereas parameters of analog parts change with time and temperature. Moreover digital processing can be fixed and copied in an identical form.
- The digital downconversion is more flexible. The downconversion and filtering done digitally can be easily modified by reprogramming while changing parameters of analog parts require modification in a circuitry.

The single bunch induced transient detection system downconverts 1.3 GHz signals using the digital downconversion. The concept used in the system is presented in Figure 2.33. The two RF signals and 1.3 GHz local oscillator are sampled at 5 GS/s by the LeCroy WaveRunner 6100A oscilloscope.

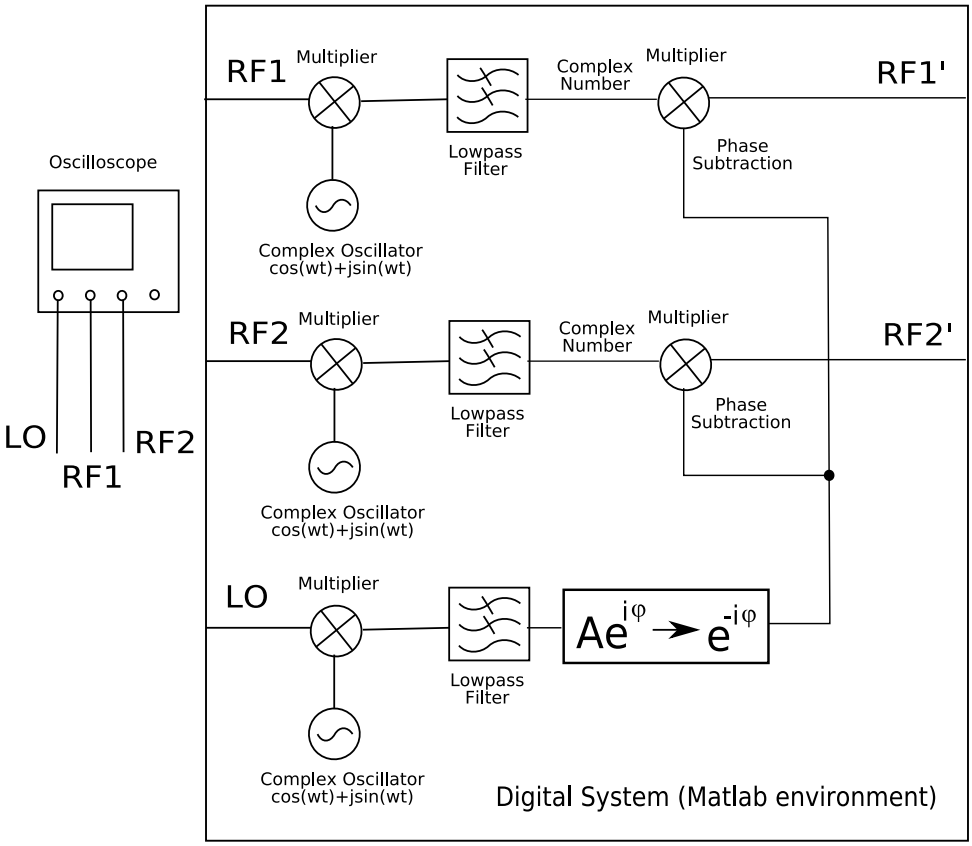

Figure 2.33: Digital downconversion.

The samples of 1.3 GHz signals are captured by the oscilloscope controlled by a Matlab script. The communication between the oscilloscope and the script is done through the LeCroy oscilloscope COM interface [46]. All the calculations are performed in the Matlab environment. The data captured by the oscilloscope is mul-

tiplied by a complex oscillator (2.34) ($\omega = 2\pi \cdot 1.3\ G\frac{rad}{s}$). The result of the multiplication of the two 1.3 GHz sines are a DC signal and 2.4 GHz signal. 2.4 GHz signal is an image of 2.6 GHz sine for a data sampled at 5 GS/s. The complex representation of the RF signals is at DC, 2.4 GHz sine has to be filtered. The first order 400 MHz lowpass Butterworth digital filter is used to filter 2.4 GHz sine and to reduce signal noise. The result is a complex representation of the signal where the phase is calculated with respect to the complex oscillator.

The phases of the vectors have to be calculated with respect to the local oscillator. The local oscillator phase is subtracted from the vectors to get the complex representation of the RF signals calculated with respect to the local oscillator.

$$CO = \cos(\omega t) + j\sin(\omega t) \tag{2.34}$$

The presented algorithm was tested successfully and is currently used in the system. The one of the advantages of this method is a phase and an amplitude linearity which is better then in analog IQ demodulators and in the phase detector based on the "Law of cosines". The disadvantage is a noise level of the signal. The high frequency signals sampled by ADC have a high noise due to the sampling clock jitter [27]. However in this application a noise level of the input signal is higher then the ADC noise. Therefore the oscilloscope noise does not degrade the signal.

2.5 Control system for transient detection

The main part in the control system is the LeCroy WaveRunner 6100A oscilloscope. All the parts in the system are controlled by the Matlab script [24] which runs on this oscilloscope. The responsibility of it are: a signal downconversion and filtering, a calculation of transient amplitude and beam phase, a control of the oscilloscope, a filter, a variable gain amplifier and a signal distribution board.

The Matlab script is controlling all the parts except the oscilloscope in the system by reading and writing to DOOCS variables (**D**istributed **O**bject **O**riented **C**ontrol **S**ystem) [13]. The oscilloscope controls itself through COM (**C**omponent **O**bject **M**odel) interface. This communication is done through the Matlab DOOCS interface [17]. All the components in FLASH are also controlled by DOOCS.

DOOCS is an object oriented system designed from a device server level up to an operator console. The system is written in C++ and runs on different operating systems including the Sun SPARC workstations under Solaris and SunOS and PC's with the LINUX operating system. The communication is performed through ONC RPC (**O**pen **N**etwork **C**omputing **R**emote **P**rocedure **C**all).

The single bunch induced transient detection system uses three DOOCS servers. The two standard servers that control DAC and the digital IO modules: ipdac08_server and ipdigi_server (appendix A.2.2, appendix A.2.3). The one special server rftransient_server (appendix A.2.1) for the transient detection, which stores measurement results and data required for the system control. Their locations in ENS (**E**quipment **N**ame **S**erver) [15] are following. ipdac08_server - server for the DAC module control. Its location is TTF2.EXP\BITD.DAC\INJECTOR. ipdigi_server - server for the digital IO module control. Its location is TTF2.EXP\BITD.DIO\INJECTOR. rftransient_server has location TTF2.EXP\BITD.DATA\INJECTOR.

As operators interface the "ddd" (**D**OOCS **D**ata **D**isplay) program is used. The "ddd" is a graphical editor for creating and running control panels. The "ddd" creates component libraries in a hierarchical way. The displays have graphics that show a status of devices. Single mouse click can invoke subwindows with detailed information or plots.

The five "ddd" panels are used for the single bunch induced transient detection system control (figure 2.34, appendix A.1). The main panel "Single Bunch Induced Transient Detection" is used for observing the measurement results. The filter is controlled using the "Beam induced transient detection filter" panel. The filter and amplifier calibration is made using the "RF Filter Calibration window" panel. The IQ modulator calibration is performed using the "IQ modulator calibration" panel. The variable gain amplifier is controlled by the "BITDAmplifier" panel.

The digital IO module controls all the relays in the system. It switches the input signal in the signal distribution board from a cavity probe to LO. It connects and disconnects the delay line in the filter and sets the IQ modulator in the filter for the normal operation or calibration. It sets a gain and an attenuation in the variable gain amplifier. The DAC converter module sets driving voltages for the I and Q inputs of the IQ modulator.

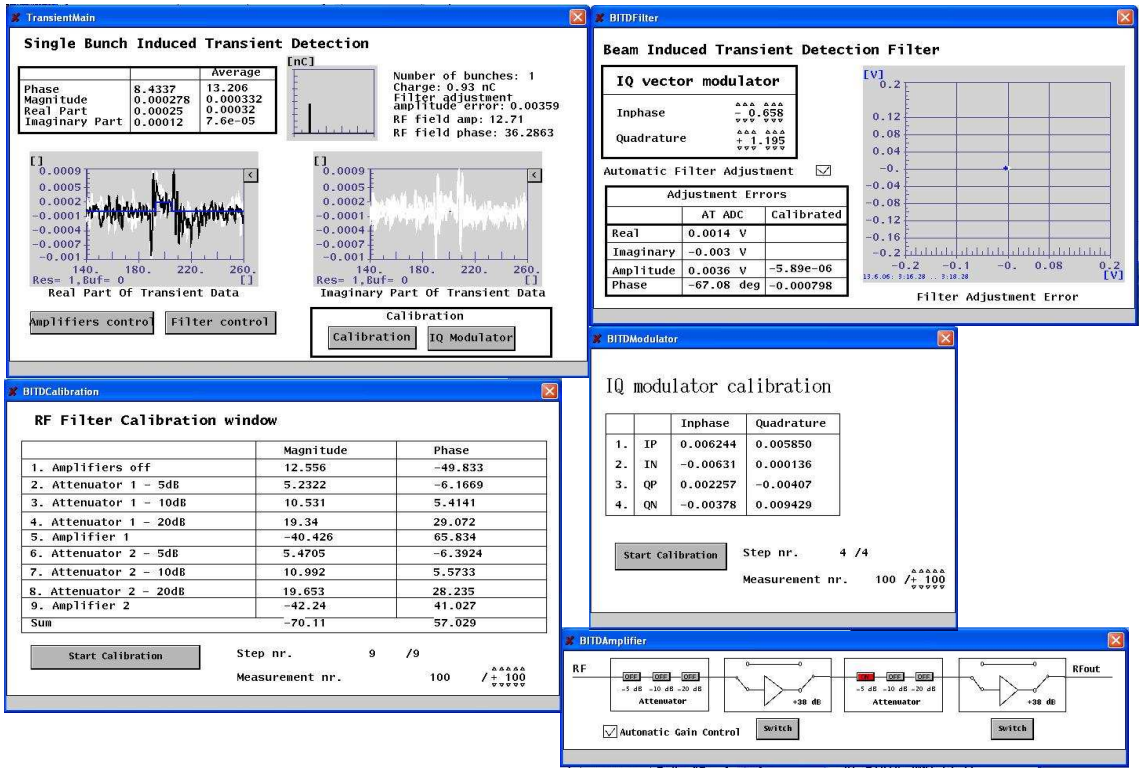

Figure 2.34: DOOCS graphical user interface panels.

The Matlab script also controls the oscilloscope and takes data from it. The communication between this script and the LeCroy oscilloscope is performed through the LeCroy Automation COM interface [46].

The script starts by initiating the oscilloscope and reading variables from DOOCS servers. Then it runs in a loop. The loop reads the DOOCS variables, checks whether it should run the calibration, takes data from the oscilloscope, performs calculations and writes results to the DOOCS variables. All the algorithms are performed automatically by the Matlab script. In particular: the calibration for measuring calibration factors, the automatic gain control, the automatic filter adjustment and the transient measurement.

2.6 Estimates of measurement accuracy

A measurement accuracy depends on measurement errors [43, 41, 51, 49]. Main experimental errors can be divided into two categories: stochastic and systematic errors.

The stochastic errors are the differences between measurements when the same value is measured with the device calibrated in the same way. These errors are often called the measurement noise. This type of errors can be reduced with averaging. The systematic errors are the errors that can arise from an incorrect calibration or from a broken device. These type of errors are constant from a measurement to measurement and can not be reduced by averaging.

The stochastic errors for a large number of measurements in statistics is normally modelled as a normal distribution. The mean value for the infinite measurements is the real value. The standard deviation is the maximum error for 68% of the measurements.

The percentage of measurements which are smaller then the measurement error is called the confidence interval. The measurement error in this case is called the confidence limit. It means that for 100 measurements with 2 % confidence limit and 95 % confidence interval, 95 of them will have the measurement error below 2 % confidence limit.

In real experiments the number of measurements is limited. For the limited number of measurements, better distribution then the normal is a student distribution. The confidence limits are calculated by multiplying the σ standard deviation by the t_{kp} factor, which depends on the confidence interval, a number of samples and is available in tables. For example the $t_{kp} = 1.6604$ for 95 % confidence interval and 100 samples.

The confidence limit for single measurement:

$$\Delta x = t_{kp} \cdot \sigma \tag{2.35}$$

Where:
Δx - confidence limit
t_{kp} - value from table, dependent on confidence interval and number of samples

σ - standard deviation

The confidence limit for an average:

$$\Delta x = t_{kp} \cdot \sigma_{av} = \frac{t_{kp}}{\sqrt{N}}\sigma \tag{2.36}$$

Where:
σ_{av} - the standard deviation of averaged samples
N - number of samples

The single bunch induced transient detection measures the transient vector. This vector is calculated according to the formula (2.37).

$$\vec{V}_{TC} = \vec{V}_T \cdot \vec{F}_C \tag{2.37}$$

Where:
$\vec{V}_{TC}$ - calibrated transient value
$\vec{V}_T$ - not calibrated transient value
$\vec{F}_C$ - calibration factor

The amplitude and phase transient measurement confidence limits calculated on the basis of the formula (2.37) are presented in the equations (2.38) and (2.39).

$$\delta_{TC} = \delta_{T0}\frac{q_0}{q}\frac{1}{\sqrt{N}} + \delta_C \tag{2.38}$$

Where:
$\delta_{TC} = \frac{\Delta A_{TC}}{A_{TC}}$ - relative calibrated transient amplitude confidence limit
$\delta_{T0} = \frac{\Delta A_{T0}}{A_{T0}}$ - relative not calibrated transient amplitude confidence limit for single bunch transient with the q_0 charge (stochastic error)
$q_0 = 1\ nC$ - reference charge
q - actual single bunch charge
$\delta_C = \frac{\Delta A_C}{A_C}$ - relative calibration factor amplitude confidence limit (systematic error)

N - number of samples when the result is averaged, the $N = 1$ when measured without averaging

$$\Delta\varphi_{TC} = \Delta\varphi_{T0}\frac{q_0}{q}\frac{1}{\sqrt{N}} + \Delta\varphi_C \tag{2.39}$$

Where:
$\Delta\varphi_{TC}$ - absolute calibrated transient phase confidence limit
$\Delta\varphi_{T0}$ - absolute not calibrated transient phase confidence limit for single bunch transient with q_0 charge (stochastic error)
$\Delta\varphi_C$ - absolute calibration factor phase confidence limit (systematic error)

The single bunch induced transient detection system accuracy can be estimated using the equations (2.38), (2.39) and some assumptions. The confidence interval in the student distribution equals 95 %. The Single transient measurement confidence limit is 3.3° in a phase and 6.5 % in an amplitude for 0.96 nC single bunch charge and 12.4 MV/m EFS amplitude (the assumptions based on the measurements presented in Section 4.10). The calibration factor measurement confidence limits are 0.3 % in an amplitude and 0.4° in a phase (the assumptions based on the calibration confidence limits measured in Section 3.1).

$$\delta_{TC} = 6.5\ \%\frac{0.96\ nC}{q}\frac{1}{\sqrt{N}} + 0.3\ \% \tag{2.40}$$

$$\Delta\varphi_{TC} = 3.3^\circ\frac{0.96\ nC}{q}\frac{1}{\sqrt{N}} + 0.4^\circ \tag{2.41}$$

From the equations (2.40) and (2.41) one can conclude that the measurement confidence limits of 0.96 nC single bunch transient measurement for 12.4 MV/m EFS amplitude are 6.8 % in an amplitude and 3.7° in a phase for 95 % confidence interval. The measurement accuracy is increased when the measured data is averaged or when the beam charge is increased. The same confidence limits for an average over 100 samples equal 0.95 % in an amplitude and 0.73° in a phase.

2.7 Conclusions

The developed system for single bunch induced transient detection consists of microwave parts, a control system and an oscilloscope. The microwave parts are responsible for a signal downconversion. The control system controls the microwave parts and stores data in DOOCS servers (**D**istributed **O**bject **O**riented **C**ontrol **S**ystem). The oscilloscope's duty is a signal downconversion, calculations and a control of the whole system. Three versions of the system were developed.

The microwave parts used in the system consist of: a signal distribution board, an RF feedforward comb filter and a variable gain amplifier. The signal distribution board's duty is to deliver probe and master oscillator signals to the oscilloscope and to the filter. The RF feedforward comb filter is the most critical part in the system and is responsible for attenuating a 1.3 GHz carrier signal while leaving the single bunch induced transients not attenuated. The variable gain amplifier amplifies the output of the filter and delivers the signal to the oscilloscope.

The RF feedforward comb filter frequency response is accurately modelled by symbolic equations. The model takes into account attenuation of the filter, a delay line cable, a splitter and a combiner. It also shows the behavior of the filter for different amplitude and phase adjustment errors. The modelled response accurately conforms measurements. On the basis of the model it is easy to find a frequency response of the filter for different cable attenuations, delay of the delay line and filter adjustment errors. Allowed maximum filter adjustment errors calculated using the model for 100 dB attenuation equal 0.001° in a phase and $2 \cdot 10^{-5}\ \frac{V}{V}$ in an amplitude.

The requirements on the filter adjustment accuracy make this part the most critical part in the system. A development of its implementation is very challenging. The filter is very sensitive to temperature fluctuations. The required amplitude and phase adjustment accuracies are very high (0.001° in a phase and $2 \cdot 10^{-5}\ \frac{V}{V}$ in an amplitude). The necessary temperature stability is relaxed by special filter implementation with fine-tuning, capable to easily compensate small phase shifts and attenuation changes caused by temperature changes in the filter. The idea is based on summing of two signals: one large used for rough adjustment and one very small used for fine-tuning. In addition the filter is roughly stabilized thermally to keep the filter attenuation and the phase shift changes in the working range of the fine-tuning circuitry.

The signal from a cavity probe and the amplified output of the RF filter are accurately downconverted using a digital downconversion. The signals are directly digitized with a 1.3 GHz carrier by an oscilloscope at 10 GS/s. The captured signals are digitally downconverted in a Matlab environment.

The whole transient detection system is controlled by a Matlab script running on the oscilloscope. The script is controlling the digital IO module and the DAC module by writing and reading variables in the DOOCS servers. These modules control directly analog parts in the system. Moreover the script controls the oscilloscope through COM interface. An operator can control the transient detection system using the "ddd" (**D**OOCS **D**ata **D**isplay) graphical user interface.

The estimated maximum filter measurement confidence limits for 0.96 nC single bunch induced transient in EFS with the amplitude 12.4 MV/m are 6.8 % in an amplitude and 3.7° in a phase for 95 % confidence interval. The measurement accuracy for the same conditions and an average over 100 samples equal 0.95 % in an amplitude and 0.73° in a phase.

CHAPTER 3

Modes of operation and algorithms

3.1 Filter and amplifier calibration

The goal of single bunch induced transient detection is to measure a transient phase with respect to RF EFS in a cavity and a transient amplitude compared to an EFS amplitude. This can be performed by dividing a transient vector (RF2) by an RF field vector (RF1). These vectors are measured separately by different oscilloscope channels (Figure 2.1).

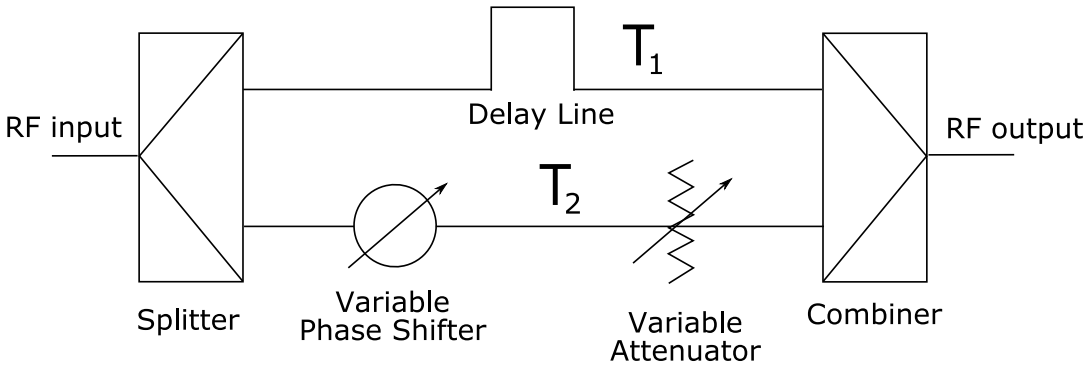

Figure 3.1: RF feedforward comb filter.

Before downconverting a signal from the cavity is splitted into two (Figure 2.1). One of them is connected directly to the oscilloscope (RF1 - the RF EFS signal) and other one is connected to a feedforward comb filter, variable gain amplifier and then to the oscilloscope (RF2 - the transient signal). Both signals are transmitted through lines with different transmittances. In order to compare them it is necessary to perform a calibration which measures transmittance differences between two different paths of these signals.

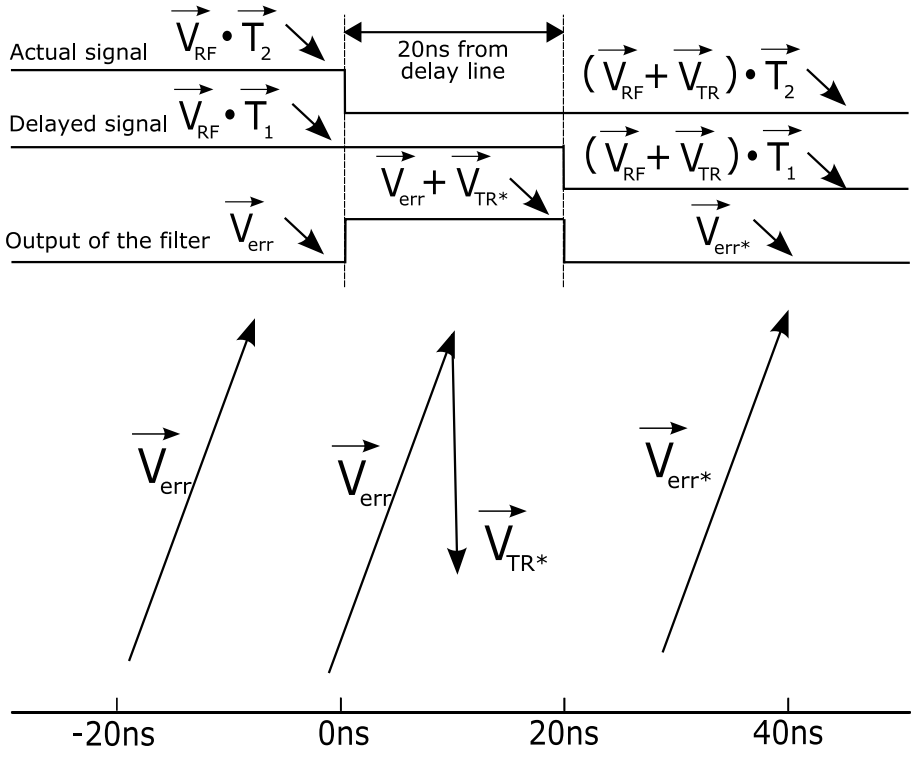

Figure 3.2: Vector analysis of a filter output.

During the calibration an input signal to the system is changed from a cavity probe to a master oscillator. It is done by switching a relay in the signal distribution board. The calibration is performed by measuring vectors at the input of channel 2 (RF1) and 3 (RF2) of the oscilloscope (Figure 2.1). To measure RF2 signal it is necessary to disconnect the delay line in the filter, otherwise it would attenuate the signal and simply zero would be measured during the procedure.

$$\vec{V}_{err} = \vec{V}_{RF} \cdot \left(\vec{T}_2 + \vec{T}_1\right) \tag{3.1}$$

$$\vec{V}_{TR*} = \vec{V}_{TR} \cdot \vec{T}_2 \tag{3.2}$$

$$\vec{V}_{err*} = \left(\vec{V}_{RF} + \vec{V}_{TR}\right) \cdot \left(\vec{T}_2 + \vec{T}_1\right) \approx \vec{V}_{err} \tag{3.3}$$

The delay line in the feedforward comb filter can be disconnected during the calibration because its transmittance does not influence a transient vector $\vec{V}_{TR*}$, it influences only a filter adjustment error vector $\vec{V}_{err}$. It can be seen in a vector analysis in Figure 3.1, Figure 3.2 and equations (3.1), (3.2), (3.3). The transient vector is only influenced by a transmittance $\vec{T}_2$ of the line with the variable phase shifter and variable attenuator inside the filter (Figure 3.1) - the line with a shorter delay. It is a result of the sum of an actual signal with a transient and a delayed signal without the transient. An actual signal with the transient is only changed by the $\vec{T}_2$ transmittance.

$$\vec{F}_1 = \frac{\vec{V}_{RF1}}{\vec{V}_{RF2}} \tag{3.4}$$

The calibration procedure of the filter and variable gain amplifier is performed with a disconnected filter delay line. It is composed of 9 steps. Each step is performed by measuring the vectors RF1 and RF2 at the input of channel 2 and 3 of the oscilloscope respectively. Each step is measured a number of times set by a user and the result is an average of all measurements performed for a single step.

Each step measures a different calibration factor:

1. Amplifiers off - $\vec{F}_1 = \vec{F}_{no\_gain}$
2. Attenuator 1, 5 dB - $\vec{F}_2 = \vec{F}_{att1\_5dB}$
3. Attenuator 1, 10 dB - $\vec{F}_3 = \vec{F}_{att1\_10dB}$
4. Attenuator 1, 20 dB - $\vec{F}_4 = \vec{F}_{att1\_20dB}$
5. Amplifier 1 - $\vec{F}_5 = \vec{F}_{amp1}$
6. Attenuator 2, 5 dB - $\vec{F}_6 = \vec{F}_{att2\_5dB}$

7. Attenuator 2, 10 dB - $\vec{F}_7 = \vec{F}_{att2\_10dB}$
8. Attenuator 2, 20 dB - $\vec{F}_8 = \vec{F}_{att2\_20dB}$
9. Amplifier 2 - $\vec{F}_9 = \vec{F}_{amp2}$

The calibration factor in the step 1 is calculated by dividing the vector RF1 by RF2 (3.4). The step 1 measures the calibration factor for the case where amplifiers gain and attenuation is turned off. The steps from 2 to 4 and 6 to 9 measure a change of the calibration factor caused by turning on one of attenuations. They are calculated by dividing the calibration factor measured in the same way as in the step 1 by the F_{no_gain} factor (3.5).

$$\vec{F}_{2,3,4,6,7,8} = \frac{\vec{V}_{RF1}}{\vec{V}_{RF2}} \cdot \frac{1}{\vec{F}_{no\_gain}} \tag{3.5}$$

In a case of step 5 and 9 when the amplifiers are calibrated these factors are measured and calculated slightly differently. To keep an input signal of the amplifiers out of a saturation range their input attenuators are set to 35 dB attenuation. The factors for these cases are calculated as in (3.6).

$$\vec{F}_{5,9} = \frac{\vec{V}_{RF1}}{\vec{V}_{RF2}} \cdot \frac{1}{\vec{F}_{no\_gain} \cdot \vec{F}_{attx\_5dB} \cdot \vec{F}_{attx\_10dB} \cdot \vec{F}_{attx\_20dB}} \tag{3.6}$$

Where:

x=1 for amplifier 1

x=2 for amplifier 2

All factors are stored in an rftransient_server DOOCS server (appendix A.2.1) as two values, an amplitude in dB and a phase in degrees. During the transient detection they are used in the transient vector calculation. A measured transient vector divided by an RF EFS vector is multiplied by calibration factors. It is multiplied by $\vec{F}_{no\_gain}$ and calibration factors of the variable gain amplifier parts that are currently turned on.

$$\vec{F}_c = \vec{F}_{no\_gain} \cdot \vec{F}_{att2\_5dB} \cdot \vec{F}_{amp1} \cdot \vec{F}_{amp2} \tag{3.7}$$

$$\frac{\Delta A}{A} = \pm 0.3\ \% \tag{3.8}$$

$$\Delta\varphi = \pm 0.4^\circ \tag{3.9}$$

The presented algorithm for the calibration is implemented and used. In order to find out how accurate the procedure is, 46 calibration measurements have been performed. The 46 samples of the measured calibration factor $\vec{F}_c$ (3.7) were used for the calculation of amplitude and phase confidence limits (Figure 3.3). A student distribution with 95% confidence interval was used during the calculations. The results are presented in equations (3.8), (3.9) and in Figure 3.3.

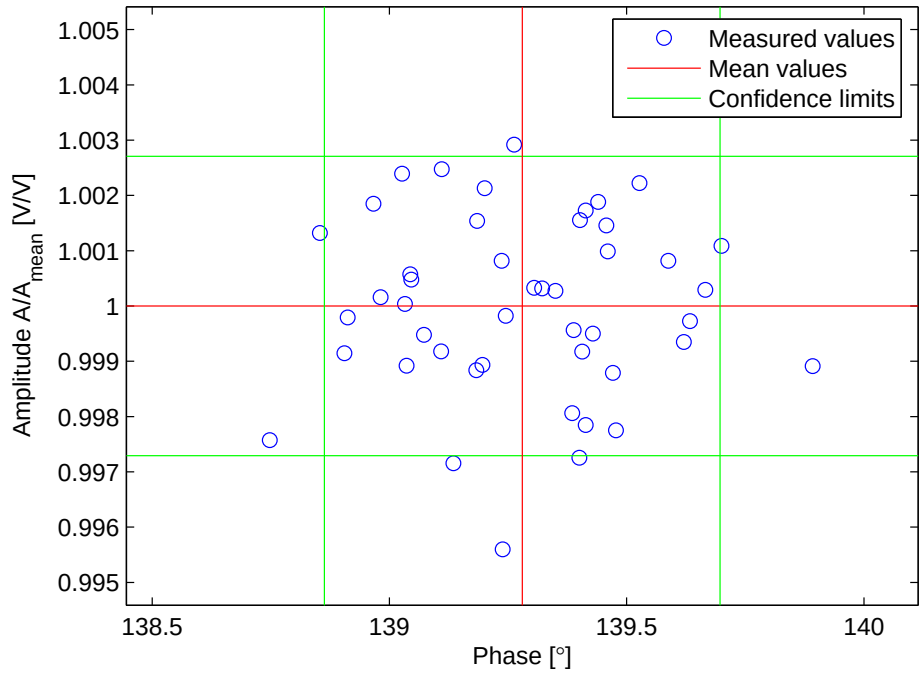

Figure 3.3: Amplitude and phase confidence limits of a calibration factor (95% confidence interval, N=46 samples).

3.2 Automatic filter adjustment

The feedforward comb filter used in a single bunch induced transient detection system has to be very precisely adjusted. The adjustment has to be performed whenever the filter is modified and also whenever filter phase shifts and attenuations are changed. As the required precision is very high these parameters fluctuate even with small temperature changes. To keep the filter adjusted with required precision it is necessary to constantly change its phase and attenuation.

The first implementation of the filter used a mechanical attenuator and mechanical phase shifter for this procedure. Adjusting a phase and amplitude with required precision was at that time very difficult. To easy the task an implementation with a fine-tuning circuitry was developed. The implementation uses an IQ modulator for fine-tuning. This device is controlled by DAC. To easy the task of an adjustment and to make continuous compensation of temperature change a special procedure was developed.

3.2.1 Calibration

To adjust the filter automatically it is necessary to find how Inphase and Quadrature inputs of the IQ modulator have to be changed to minimize filter adjustment errors. This is a mainly a problem of changing one coordinate system into another one. The first coordinate system is a complex space which shows a measured error vector. The second coordinate system is a complex space of Inphase and Quadrature voltages that drive the IQ modulator and control the filter adjustment error vector.

Before starting an automatic filter adjustment algorithm it is necessary to calibrate the IQ modulator. The calibration measures how changes of the IQ modulator inputs change a vector measured by the oscilloscope. During the calibration the delay line in the filter and the parallel line to the IQ modulator are disconnected using relays (Figure 2.24). When they are disconnected the oscilloscope measures only an output of the modulator.

The calibration consists of 4 steps. Every step is a measurement of the IQ modulator output for different input voltages controlled by DAC. The first two steps measure an output for 0 V at the quadrature input, +5 V and -5 V for respectively IP and

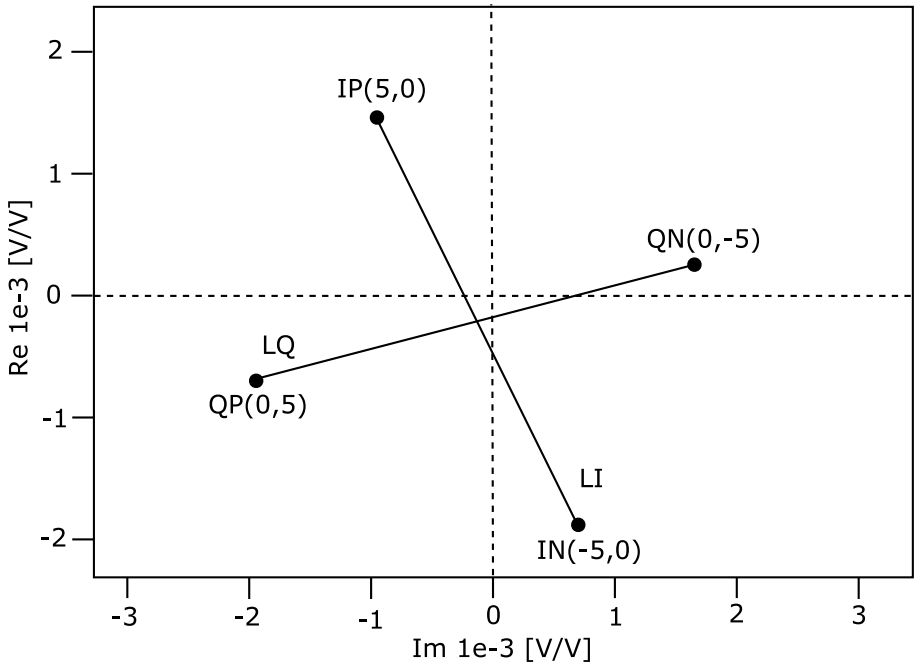

Figure 3.4: Calibration.

IN at the inphase input. The following two steps measure an output for 0 V at the inphase input, +5 V and -5 V for respectively QP and QN at the quadrature input (Figure 3.4). The measurement is performed with both amplifiers, 10 dB and 20 dB attenuations in second attenuator of the variable gain amplifier turned on. The measured vector for every step is calculated using the formula (3.10), the factors used in this formula are measured during the filter and amplifier calibration. Every step is repeated a number of times, which is set by a user. Averages of the measured calibration factors are saved to DOOCS variables (appendix A.2.1).

$$\vec{F}_{mod} = \frac{\vec{V}_{RF2}}{\vec{V}_{RF1}} \cdot \vec{F}_{no\_gain} \cdot \vec{F}_{amp1} \cdot \vec{F}_{amp2} \cdot \vec{F}_{att2\_10dB} \cdot \vec{F}_{att2\_20dB} \tag{3.10}$$

The next step in the calibration is a calculation of factors of lines, which connect the measured points. The lines can be expressed as in (3.11). The most important parameter in the equation is "a" factor.

$$y = a \cdot x + b \tag{3.11}$$

The factors for LI line that connects two points IP with IN presented in Figure 3.4

are calculated in the following way:

$$a_I = \frac{Im\{IP\} - Im\{IN\}}{Re\{IP\} - Re\{IN\}} \tag{3.12}$$

$$b_I = Im\{IN\} - a_I \cdot Re\{IN\} \tag{3.13}$$

The factors for the that connects two points QP with QN presented in Figure 3.4 are calculated in the following way:

$$a_Q = \frac{Im\{QP\} - Im\{QN\}}{Re\{QP\} - Re\{QN\}} \tag{3.14}$$

$$b_Q = Im\{QN\} - a_Q \cdot Re\{QN\} \tag{3.15}$$

The IQ modulator calibration is required for the automatic filter adjustment algorithm to work.

3.2.2 Feedback

The idea behind the feedback algorithm is presented in Figure 3.5. The filter adjustment error vector is presented as $P1$. $P3$ is an optimal filter adjustment where the filter adjustment error vector equals zero.

The line LI calculated during the calibration is fitted to the $P1$ point. The parameters of the fitted line LI to the $P1$ point are presented in (3.16), (3.17).

$$b_{LI} = Im\{P1\} - a_I \cdot Re\{P1\} \tag{3.16}$$

$$a_{LI} = a_I \tag{3.17}$$

The line LQ is fitted to the $P3$ point by setting the b factor to zero. The next step is to find the $P2$ point where the fitted lines LI and LQ cross. The point is calculated using equations (3.18) (3.19).

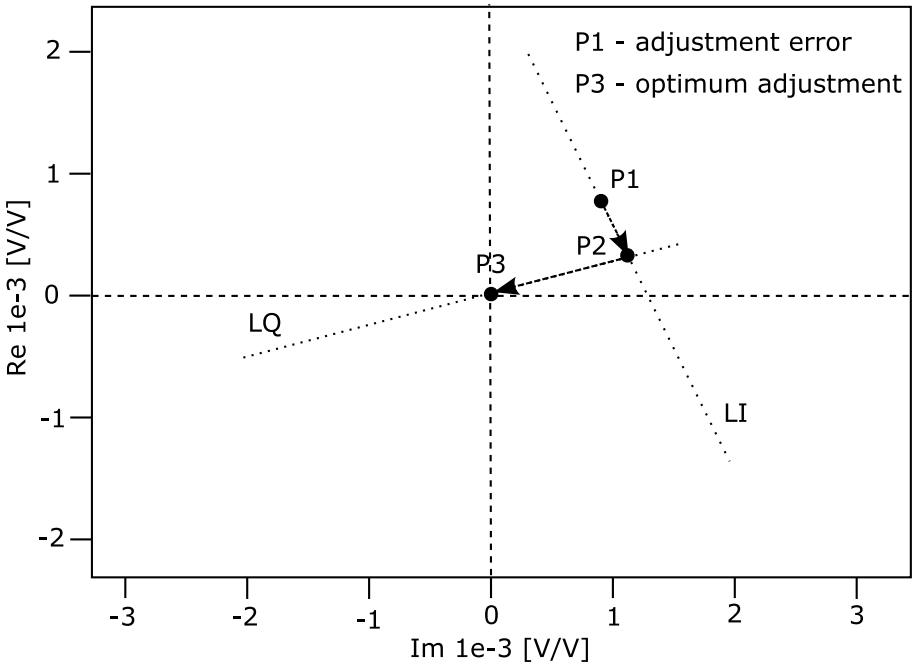

Figure 3.5: Filter adjustment.

$$Re\{P2\} = \frac{b_{LI}}{a_Q - a_I} \tag{3.18}$$

$$Im\{P2\} = a_I \cdot Re\{P2\} + b_I \tag{3.19}$$

When the $P2$ point is calculated, the distance from the point $P1$ to $P2$ gives a value that after scaling and setting a sign is used as the Inphase error at the input of the IQ modulator (3.20). The distance from the point $P2$ to $P3$ gives a value which after scaling and setting a sign is used as the Quadrature error at the input of the IQ modulator (3.21).

$$I_{err} = sqrt\left\{ \left(Im\left\{P2\right\} - Im\left\{P1\right\} \right)^2 + \left(Re\left\{P2\right\} - Re\left\{P1\right\} \right)^2 \right\} \cdot I_{scale} \cdot I_{sign} \tag{3.20}$$

$$Q_{err} = sqrt\Big\{ Im\{P2\}^2 + Re\{P2\}^2 \Big\} \cdot Q_{scale} \cdot Q_{sign} \tag{3.21}$$

A sign of I_{err} depends on the directions of the vectors from the point IN to IP and

from the point P1 to P2 (3.22). A sign of Q_{err} depends on the directions of the vectors from the point QN to QP and from the point P2 to P3 (3.23).

$$I_{sign} = sign\Big\{Re\{IP\} - Re\{IN\}\Big\} \cdot sign\Big\{Re\{P2\} - Re\{P1\}\Big\} \tag{3.22}$$

$$Q_{sign} = sign\Big\{Re\{QP\} - Re\{QN\}\Big\} \cdot sign\Big\{-Re\{P2\}\Big\} \tag{3.23}$$

Scaling of I_{err} is calculated on the basis of the distance between the point IP to IN and the difference of voltages applied during the calibration to the inphase input which is for the case 10V (3.24). Scaling of Q_{err} is calculated on the basis of the distance between the point QP to QN and the difference of voltages applied during the calibration to the quadrature input which is for the case 10V (3.25).

$$I_{scale} = \frac{10V}{sqrt\Big\{\Big(Im\{IP\} - Im\{IN\}\Big)^2 + \Big(Re\{IP\} - Re\{IN\}\Big)^2\Big\}} \tag{3.24}$$

$$Q_{scale} = \frac{10V}{sqrt\Big\{\Big(Im\{QP\} - Im\{QN\}\Big)^2 + \Big(Re\{QP\} - Re\{QN\}\Big)^2\Big\}} \tag{3.25}$$

I_{err} and Q_{err} are used for the calculation of new voltages at the inputs of the IQ modulator driven by the DAC IndustryPack module (3.26), (3.27).

$$I_{mod\_new} = I_{mod} + G \cdot I_{err} \tag{3.26}$$

$$Q_{mod\_new} = Q_{mod} + G \cdot Q_{err} \tag{3.27}$$

The G factor which is a gain was added to the feedback algorithm because of instabilities observed at high filter attenuations. For the reason G is a variable of an attenuation of the carrier by the feedforward comb filter (3.28) (where the L is an attenuation of the carrier by the filter):

$$G = \begin{cases} 1 & L \leq 70dB \\ 0.1 \quad for & 70dB < L \leq 80dB \\ 0.01 & 80dB < L \end{cases} \tag{3.28}$$

3.3 Measurement of transient vector

The goal of the single bunch induced transient detection system is to measure a transient vector with respect to RF EFS in the cavity. Amplified single bunch induced transients at the output of the feedforward comb filter look like pulses. An algorithm for the transient vector measurement calculates the transient vector from the pulses.

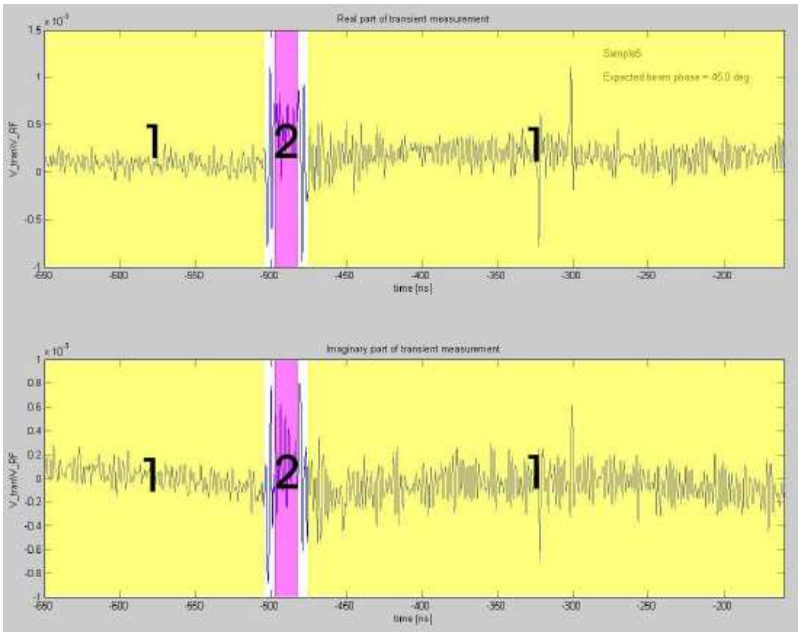

Figure 3.6: Real and imaginary parts of the single bunch induced transient.

A waveform with the transient captured and downconverted by the oscilloscope can be divided into two parts (Figure 3.6). The first one (number 1) is a filter adjustment error, the second one (number 2) is a sum of the filter adjustment error and the pulse that has information about the transient vector. In order to measure the pulse vector, the filter adjustment error vector has to be removed from the data. The two slightly different methods for the pulse measurement were implemented.

$$\vec{V}_{TR\_cal} = \frac{\vec{V}_{TR}}{\vec{V}_{RF}} \cdot \vec{F}_{no\_gain} \cdot e^{i\pi} \cdot \prod \vec{F}_i \tag{3.29}$$

Where:
$\vec{F}_i$ - calibration factors of all turned on parts in the variable gain amplifier
$e^{i\pi}$ - conversion from the transient phase to the beam phase

3.3.1 Polynomial fitting

The filter adjustment error in the data captured by the oscilloscope (number 1 in Figure 3.6) is slowly changing. It can be removed by fitting a 10-th order polynomial function to the data number 1 and subtracting the polynomial function from the data. Fitting and subtraction is performed for both real and imaginary parts of the captured data. It is done with "polyfit" matlab function.

The waveform after subtraction of the polynomial function is used for the transient measurement. The data number 2 in Figure 3.6 is averaged and the result is the single bunch induced transient vector. The vector is later multiplied by calibration factors and divided by the RF EFS vector measured by another oscilloscope channel to give the calibrated value of the transient vector (3.29).

3.3.2 Pulse integration

Another algorithm for the transient measurement uses a filter and an integrator. The filter adjustment error is removed by filtering the data with 8 MHz to 400 MHz 1-st order butterworth bandpass filter. The captured pulses (the data number 2 in Figure 3.6) with the filtered filter adjustment error is integrated. The integrated value is divided by a number of samples used during the integration. The calculated value is divided by the RF EFS vector and multiplied by the calibration factors to give a calibrated single bunch induced transient vector (3.29).

The reason for implementing this method was to test the concept for a low cost implementation of the single bunch induced transient detection system. The method would not require an expensive oscilloscope or a high sampling rate ADC instead it might use slow ADC's, IQ demodulators and integrators for downconversion.

3.3.3 Conclusions

Both methods for the transient measurement were implemented in a matlab script and tested. The results showed that they work correctly and give expected results. A smaller measurement noise was observed during measurements with the polynomial fitting method.

3.4 Conclusions

A correct single bunch induced transient measurement requires comparison of a transient vector, measured using the oscilloscope channel 3 to an absolute RF EFS vector from a cavity probe measured using the channel 2. Because the signals are measured with different channels of the oscilloscope and they are sent through lines with different transmittances it is necessary to perform a calibration. The calibration measures a vector factor required for the comparison of the transient vector to the RF EFS vector. A special automatic calibration procedure consists of 9 steps. Every step measures transmittances of different parts of the system. The calibration results are stored in a DOOCS server.

The developed RF feedforward comb filter implementation with a fine-tuning is able to perform an automatic filter adjustment. This procedure is based on calculating required changes of Inphase and Quadrature inputs of a fine-tuning IQ modulator in order to minimize a filter adjustment error vector. Before starting the algorithm an IQ modulator must be calibrated in order to work properly.

Single bunch induced transients are measured by calculating an average of a pulse captured by the oscilloscope at the output of an amplifier. However the filter adjustment error vector does not always equal zero. Therefore it is necessary to filter the pulse using a bandpass filter. The bandpass filter attenuates the filter adjustment error vector and also reduces a signal noise level. Another method tested for the transient measurement was based on fitting of a polynomial function to the filter adjustment error vector and removing this error by subtracting the polynomial function from a captured waveform. Then the pulses are also calculated by averaging their value.

CHAPTER 4

Experimental results

The single bunch induced transient detection system has been tested during a special accelerator study periods. The goal was to verify that the concept is correct and the system is working with expectations. The tests were based on the comparison of the new method with the old method used for the calibration and on comparing the measurement results with the theory.

4.1 Beam phase and transient amplitude measurement

The presented measurements are the first successful measurements of a beam phase and a transient amplitude. They were performed in the module ACC1 of TTF2, cavity 3 on 17-th January 2005. The beam phase was expected to equal $-10°$.

Transients were measured with an early version of the system. The downconversion was performed with an amplitude and phase detector based on the "Low of cosine". The data was taken with a LeCroy WaveRunner 6100A oscilloscope. The waveforms were averaged over 100 samples to reduce a noise level. A transient measurement

Charge [nC]	Re [V]	Im [V]	Mag [V]	Phase [°]	Error [°]
1	0.183	-0.0399	0.187	-12.3	-2.33
2	0.321	-0.0482	0.325	-8.53	1.47
3	0.464	-0.107	0.476	-13.0	-3.04

Table 4.1: Single bunch induced transient measurement results

results were calibrated only in a phase. Therefore an absolute value of a transient amplitude is not known.

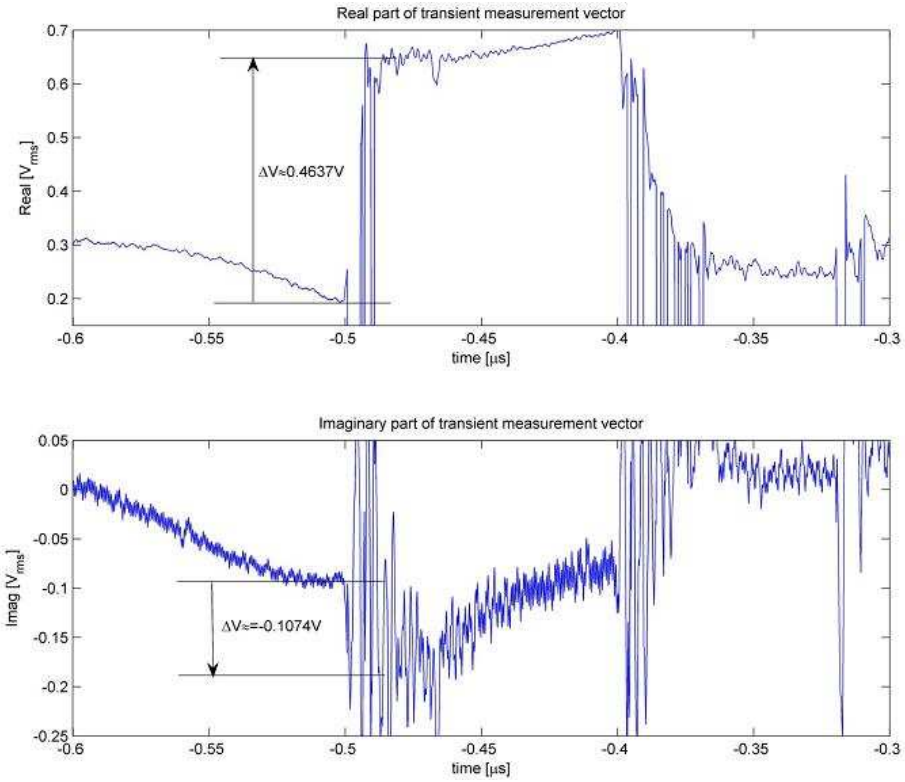

Figure 4.1: 3 nC single bunch induced transient.

The experiment was performed for three beam charges: 1 nC, 2 nC and 3 nC. A beam phase was fixed. Figure 4.1 presents one of the captured transients. Table 4.1 shows calculated results. As it can be seen, a transient amplitude increases with the charge as it is expected by a theory. The measured beam phase is also close to the expected value ($-10°$). The differences between the measured beam phase and the expected are small.

4.2 Beam phase and transient amplitude measurement

The experiment was performed in the ACC1 module cavity 3 for the EFS amplitude 13.7 MV/m with feedback turned off on 28-th May 2005. The measurement was performed on a single bunch beam with 1 nC charge.

The system was a bit different then in the previous measurement. Signals were directly downconverted by an oscilloscope using a digital downconversion. The calculations were done online with a matlab script running on the oscilloscope.

Beam phase set point	Measured phase	Measured amplitude	Measured beam phase error
-90	-90.9	4.19e-4	0.9
-45	-48.2	4.37e-4	3.2
0	1.7	3.95e-4	-1.7
45	41.6	4.09e-4	3.4
90	44.9	1.19e-4	45.1
180	35.6	8.92e-5	144.4

Table 4.2: Single bunch induced transient detection results

The results are presented in table 4.2. The starting point for the measurement was 0° beam phase set point. The RF EFS phase was changed according to the table by +45°, +90°, +180°, −45° and −90° from the set point. Measured phase differences between expected and measured values for the set points in the range from −90° to +45° are small and show that the system works correctly. The phase results for +90° and +180° are incorrect as the errors are higher then 45°. For these two points transients amplitudes are also improperly smaller then in other points. The explanation could be that the beam was decelerated for these phases, therefore the transmission was not good and the beam did not reach the third cavity properly. Hence these results can not prove that the transient detection system is working incorrectly.

4.3 Comparison of high and low charge transients

The measurement presented in this section was performed on 2 June 2005. The results show a comparison of a transient measurement using an old method and the new. The experiments with the old method that measures high charge transients were performed for around 110 nC charge transients (30 bunches, 3.67 nC single bunch charge) in the ACC1 module cavity 3, EFS amplitude 14.75 MV/m and a feedback off. The measurements with the new method that detects small charge transients where performed for 2 nC transients (1 bunch, 2 nC single bunch) in the ACC1 module cavity 3, EFS amplitude 14.75 MV/m and a feedback off.

Beam phase set point	Measured beam phase for 110 nC transient	Measured beam phase for 2 nC transient	Beam phase error calculated with respect to set point	Beam phase error calculated with respect to 110 nC transient phase
-90	-63.2	-67.1	-22.9	-3.89
-45	-39.6	-39.7	-5.3	-0.14
0	4.86	4.7	-4.7	-0.16
45	51.0	46.50	-1.5	-4.54
90	66.9	71.9	18.1	5.01
180	46.86	38.4	141.6	-8.46

Table 4.3: Beam phase measurement results

The results are presented in two tables table 4.3 and table 4.4. Table 4.3 shows a comparison of measured beam phases. The beam phase set point shows a beam phase, which was expected by an accelerator operator. However this value can be a different from a real one. The real one should be detected by the transient detector. As one can see the measured beam phases are slightly different from the phase set points for a high charge and a low charge transients measurements. However the differences between the beam phase assumed by an operator and detected using the new method are not large (the beam phase error calculated with respect to the set point). The real measurement errors should be shown by comparing the results achieved by the two methods for transient detection. The comparison is presented in the "Beam phase error calculated with respect to 110 nC transients". These errors are smaller than the previous, the maximum is around 8°, hence proving that the system is working as expected.

Beam phase set point	Measured transient amplitude for 110 nC transient	Measured transient amplitude for 2 nC transient
-90	3.53e-2	8.10e-4
-45	3.50e-2	8.21e-4
0	3.60e-2	8.29e-4
45	3.49e-2	7.98e-4
90	1.42e-2	5.52e-4
180	0.17e-2	8.43e-4

Table 4.4: Transient amplitude measurement results

4.4 Transient amplitude measurement

The measurement was performed in the ACC1 cavity 3 for different beam charges on 2 July 2005. The charge was set to 1 nC, 1.5 nC and 2 nC. The beam phase was fixed at 0°.

In Figure 4.2 transient amplitude is changing proportionally with a beam charge as expected. The measured beam phase does not change, only a measurement noise is increasing when the transient amplitude is decreasing.

The measurements made for the similar conditions are presented in table 4.5. The experiments were performed for the cavity 5 in the module ACC3 with conditions: EFS amplitude 11.1 MV/m, a beam phase on crest. A mean value and confidence limits were calculated for 299 samples. The confidence limits for single measurements were calculated from 299 samples for 95 % confidence interval using the Student distribution. A beam phase and a transient amplitude were measured with the beam induced transient detection system with a new DOOCS interface.

Set charge $[nC]$	Toroide mean charge $[nC]$	Toroid Δq CI=95% $[nC]$	Measured mean phase [°]	Measured $\Delta\varphi$ CI=95% [°]	Measured mean tr. mag. $[V/V]$	Measured ΔA CI=95% $[V/V]$
0.5	0.51	0.024	-1.44	26.53	1.40e-4	0.59e-4
1.0	1.06	0.048	-0.46	12.04	3.08e-4	0.63e-4
1.5	1.66	0.046	0.52	7.66	4.62e-4	0.56e-4
2.0	2.21	0.060	2.93	5.87	5.94e-4	0.63e-4

Table 4.5: Transient measurement results

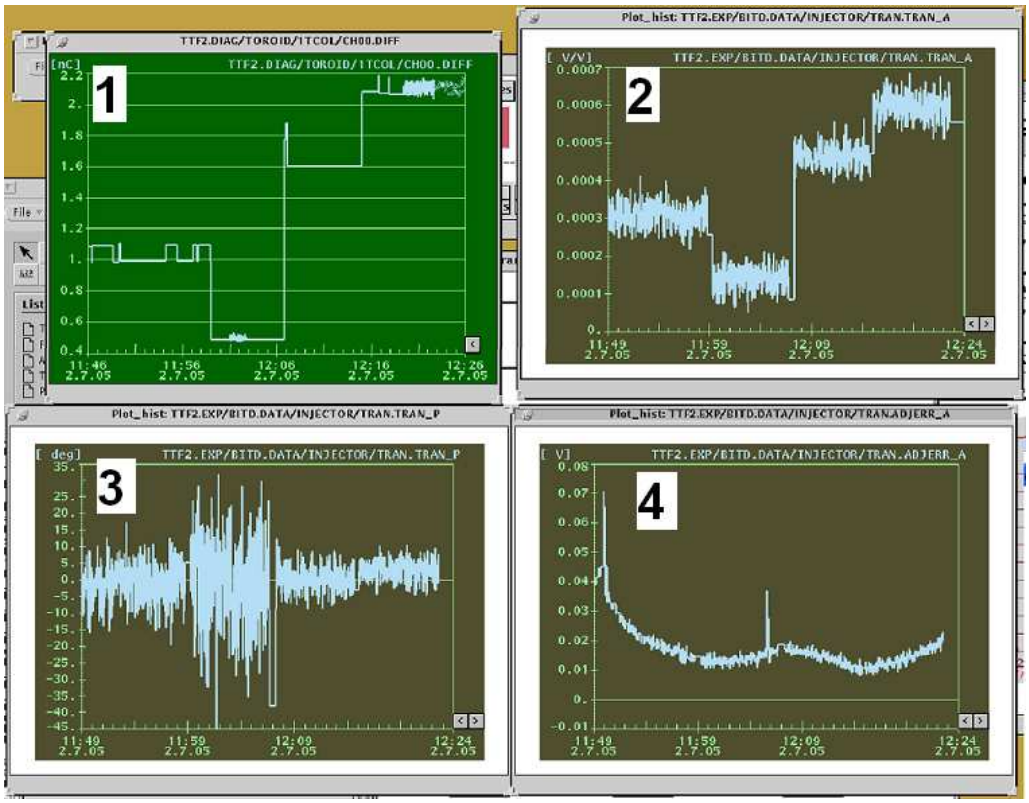

Figure 4.2: Measurement results: 1 - Charge measured with toroid [nC]; 2 - Transient amplitude [V/V]; 3- Beam phase [°]; 4 - Filter adjustment error [V].

The measured beam phase for a fixed RF EFS phase is slightly changing with a beam charge. This is not a measurement error but known behavior of the particle beam. A confidence limit of the beam phase increases with a decreasing transient amplitude since the measurement noise is at the same level while real and imaginary parts used to calculate a phase are becoming smaller. A transient amplitude is increasing proportionally to a beam charge which also conforms expectations.

4.5 Energy measurement

This experiment was performed in the cavity 3 module ACC1 on 18-th March 2006. The goal was to measure beam energy at the output of the ACC1 module in the function of a beam phase measured by the transient detector in the cavity 3 and compare it with theory. A camera "3BC2" in a bunch compressor 2 was used for the beam energy measurement. During the experiment an RF EFS in the cavity

3 was not included in a vector sum control. An RF EFS in all cavities except the cavity 3 was on crest. A phase in the cavity 3 was changed by a waveguide tuner. A single result is an average over 100 samples taken by the single bunch induced transient detection system. The measurement results are presented in Figure 4.3. The measured beam energy and phase are fitted with a cosine function. Calculated parameters of the fitted cosine function are presented in the figure.

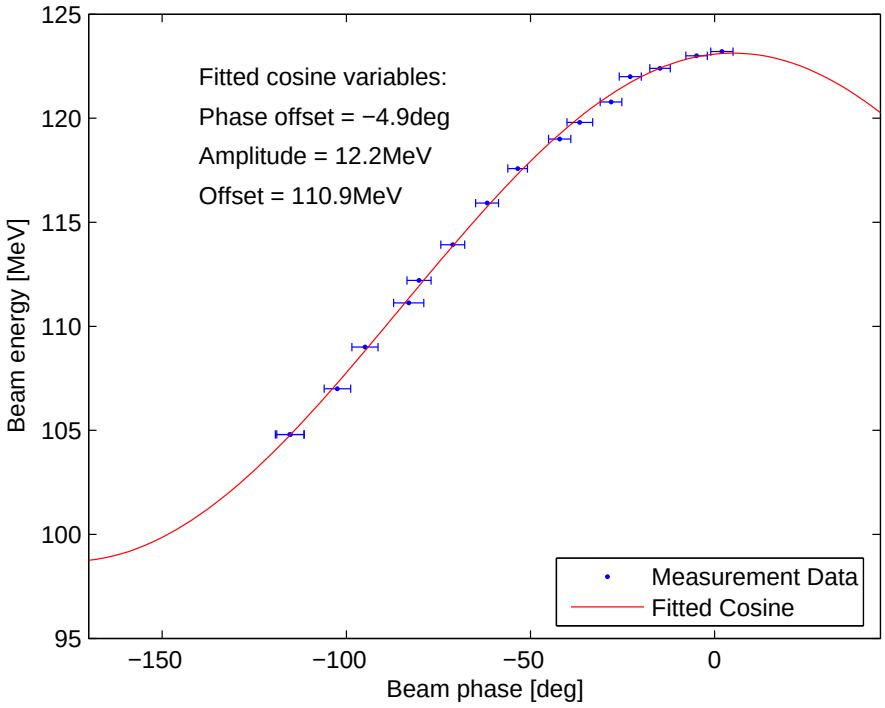

Figure 4.3: Energy measurement.

An amplitude of the fitted cosine function is 12.2 MeV. An expected amplitude of the function would be beam energy gained in the cavity 3 - EFS amplitude in this cavity. Because the EFS amplitude in the cavity and the cosine amplitude are very close, it proves that the measurement is correct. The measured offset 110.9 MeV should be the energy gained by the beam in all cavities except the cavity 3. This offset is close to the sum of all EFS amplitudes in all cavities in the module ACC1 except the cavity 3. It is another proof that the measurement was correct. The measured phase offset is small and close to 0°. Therefore the transient detection system measures a beam phase correctly.

4.6 Amplitude and phase measurement

The measurement was performed with the single bunch induced transient detection system in the ACC1 cavity 3 on 26-th March 2006. The goal of the experiment was to measure the single bunch induced transient amplitude for different bunch charges and compare the results with theory. A bunch charge was changed from 0.5 nC to 3 nC in 0.5 nC steps. Every measurement is an average of 100 samples taken by the single bunch induced transient detection system. The bunch charge was measured with a toroid.

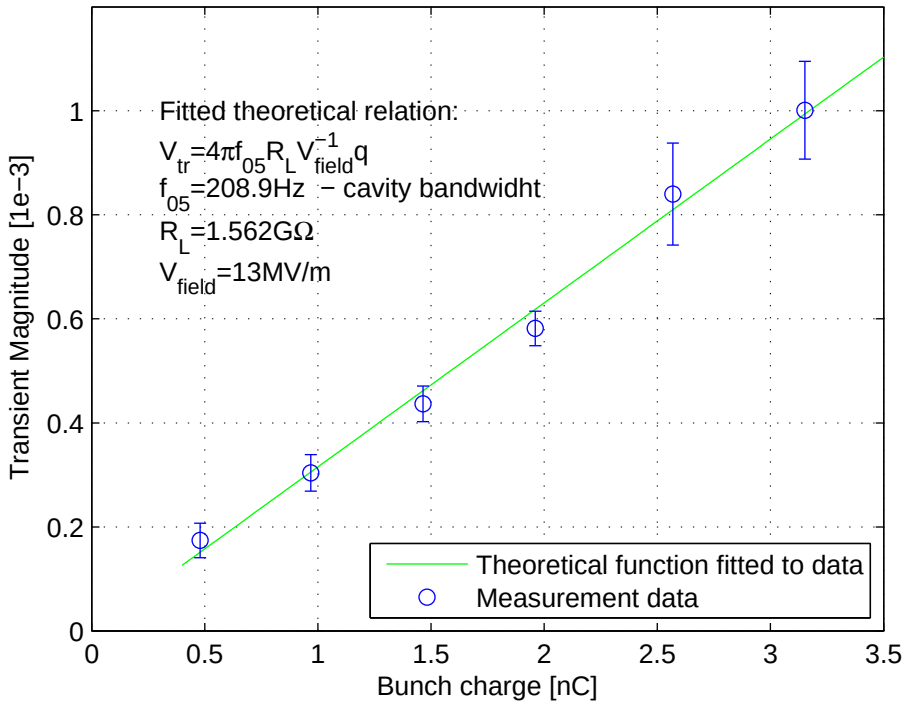

Figure 4.4: Transient amplitude as a function of charge.

The measurement result is presented in Figure 4.4. The theoretical line was fitted to the measured data with the following assumptions: the cavity 3 EFS amplitude was 13 MV/m, the R_L was 1.562 $G\Omega$. A variable during the line fitting was a cavity half bandwidth $f_{0.5}$. The calculated cavity half bandwidth during the line fitting was 208.9 Hz were an expected bandwidth is 208 Hz. The result proves that the transient amplitude measured with the single bunch induced transient detection system is correct.

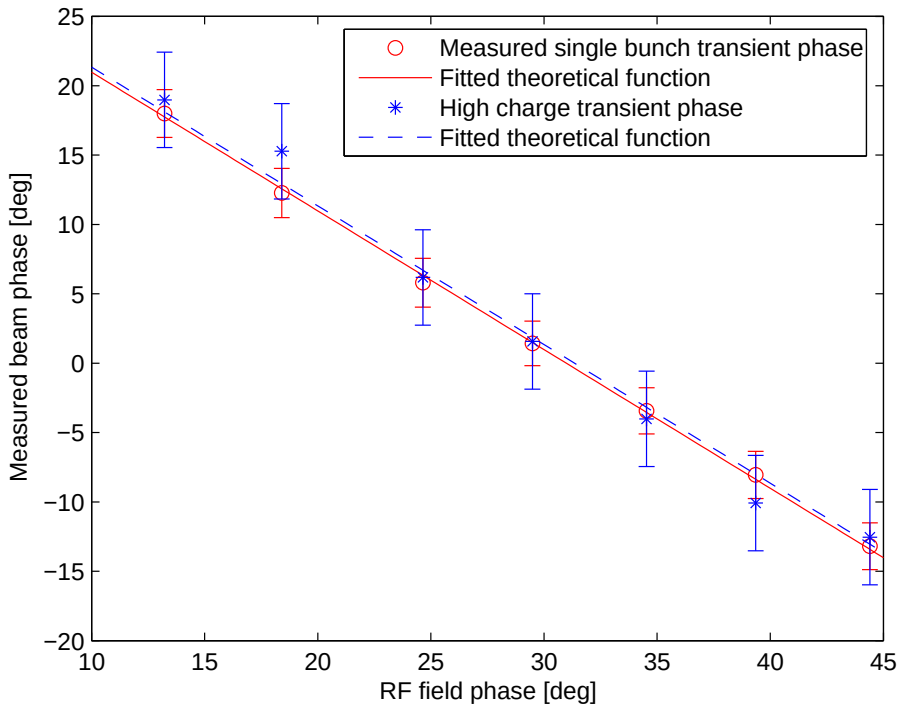

Figure 4.5: Measured phases comparison.

The second experiment was also performed in the ACC1 cavity 3. The goal of the measurement was to compare the beam phase measured with the two different methods: the single bunch induced transient detection and a large high charge induced transient detection (a reference method). The beam charge was set to 1 nC. The phase was changed in 5° steps from −15° to +15°. During the experiment, the RF EFS phase and the beam phase with two methods was measured.

The result is presented in Figure 4.5. The x axis shows the RF EFS phase, y axis presents the measured beam phase with the two different methods. The measured data was fitted with the theoretical function. The theoretical line was a linear equation (4.1). The "x" is the RF EFS phase and "y" is the measured beam phase. A variable during fitting was "b" - a phase offset between the beam phase and the RF EFS phase. The beam phases measured with the two different methods are very similar. It proves that the beam phase measured with the single bunch induced transient detector is correct.

$$y = x + b \tag{4.1}$$

4.7 Transient phase and amplitude measurement in different cavities

The measurement was performed on 1 August 2006 in the module ACC1. The single bunch induced transient detector was connected to all cavities in the module using an RF relay. The measurement was done for every cavity in the module. The transients were measured with the two methods: using the single bunch induced transient detection and with the high charge induced transient detection. The single 1.7 nC bunch induced transient amplitudes and phases were measured 100 times with the single bunch induced transient detector and averaged. The high charge transients made of 30 bunches with 1.7 nC charge were measured with probe monitoring ADC's.

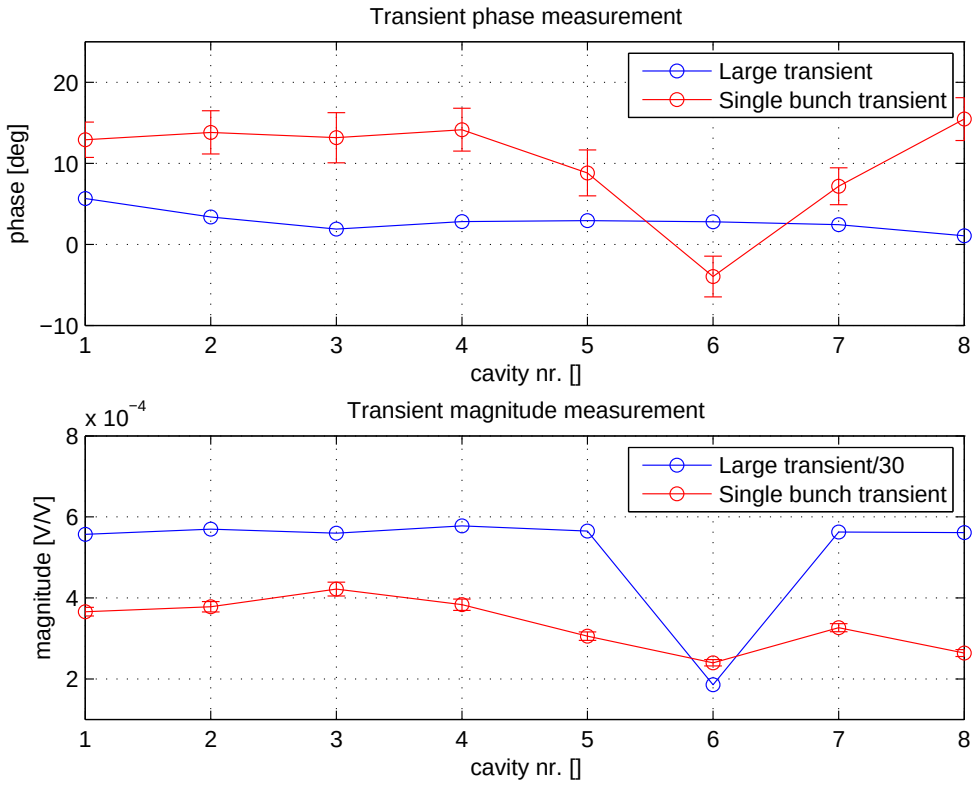

Figure 4.6: Transient amplitude and phase in different cavities.

The results are presented in Figure 4.6. The transient amplitudes and phases are calculated with respect to the RF EFS in cavities. High charge transients measurement results are used as a reference. The differences between the two methods, show the single bunch induced transient detector measurement errors.

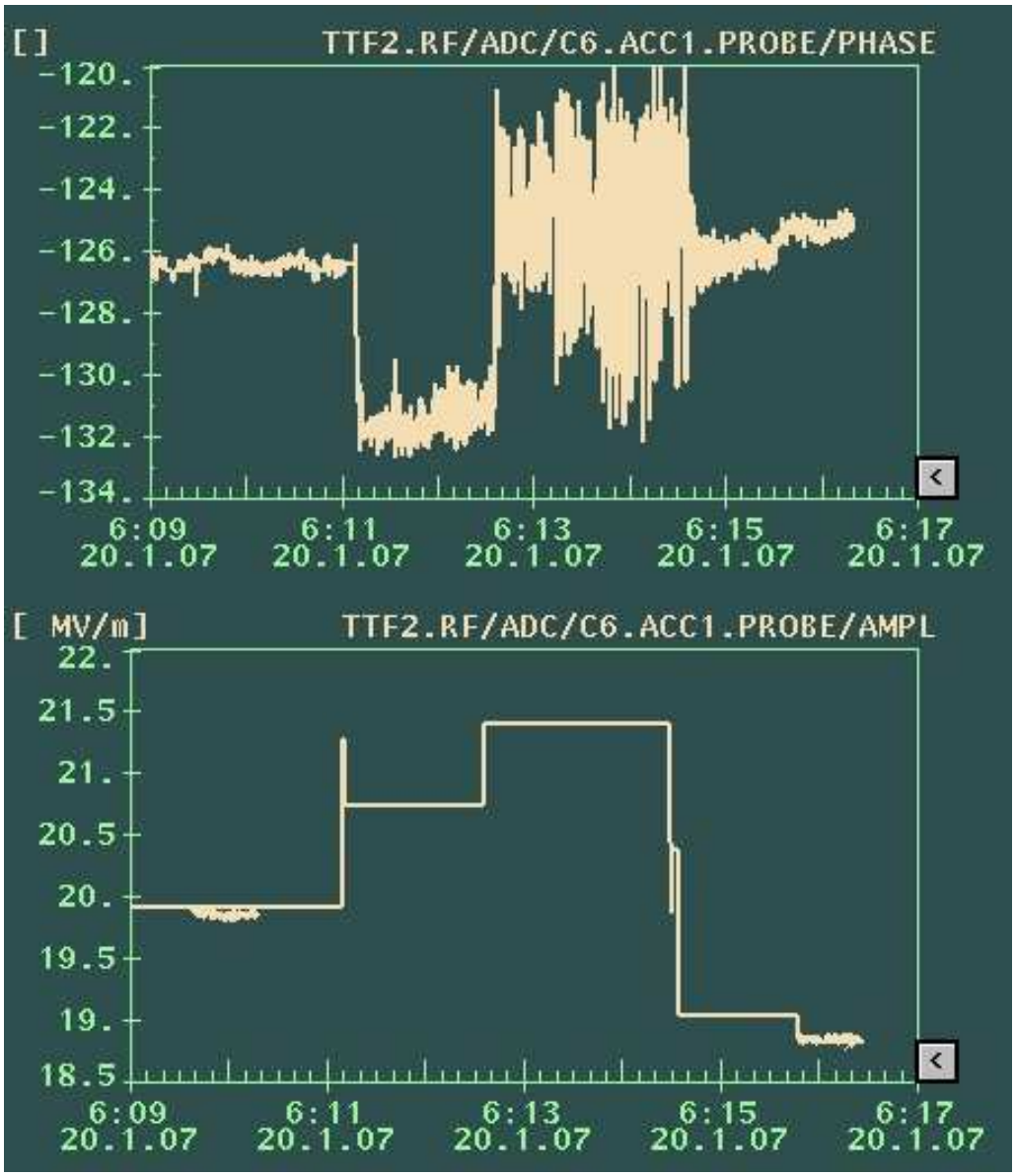

Figure 4.7: Phase jumps in cavity 6 depends on an amplitude: upper picture - EFS phase [°]; lower picture - EFS amplitude [MV/m].

The presented results show that the single bunch induced transient detection has two measurement errors. The one is systematic - the same for all cavities except the cavity 6 (an offset). The second one is stochastic - different for the cavity 6.

The offset in the phase and amplitude measurement (a systematic error) can be explained by a calibration error. Every result of the single bunch induced transient detection is calculated by multiplying the measured transient with respect to the RF EFS by a calibration factor. The factor is the same for all measurements hence

it can be a source of the systematic error. During the experiments the system was tested with a different method for the calibration then normally. During the tests, the signal from the cavity probe was used as a reference signal during the calibration instead of a local oscillator. In the case the probe signal was stable the calibration procedure should give the correct values. Unfortunately the probe signal is not fixed, its phase and amplitude are changing. Therefore these changes add errors to the calibration factor. This problem is fixed already by connecting the local oscillator as a reference during the calibration instead of the cavity probe.

The second problem is a measurement error in the cavity 6. As one can see in Figure 4.6 this error is different than in other cavities. Therefore it is not the systematic error present in other cavities. It is known that the cavity 6 has the highest EFS amplitude then any other cavity in the module. It is also known that for the highest amplitudes signal in the cavity 6 behaves in a strange manner (Figure 4.7). When the EFS amplitude is increased to the highest value its phase in the cavity 6 is jumping by up to 10° peak to peak. The transient measurements were performed for the highest EFS amplitudes. Therefore the strange behavior could have been a source of the transient measurement error.

4.8 Transient measurements in different cavities

The measurement was performed on 27-th November 2006 in ACC1 to investigate the problem with the measurement on 1 August 2006. The single bunch induced transients were measured 100 times in every cavity. The results were averaged and stochastic measurement errors were estimated. The measurement results are presented in Figures 4.8, 4.9, 4.10.

The presented measurements are different than expectations. The phases in all cavities should have similar phases, whereas measured phases are different by up to ±10°. The measured amplitudes are also incorrect. The amplitudes in the cavities 1 to 4 should be very similar, on the measurement they are different by up to ≈ ±20 %.

The measured transient amplitude, phase and the signal amplitude for all cavities look similar. Therefore it seams that the measured transient vector phase and amplitude may depend on the signal power from the cavity probe. In order to find out what is the source of these errors more measurements must be performed.

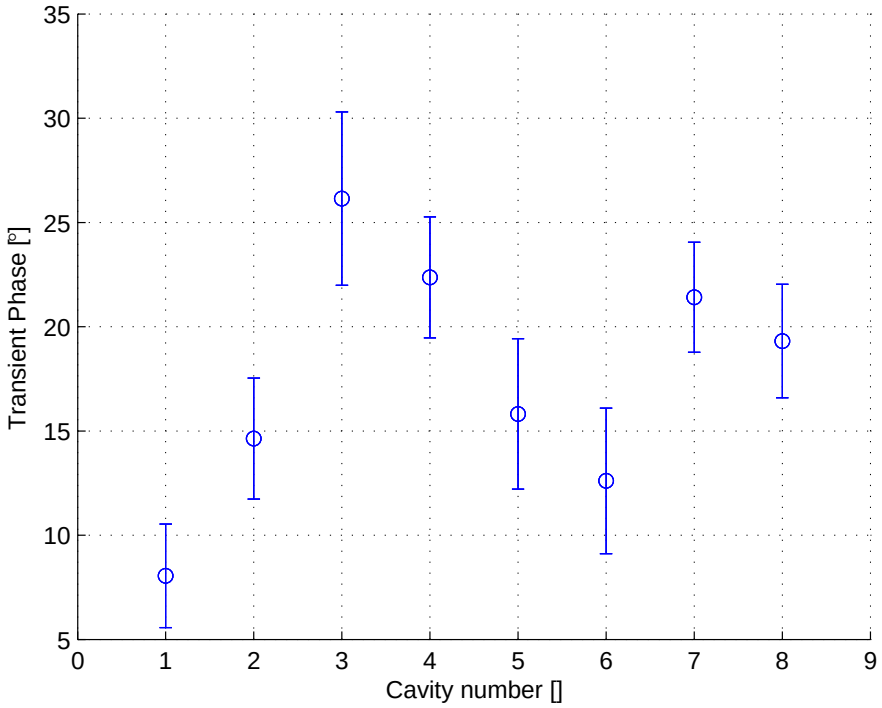

Figure 4.8: Transients phases in different cavities.

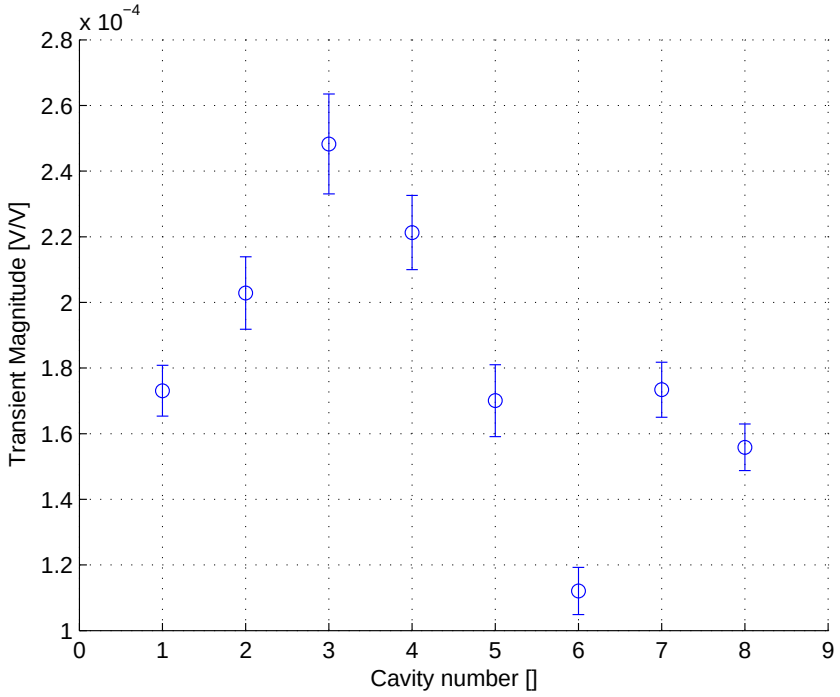

Figure 4.9: Transients amplitudes in different cavities.

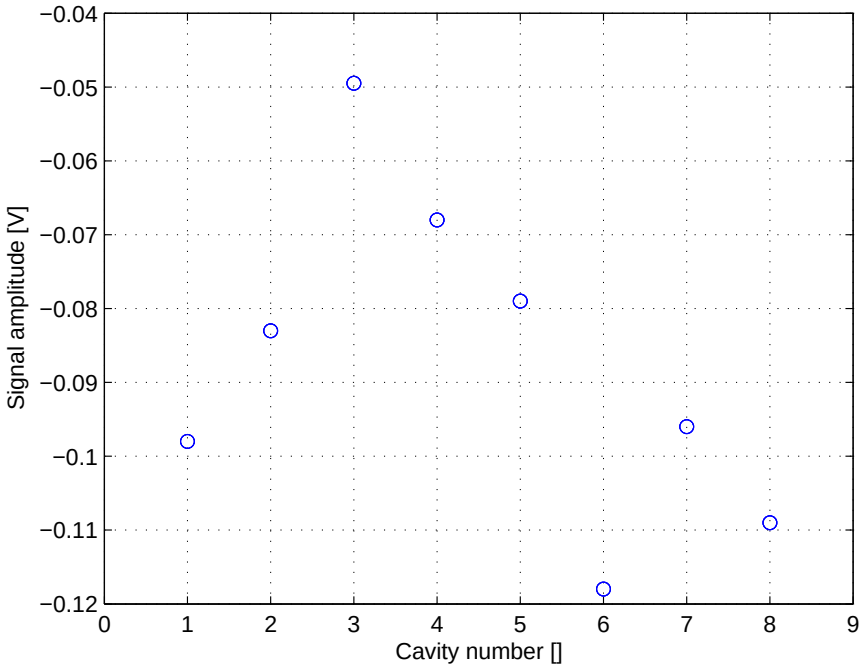

Figure 4.10: Negative amplitude of the signal from a cavity probe measured by the oscilloscope channel 2.

4.9 Transient detection system sensitivity to signal power level

The measurements on 27-th November 2006 in ACC1 show that the measurement errors possibly depend on the signal power. In order to find out what is the source of the measurement errors, the measurement with the single bunch induced transient detection system was performed on 15-th December 2006.

A manual mechanical variable attenuator was installed in front of the system. The delay line in the filter was disconnected and relays were connected to 50 Ω loads in order to measure a constant signal transmitted by the filter. The 60 dB attenuator was installed between the amplifier and the filter to simulate transients 60 dB smaller than a carrier. The signal measured by the channel 2 of the oscilloscope was divided by the signal measured by the channel 3. An amplitude and phase of the result was recorded with an amplitude of the signal in the channel 2. During the measurement attenuation of the variable attenuator was changed manually. The variable gain amplifier was set to the maximum gain. The results are presented in Figure 4.11 as

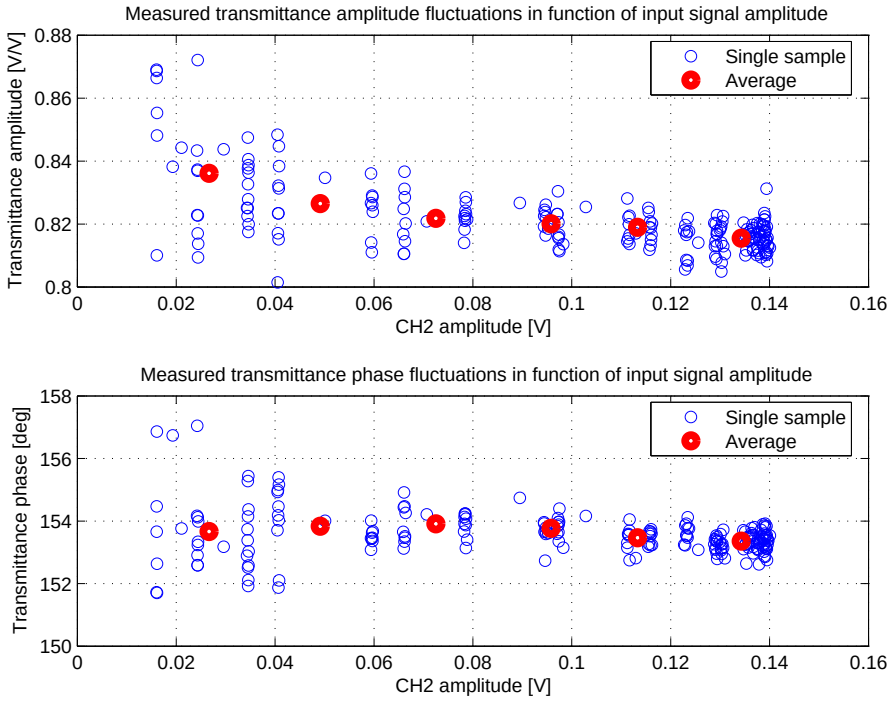

Figure 4.11: Measured transmittance fluctuations as function of an input signal amplitude.

a single measurements and as averages.

The results show that the transient phase measurement with the transient detection system is insensitive to a signal power level. An amplitude is sensitive to a signal power level but only to around 3 %. As a conclusion the transient detection system is not a source of the errors which depend on a signal power level and can reach ±20 % for an amplitude, ±10° in a phase.

4.10 Single bunch induced transient measurements

The measurement was performed on 15-th December 2006 in ACC1 cavity 1. The RF EFS amplitude was set to 12.4 MV/m. Figure 4.12 shows an image of the 1 nC single bunch induced transient at the output of the RF feedforward comb filter taken by an oscilloscope. The picture shows that the transient is several times higher than the noise visible in front and at the back of the pulse.

Figure 4.12: 1 nC single bunch induced transient.

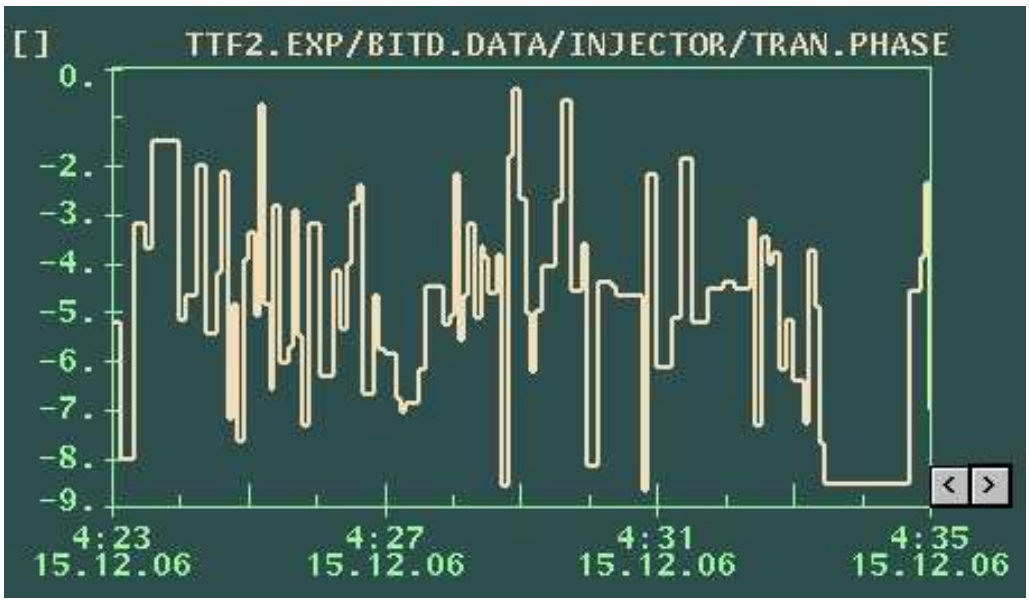

Figure 4.13: Single bunch induced transient phase [°].

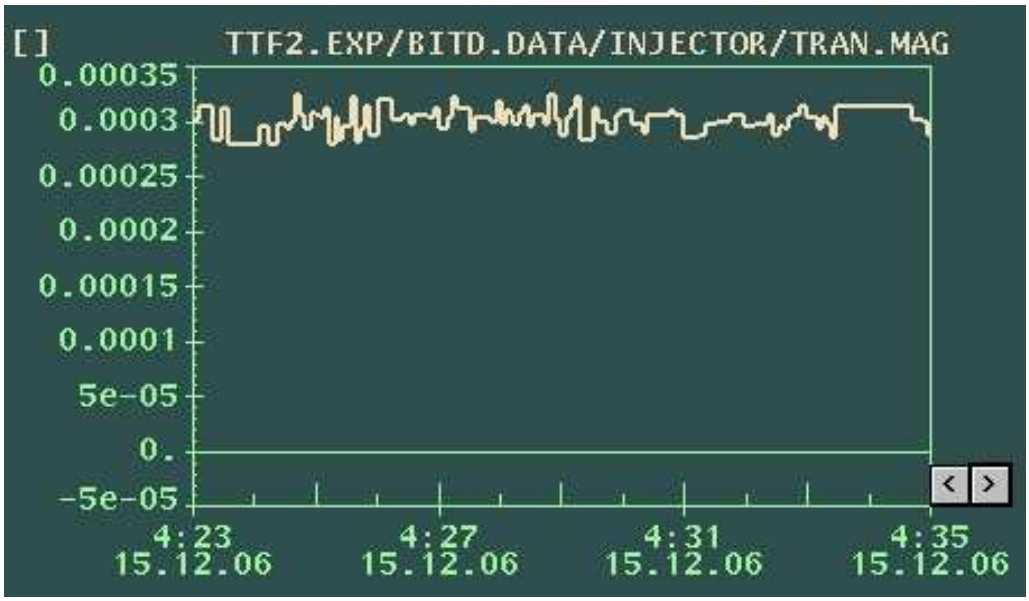

Figure 4.14: Single bunch induced transient amplitude $[V/V]$.

Figures 4.13 and 4.14 present a series of transient phase and amplitude measurements. The measurements were performed 100 times and a stochastic measurement error was estimated. The stochastic measurement error for 0.96 nC single bunch induced transient in ACC1 cavity 1 with 95 % confidence interval and for 12.4 MV/m EFS amplitude equals:

$$\Delta M = \pm 6.5\ \% \tag{4.2}$$

$$\Delta \varphi = \pm 3.3^{\circ} \tag{4.3}$$

Figure 4.15 presents the single bunch induced transient measurement using a main DOOCS panel for the transient measurement. Figures 4.16, 4.17 and 4.18 show the measured transient amplitude and phase during an RF gun startup. The measured transient amplitude (Figure 4.17) changes linearly with the beam charge (Figure 4.16) which is a prove that the system measures the single bunch induced transients correctly.

The presented results show that it is possible to measure the single bunch induced transient with a low noise level and low stochastic errors $\Delta M = \pm 6.5$ % in an

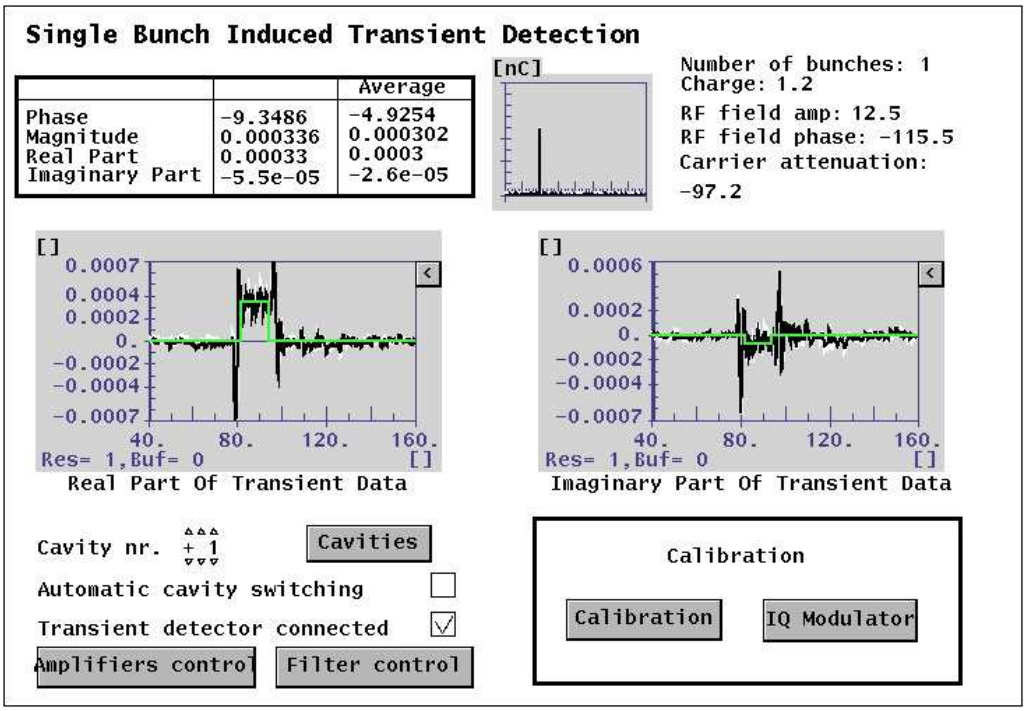

Figure 4.15: Single bunch induced transient measurement using a DOOCS graphical user interface.

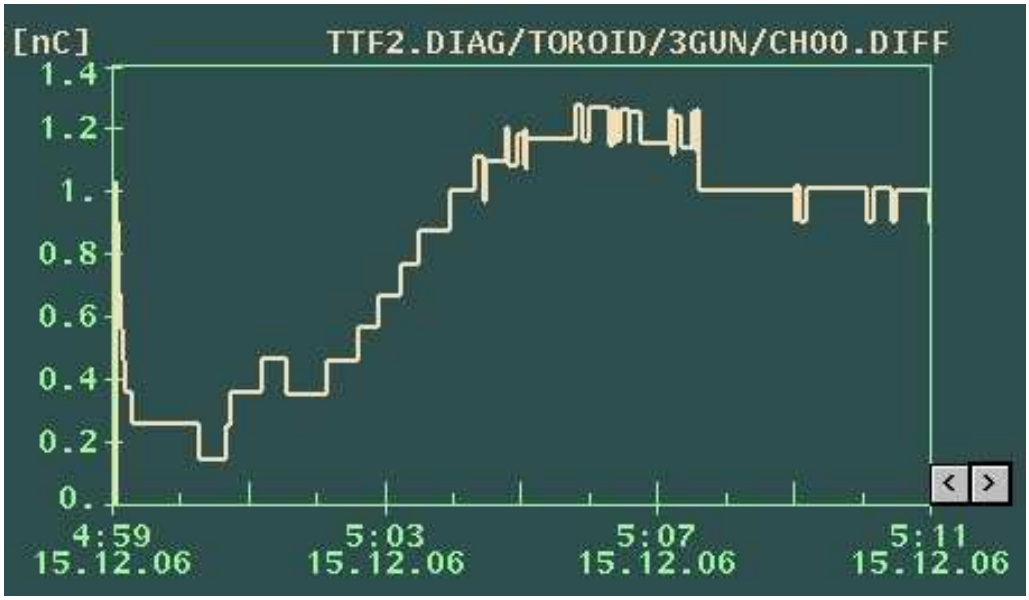

Figure 4.16: Beam charge measured by toroid [nC].

Figure 4.17: Single bunch transient amplitude $[V/V]$.

Figure 4.18: Single bunch transient phase [°].

amplitude and $\Delta\varphi = \pm 3.3°$ in a phase.

The measured transient phase and amplitude were also compared with expected values. The phase was expected to be $0° \pm 5°$. The amplitude was estimated on the basis of the measured beam charge, the EFS amplitude and the known cavity parameters (1.3). The comparison is presented in Figure 4.19. The differences between the measured values and the expected are around 20% in an amplitude and 11° in a phase. The source of the differences is currently unknown and will be investigated.

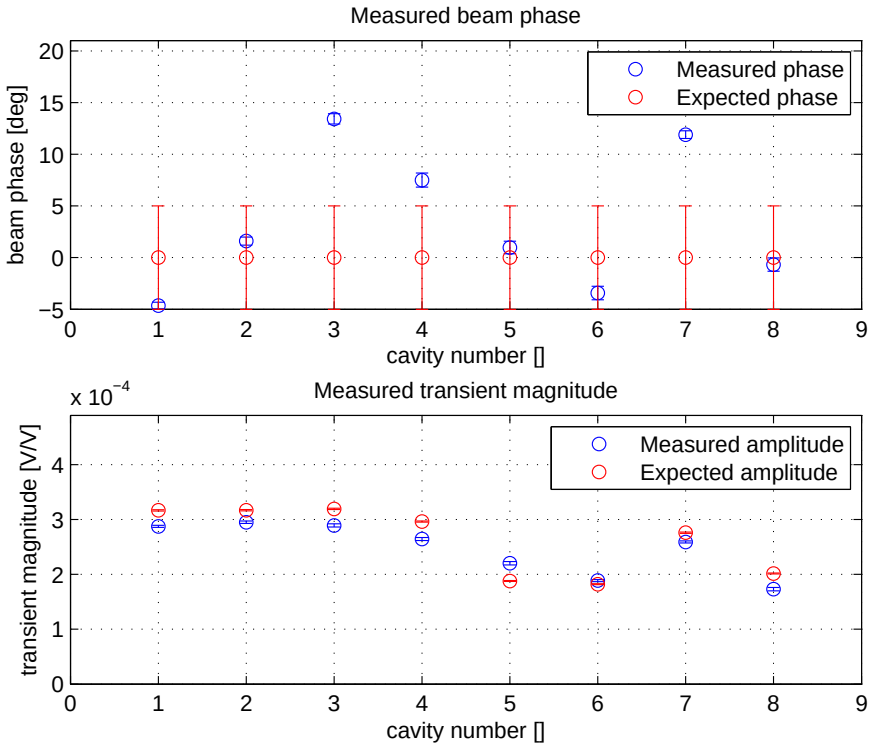

Figure 4.19: Comparison of measured and expected transient amplitude and phase.

4.11 An influence of a signal power on single bunch induced transient measurements

Single bunch induced transient detection measurements show the correlation between the measured transient phase and a signal power (Section 4.8). In order to verify if the errors are caused by the single bunch induced transient detection system, a variable attenuator was installed between the system and a relay connected to the cavities. The measurement was performed on 18-th December 2006 in ACC1.

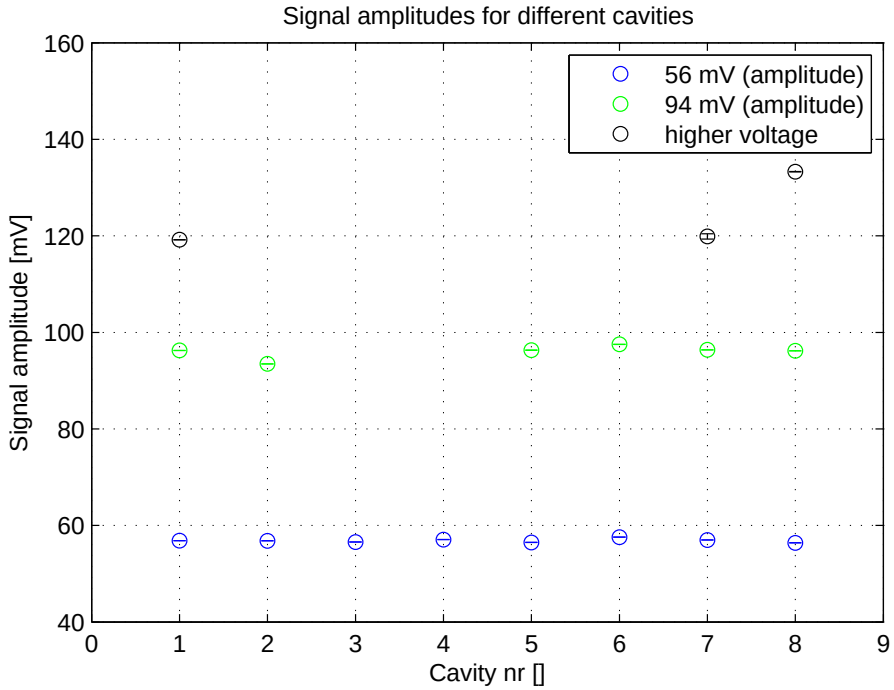

Figure 4.20: Signals amplitudes.

The signal amplitudes measured by an oscilloscope for every cavity are presented in Figure 4.20. Every point presented in Figure 4.20 and Figure 4.21 has a color. One color corresponds to one power level. The presented measured transient phases have small dependence on the signal power at an input of the single bunch induced transient detection system (Figure 4.21). Therefore the transient detection system does not cause the large systematic measurement errors in a phase which are correlated to the signal power and can reach up to $\pm 10^{\circ}$ (Section 4.8).

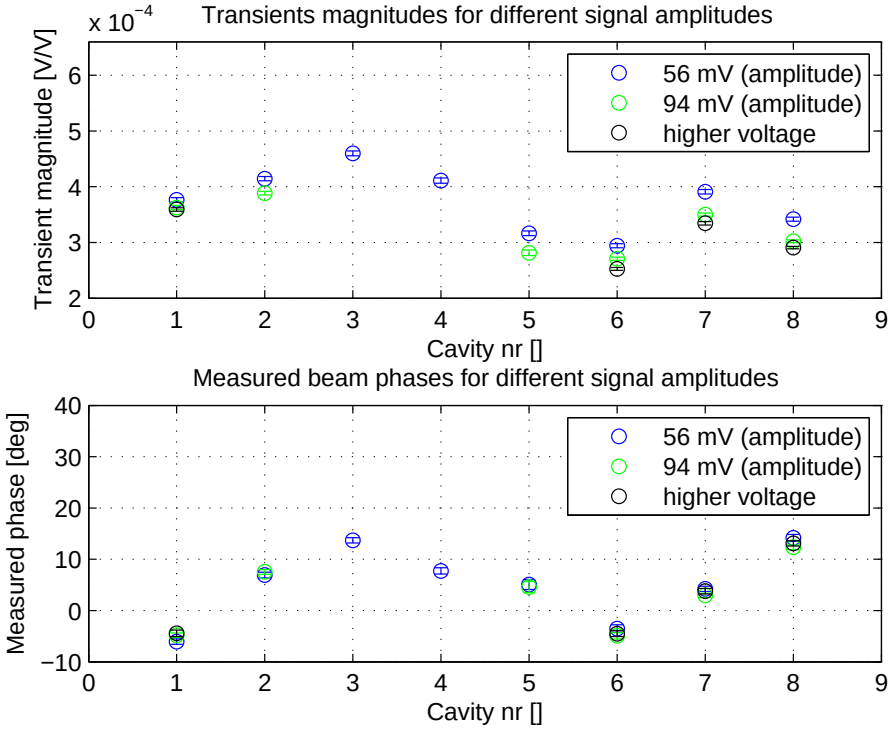

Figure 4.21: Transient measurement sensitivity to a signal power.

4.12 An influence of directional couplers on a transient measurement

The signal power level at an input of the single bunch induced transient detection system has a very small influence on the measured transient phase. Therefore it does not explain why the transient phase systematic measurement errors are correlated to the signal power. The part which might influence the measurement is a directional coupler installed between the transient detection system and the cavity probe.

In order to verify it, the transient phase was measured for different RF EFS amplitudes in the cavity. When the EFS amplitude in the cavity is changed it also changes the signal power level at the input of a directional coupler. A real transient phase should not depend on the EFS amplitude in the cavity. Therefore the transient phase changes due to an amplitude for the fixed RF EFS phase are caused by the directional coupler and they are not real changes of the beam phase.

The measurement was performed in ACC1 cavity 6 on 18-th December 2006. As seen

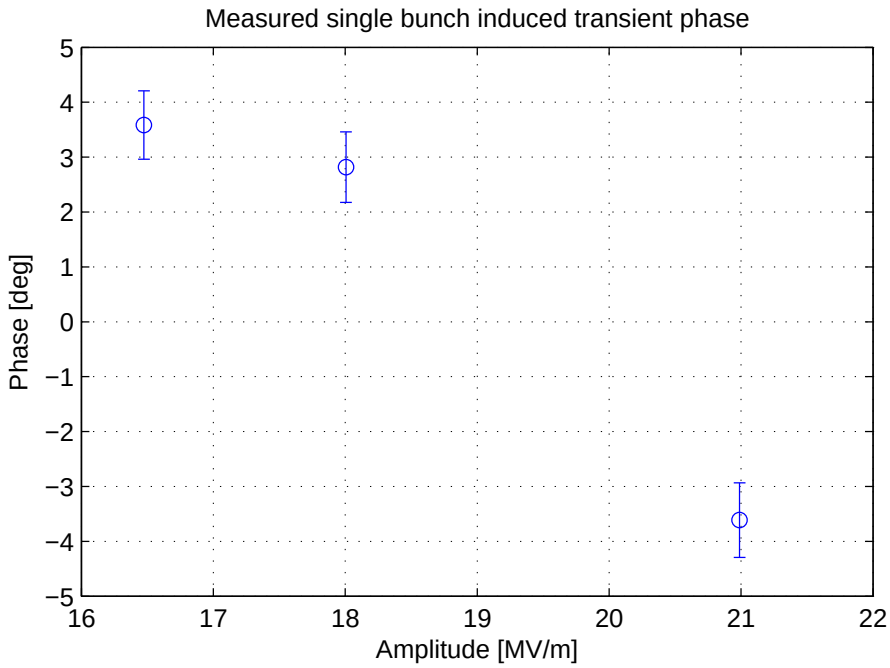

Figure 4.22: Influence of directional couplers on transient measurements.

in Figure 4.22 amplitude changes cause a significant change in the measured transient phase (changes of the RF EFS phase in the cavity was removed by subtracting these changes from the measured transient phase). As a result it might suggest that the systematic measurement errors of the single bunch induced transient detection system are caused by the directional couplers installed between the cavities and the transient detection system.

The directional couplers installed between the system and the cavities have transformers. They are not passive microstrip devices. Therefore they are dependent on a temperature, load, can heat and cause measurement errors. These device are going to be replaced with passive couplers.

4.13 Transient amplitude and phase measurement

The measurement was performed on 13-th January 2007 in ACC1. The measurement presented in Figure 4.23 compares measured transient phases for three different RF EFS phases. When the EFS phase in a cavity is changing the same should happend with a relative transient phase. The transient phase should change by the same value as the EFS phase. The results presented in Figure 4.23 conform the theory.

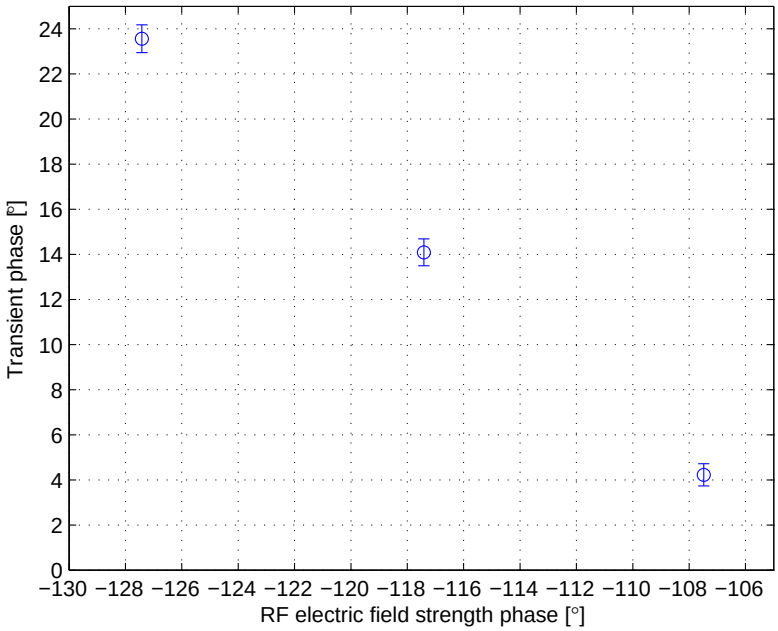

Figure 4.23: Single bunch transient measurement for different RF electric field strength phases in cavity 3 ACC1.

The following experiment (Figure 4.24) checks weather the single bunch induced transient amplitude is changing proportionally to a beam charge. The measured transient amplitude presented in Figure 4.24 is changing proportionally to the beam charge as expected.

Another experiment (Figure 4.25) measures an EFS amplitude influence on a relative transient amplitude. The transient amplitude measured by the transient detector is a relative value. It is an absolute value of a transient amplitude divided by an absolute RF EFS amplitude in the cavity. Therefore when the absolute EFS amplitude is increasing for the fixed transient amplitude, the measured relative transient amplitude should decrease. The measurement result presented in Figure 4.25 conforms

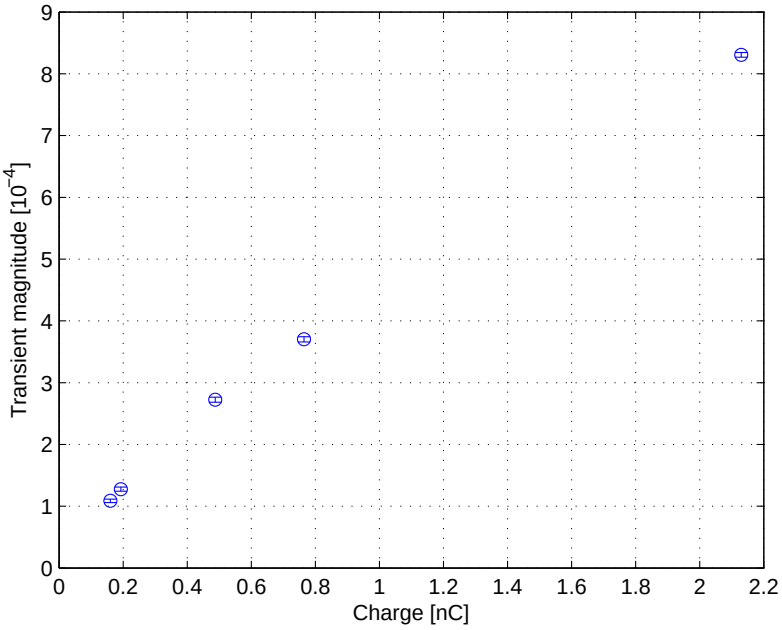

Figure 4.24: Single bunch induced transient measurement for different charges in cavity 3 ACC1.

the theory. It proves that the transient detection system measures single bunch induced transients correctly.

To verify if the transient phase measured by the transient detector for the on crest beam acceleration (maximum acceleration) equals 0°, three different methods for the beam phase measurement were used. The measurement was performed for three different detunings to verify if it gives the same results independently from detuning. The measurement result for the cavity 3 is presented in Figure 4.26 and for the cavity 4 in Figure 4.27. To make sure that the beam has a certain phase the beam phase was set to 90° using an energy measurement. Firstly an RF EFS in a cavity was reduced close to zero by maximally detuning the cavity. An energy of the whole module was measured (energy E0). Then the cavity was tuned back to a normal state and the phase of only this cavity was changed until the beam energy of the whole module equals again E0. For this condition the beam has 90° phase off crest in the cavity. Then the beam phase was measured with the single bunch induced transient detector and using an old method with the high charge transient measurement.

The results presented in Figures 4.26 and 4.27 show that the transient measurement has a small dependence on the cavity detuning. It is also visible that the high

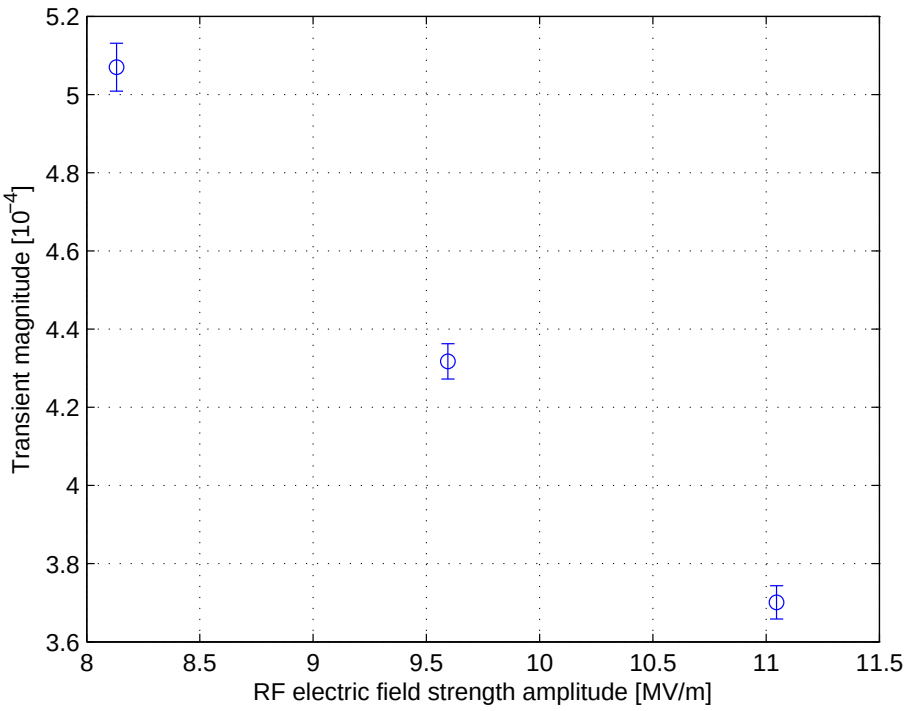

Figure 4.25: Single bunch induced transient measurement for different RF EFS amplitudes in the cavity 3 ACC1.

charge transient measurement is more accurate then the single bunch induced transient measurement. The measurement error of the single bunch induced transient measurement is higher then the measurement noise therefore it is a systematic error. The source of this error is currently unknown and it will be investigated.

4.14 Single bunch induced transient measurement

The single bunch induced transient detection system tests show that the transient detector measures transients with systematic errors (Section 4.10 and 4.13). The possible explanation is that the single bunch induces significant transients not only in a fundamental resonance mode (1.3 GHz) of the cavity but also in other passband modes. As a result other passband modes have an influence on the measured transient amplitude and phase and can be a source of the systematic error.

The measurement of a single bunch induced transient without an EFS in the cavity

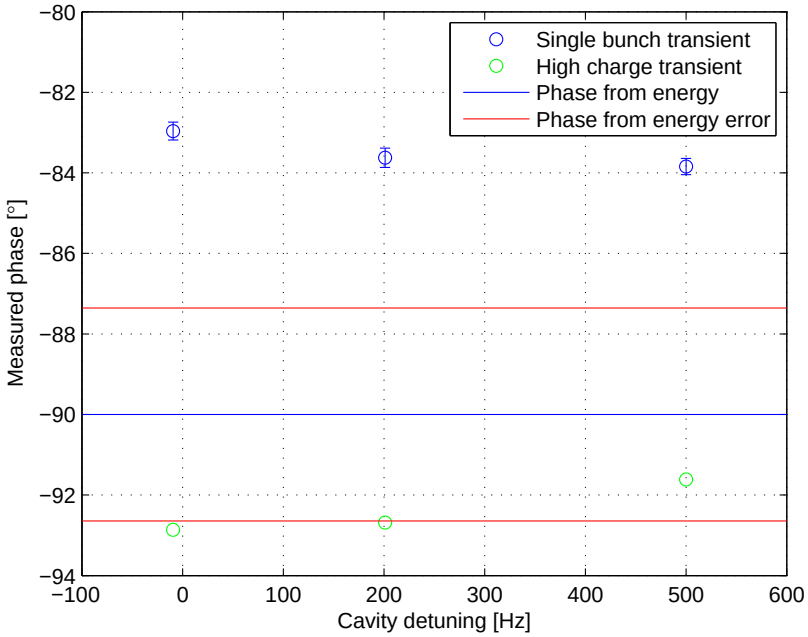

Figure 4.26: Comparison of 3 beam phase measurements for different cavity detunings in cavity 3.

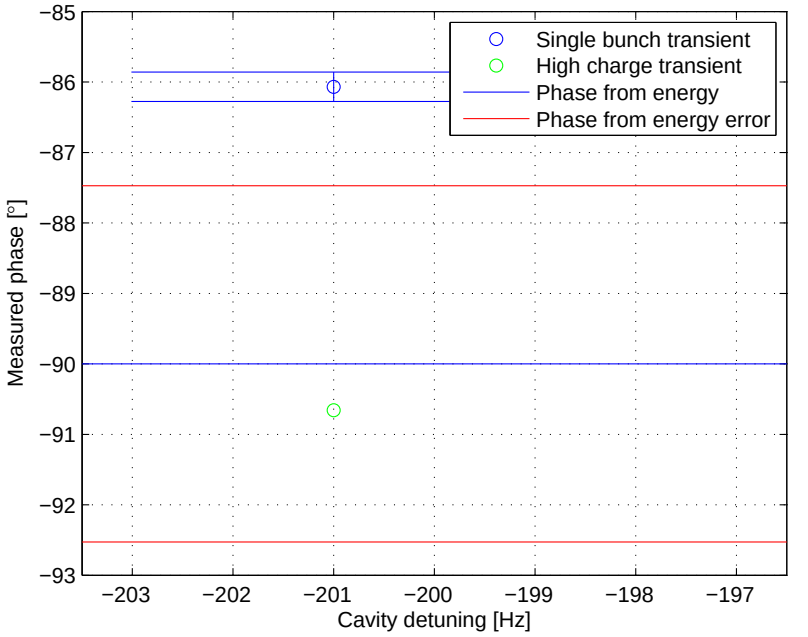

Figure 4.27: Comparison of 3 beam phase measurements for one cavity detunings in cavity 4.

was performed in order to verify if other passband modes of the cavity have influence on the single bunch induced transient measurement. The measurement was performed on 20-th January 2007. The results are shown in Figure 4.28 and 4.29. Figure 4.28 presents the measured EFS in the cavity without beam. The small signal is visible which is a coupling from an RF gun. Figure 4.29 presents a single bunch induced transient. It is evident that the single bunch induced transient spectrum is composed of a frequency component at the fundamental mode of the cavity and at frequencies of other passband modes of the cavity (1300.091 MHz, 1299.260 MHz, 1296.861 MHz, 1293.345 MHz, 1289.022 MHz, 1284.409 MHz [52]). The signal at frequency 1299.260 MHz has the highest value of all signals at frequencies other then the fundamental resonance mode of the cavity. Therefore the passband mode at this frequency has the most significant influence on the measured single bunch induced transient.

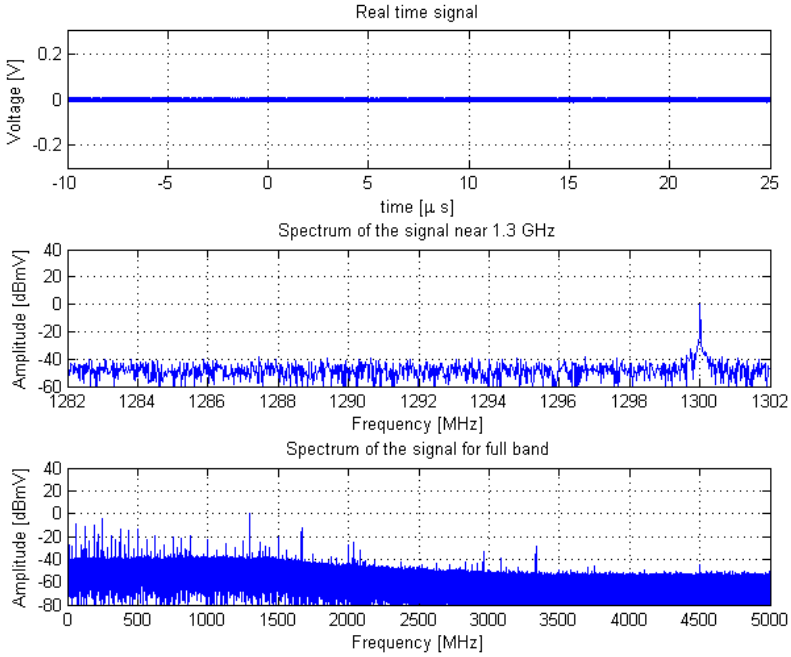

Figure 4.28: Measurement without beam.

The goal of the single bunch induced transient measurement is to measure the transient induced in the fundamental mode of the cavity (1.3 GHz). Only the fundamental mode of the cavity is responsible for a beam acceleration. Therefore the composition of all transients will give the transient amplitude and phase different than expected. The beam will have a maximum energy for a different phase than

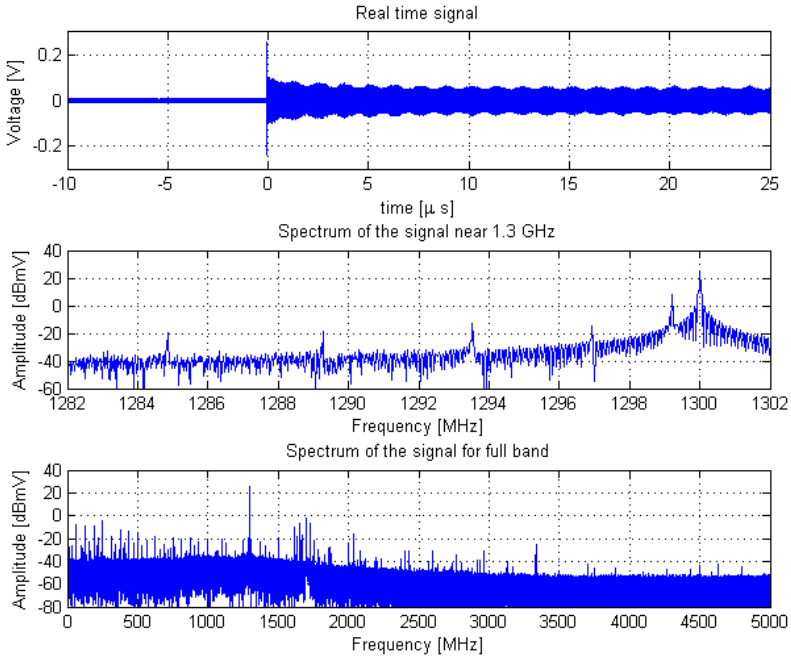

Figure 4.29: Measurement with beam.

0°, measured using the single bunch induced transient detector. The difference will depend on the phases and amplitudes of the transients induced in other passband modes of the cavity. Because these transients are smaller then the transient induced in the fundamental mode (1.3 GHz), therefore the difference is smaller then ±20 % in an amplitude and ±10° in a phase (Section 4.10 and 4.13).

Why transients measured using the old method with a high charge beam give more accurate results then using the system for the single bunch induced transient detection. The old method uses probe monitoring ADC's and measures a long transients (30 μs). The monitoring ADC's use 250 kHz intermediate frequency and have a small bandwidth below 250 kHz. Therefore the transients induced in other passband modes are filtered by the input bandwidth of the downconverting ADC's. As a result the transients induced in other passband modes have neglectable influence on the measurement of the transient at the fundamental mode of the cavity. The single bunch induced transient measurement has higher measurement errors, because the single bunch induced transient detection system measures transients with a higher bandwidth $\approx$ 400 MHz. It is necessary to measure them with a high bandwidth, because the measurement with a low bandwidth (for example below 500 kHz) would

have 318 ns time constant which is much longer than a length of the measured transient pulse, which is 20 ns. As a result the transients induced in other passband modes would be filtered with the transient induced in the fundamental mode of the cavity (1.3 GHz). Therefore the system would not be able to measure any transient.

4.15 Measurement of single bunch induced transients in non-fundamental passband modes of cavity

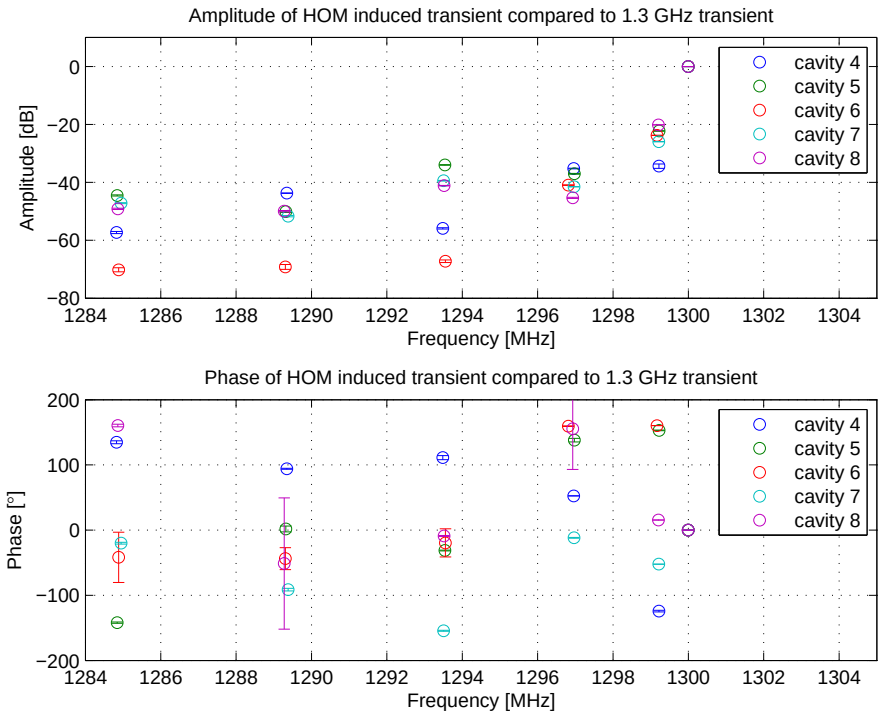

Figure 4.30: Comparison of single bunch induced transient vector spectrum maximums at other passband modes of cavities.

The measurement was performed on 14-th February 2007 in ACC1. The goal of the measurement was to compare the transients induced in the passband modes of cavities. The experimental results are presented in Figure 4.30. During the measurement the EFS in the cavities was reduced to the minimum. A klystron used as an EFS source for ACC1 was turned off. Figure presents vector values of

the frequency components in the transient spectrum at cavity passband modes. The measured vectors are divided by the vector taken from the spectrum at the frequency of the fundamental mode of the cavity (1.3 GHz) - the vector measured at the frequency of the fundamental mode of the cavity is a reference. The measurement was performed for cavities 4 to 8 in the module. It is visible that the maximums which represent other passband modes of the cavity have different frequencies for different cavities. Moreover they also have different amplitudes and phases measured with respect to the signal at the frequency of the cavity fundamental mode. This is an additional prove that other passband modes of the cavities can be a source of the systematic errors during the single bunch induced transient measurements. In case they all have the same amplitudes and phases for every cavity, they would not be a source of the systematic errors which are random between cavities.

4.16 Dependence of single bunch induced transient spectrum on beam position

The passband modes of a 9-cell superconducting TESLA cavity can be a source of the beam phase and transient amplitude systematic measurement errors. The errors are different between cavities. The transient spectrum within the cavity passband modes is also different between cavities. In case the transient spectrum is fixed in a single cavity and do not change then it would be possible to remove the systematic errors using correction factors. The correction factor could be measured for every cavity and used during the single bunch induced transient measurements.

In order to find out if the transient spectrum within the cavity passband modes change, the dependence of the spectrum on a beam position was measured. The result is presented in Figures 4.31 and 4.32. Figure 4.31 presents the different beam positions measured at the output of the ACC1 module. The amplitudes and phases of the spectrum of other passband modes compared to the fundamental mode (1.3 GHz) for the different beam positions is presented in Figure 4.32. It is visible that the spectrum at other modes have a very small dependence on the beam position. It might prove that the single bunch induced transient spectrum within the cavity passband modes is fixed and does not change. Therefore the systematic measurement errors can be removed using correction factors.

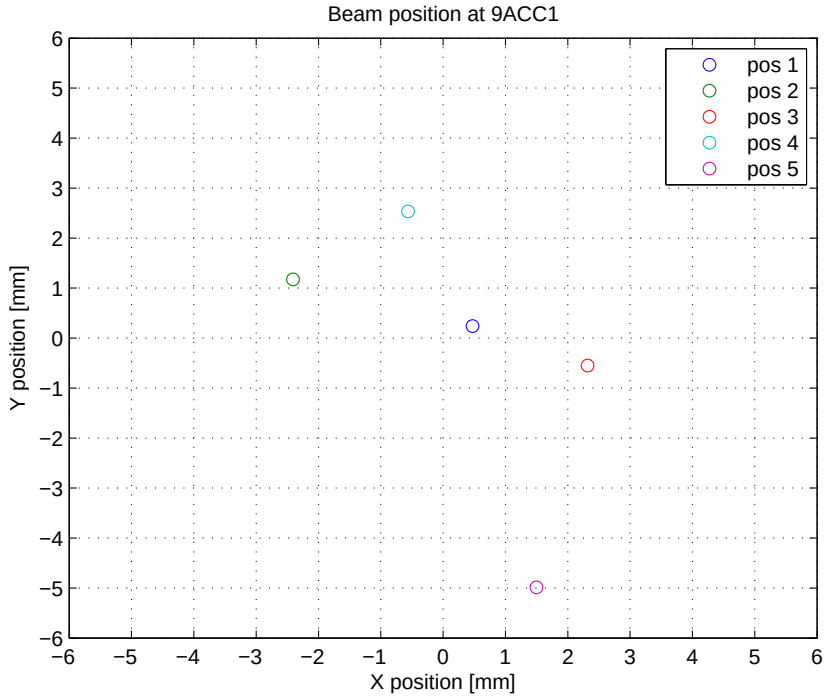

Figure 4.31: Beam positions measured at an output of ACC1.

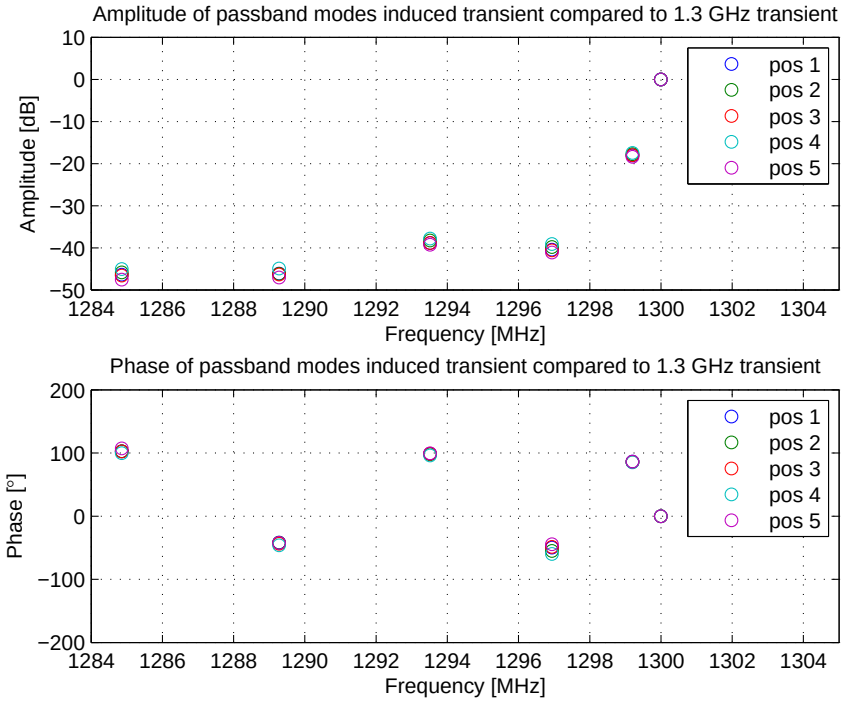

Figure 4.32: Single bunch induced transients in the cavity passband modes compared to the transient at 1.3 GHz.

4.17 Conclusions

The single bunch induced transient detection system was validated with a number of measurements. The measurements made by the transient detection system were compared to the old calibration method based on detecting high charge induced transients. The single bunch induced transient measurements were compared to a beam charge. The transient magnitude was checked if it increases linearly with a charge. Moreover the transient detection was validated by comparing beam energy measurements with the single bunch induced transient phase measurements. The beam energy should depend on the beam phase as a cosine function. These tests proved that the system works correctly however it has some systematic errors.

The causes of the systematic errors were studied. The measurements on the single bunch induced transient detection system showed that this system can not be a source of the errors. The errors on the phase were up to 11° in phase and 20 % in an amplitude and they were correlated to a signal power (section 4.10 and 4.13). Directional couplers installed between the system and cavities probes were suspected to be the source of these errors. Measurements showed that they were not the source of the systematic errors. The errors were probably caused by the EFS transients induced in other passband modes of cavities than fundamental. Currently an influance of cavities fundamental modes on the transient measurement could be possibly eliminated in the single bunch induced transient detection system by using correction factors for every cavity separately.

CHAPTER 5

Conclusions and outlook

In this work it has been shown that it is possible to make a system for beam phase monitoring, an amplitude calibration and a phase calibration in linear particle accelerators based on single bunch induced transient detection. All the thesis have been proven. In particular, Thesis 3 was proven by using an RF feedforward comb filter in the measurement system and experimental results (Chapter 4). Single bunch induced transients used during measurements and experimental results prove Thesis 2. Single bunch induced electric field strength changes used in the method are detectable during a normal accelerator operation, which prove Thesis 1.

Detailed conclusions:

- It is possible to perform a long term transient measurement (a feedforward comb filter with an automatic filter adjustment and thermal stabilization).
- It is possible to automatically adjust the filter with a precision of $2 \cdot 10^{-5}$ V/V in an amplitude and 0.001° in a phase (Section 2.2.3).
- Stochastic measurement confidence limits for 95 % confidence interval, 0.96 nC single bunch induced transient and a 12.4 MV/m electric field strength amplitude are 6.8 % in an amplitude and 3.7° in a phase. The confidence limits of

average over 100 samples for the same conditions are 0.95 % in an amplitude and 0.73° in a phase (Section 2.6). The systematic measurement errors equal ±20 % in an amplitude and ±11° in a phase and can probably be eliminated using correction factors.

The presented system was developed at DESY in Hamburg. It was tested in a real working linear accelerator (FLASH). The results of the tests prove correctness of the concept presented in the work. The system has features not available before:

- Detection of single bunch induced transients, 3000 to 10000 times smaller then an electric field strength in a cavity
- Measurement of the transients with respect to an electric field strength in the cavity
- A beam phase monitoring during a normal accelerator operation

A previously used method for the transient detection was not able to measure the beam phase during a normal accelerator operation. It was only possible to measure the beam phase and perform an amplitude and phase calibration in rear occasions. Currently with the new method it will be possible to perform the calibration without disturbing an accelerator operation.

The superior feature of the new method is an ability to measure the beam phase during a normal accelerator operation using a single low charge bunch (1 nC). The disadvantage of the method is a systematic measurement error. The sources of the error are most probably cavity passband modes other then a fundamental mode. The single bunch induces transients not only in the fundamental mode of the cavity (π mode) but also in other passband modes ($\frac{8}{9}\pi$ - $\frac{1}{9}\pi$). The frequencies of other modes ($f_{8/9\pi} = 1299.260\ MHz$, $f_{7/9\pi} = 1296.861\ MHz$, $f_{6/9\pi} = 1293.345\ MHz$, $f_{5/9\pi} = 1289.022\ MHz$, $f_{4/9\pi} = 1284.409\ MHz$) are close to the frequency of the fundamental mode ($f_{\pi} = 1300.091\ MHz$). A filter which could attenuate signals at the frequencies of other passband modes of the cavities must have a bandwidth smaller then 0.5 MHz. Unfortunately the filter with such a small bandwidth has also a big time constant, which in this case equals 318 ns. The filter with this time constant is inappropriate for filtering in the single bunch induced transient detection

system, because it would filter the signals at frequencies in other passband modes of the cavity and also the 20 ns pulse at the fundamental mode of the cavity. However, the transient spectrum at the cavity passband modes seems to be fixed. Therefore it might be possible to remove the systematic errors using correction factors.

The developed method can be used for an amplitude and a phase calibration in the future X-FEL accelerator. It can be especially useful during an accelerator startup. While the accelerator startup the beam phase is not known and random, the new method can be much safer then an old one. When the beam phase is incorrect it does not have a correct transmission. In these circumstances it can collide with an equipment installed inside an accelerator tunnel. The single 1 nC bunch used for the calibration will have less harming influence as the calibration with high charge transients where many high charge bunches are required for the measurement. More bunches with a higher charge increases the risk of harming an equipment inside the tunnel.

The main goal in the presented work was to prove that the concept can be used for a correct beam phase and transient amplitude measurement. The developed prototype system is currently expensive. In the future the system cost has to be reduced. The system is also big and it will be necessary to work on the system minimization.

APPENDIX A

Appendix

A.1 The DOOCS graphical user interface

The control of the single bunch induced transient detection system is performed with the "ddd" (**D**OOCS **D**ata **D**isplay) program. The program is used for a graphical user interface editing and running. To start the interface, the FLASH accelerator control panel has to be started with the console command "ttf_ddd_run" on the one of the TTF Solaris machines. Then the following buttons have to be pushed the "Diagnostics" and the "Beam phase" in the "Phase" group. As a result the main panel for the control of the single bunch induced transient detection system should be visible (Figure A.1).

The main panel (Figure A.1) is used for the transient measurements. It shows measurement results: transient amplitude, a beam phase, transient real and imaginary parts. The measured transients are very small and noisy. The results are presented as samples and as an average over 100 samples to reduce measurement noise. The transient vector is calculated with respect to the RF EFS in the cavity. The beam phase is calculated by subtracting 180° from the measured transient phase with respect to the absolute RF EFS. The two shown waveforms present also the real and

imaginary parts of the transient vector. The waveforms show the data measured and downconverted by an oscilloscope (black lines) and a transient approximation based on the calculation result (blue lines). The panel presents also a beam charge measured with a toroid, number of bunches and the absolute RF EFS amplitude with phase. Additional detector control features are available in four panels, which are started by pushing the buttons: "Amplifiers control", "Filter control", "Calibration" and "IQ Modulator".

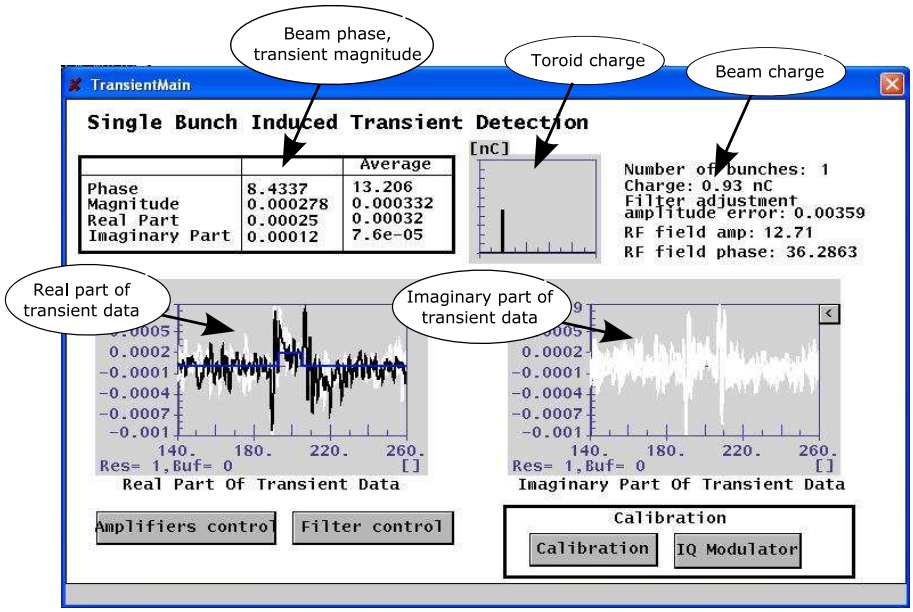

Figure A.1: Main panel.

The RF feedforward comb filter can be controlled with the filter control panel (Figure A.2). The panel is started by pushing the "Filter control" button in the main panel. It has control boxes for changing manually the DAC voltages, which drive I and Q inputs of the IQ modulator used for the filter fine-adjustment. These inputs can be adjusted manually or automatically when the "Automatic Filter Adjustment" is activated. The panel has also a diagram that presents a filter adjustment error vector in complex space. The error vector is shown as a point. The x-axis is a real and y-axis is an imaginary value of the vector. The values are presented in voltages measured by the oscilloscope without any additional scaling. In addition the table "Adjustment Errors" shows the filter adjustment errors as real, imaginary parts and amplitude, phase measured by the oscilloscope. The column "Calibrated" presents the calibrated filter adjustment errors.

The variable gain amplifier is controlled using the amplifier control panel (Fig-

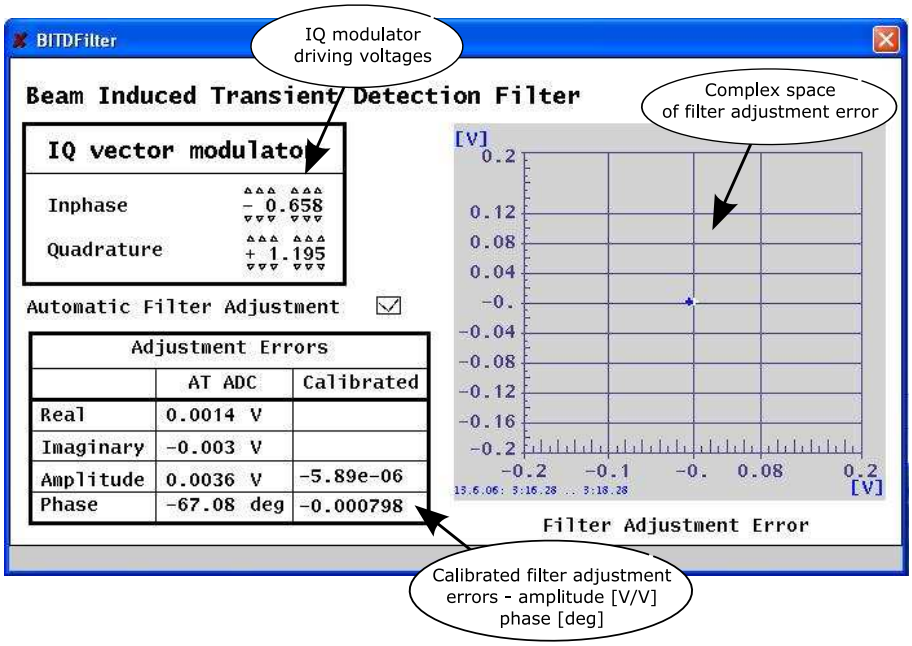

Figure A.2: Filter control panel.

ure A.3). The panel is started using the "Amplifiers control" button in the main control panel. It can be controlled manually or automatically depending on the "Automatic Gain Control" setting. An attenuation of the variable attenuators is controlled by pushing the buttons that enable or disable certain attenuations. The amplifiers are connected or disconnected by pushing the "Switch" buttons. Current settings are visible on graphics. The active attenuators are in red. The active amplifiers are connected to a main transmission line.

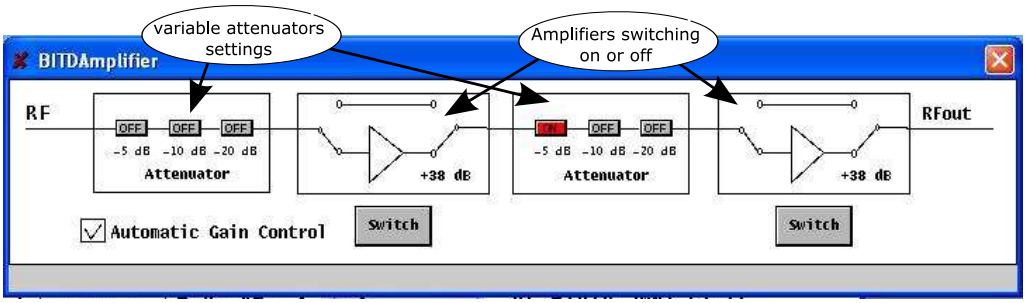

Figure A.3: Amplifier control panel.

Before starting any measurement the system has to be calibrated. The calibration does not have to be done often it is only required to perform it when the hardware was modified (for example the cabling was changed). The calibration is performed

using the calibration panel (Figure A.4). The panel is started by pushing the "Calibration" button in the main panel.

The calibration panel shows a table with 9 calibration measurements and a sum. The first column has descriptions about the measurements. The second column presents the amplitudes of the calibration vectors. The amplitudes are shown in dB units as attenuations (positive values are attenuations, negative are gains). The third column presents phases of the calibration vectors in degrees.

The calibration consists of 9 measurement steps. The every measurement is repeated a number of times and the result is an average of all the results for a single step. A number of repetitions is set using the control box named "Measurement nr.". The first measurement "1. Amplifiers off" is made for the case when the amplifiers and the attenuators are switched off. The result is presented as an absolute value of a transfer function. The following results show instead a change in the transfer function caused by connecting a measured part. For example, the measurement 2 presents a change of the transfer function, induced by turning on the 5 dB attenuator in the first variable attenuator, instead of the absolute value.

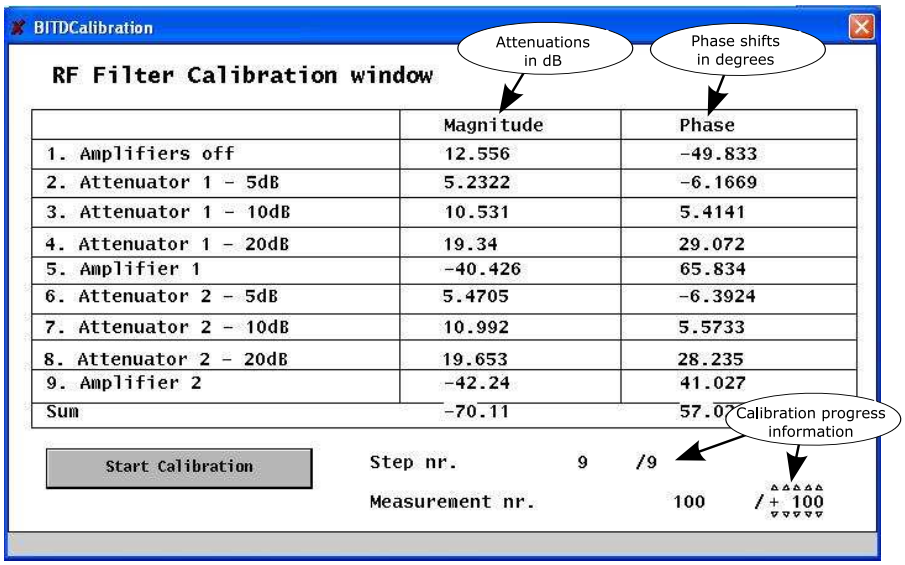

Figure A.4: Calibration panel.

The calibration is started by pushing the "Start calibration" button. The progress of the calibration is presented as the "Step nr." and the "Measurement nr.". The "Step nr." is a measurement step number. The "Measurement nr." it the repetition of measurements for the single step. The result presented as the "Sum" is the sum of

the transfer functions for the maximum gain. It is the sum of the gains and phases for the measurements number: 1, 5 and 9.

The filter can be automatically adjusted by turning on the automatic filter adjustment in the filter control panel (Figure A.2). The IQ modulator has to be calibrated before activating the feature. The amplifier and the filter calibration has to be performed prior to it. The calibration has to be performed whenever the hardware of the system was modified. The IQ modulator calibration is performed using the IQ modulator calibration panel (Figure A.5).

The IQ modulator calibration panel is started by pushing the "IQ Modulator" button in the main panel. It has a table with measured real and imaginary parts of the calibration vectors. The vectors are measured with all the relays in the filter switched to 50 Ω loads.

The measurement is performed in four steps. The first two steps, IP and IN are with the quadrature input of the IQ modulator set to 0 V and the inphase input to +5 V and -5 V respectively. The following two steps QP and QN are with the inphase input set to 0 V and the quadrature input set to +5 V and -5 V respectively.

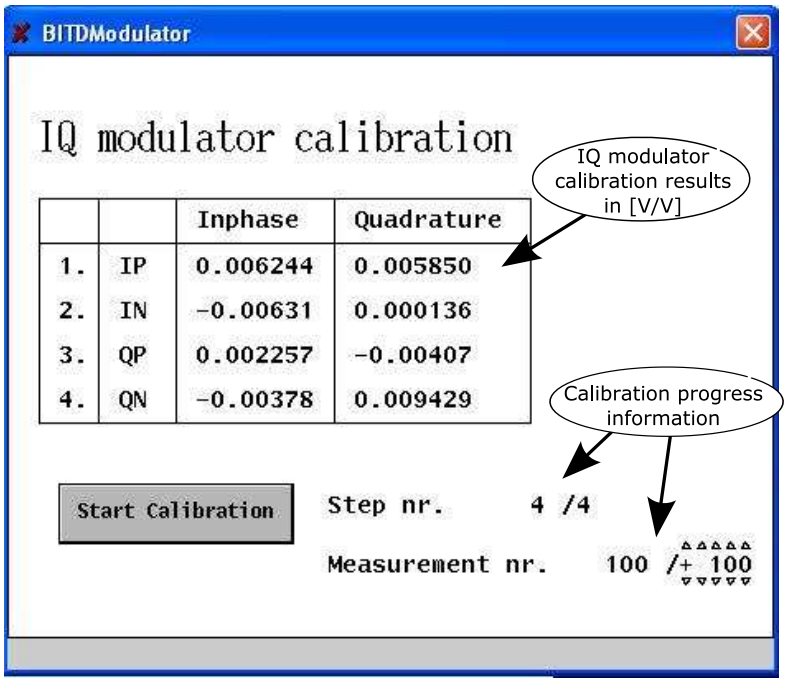

Figure A.5: IQ modulator calibration panel.

The calibration is started by pushing the "Start Calibration" button. During the

calibration a user can observe the calibration progress by looking at the "Step Nr." and the "Measurement Nr.". The measurement number sets the number of measurements used for averaging.

A.2 DOOCS servers variables

A.2.1 rftransient_server

DOOCS variables in rftransient_server (TTF2.EXP\BITD.DATA\INJECTOR).

ADJ_ERR.I	not calibrated filter adjustment error inphase
ADJ_ERR.Q	not calibrated filter adjustment error quadrature
ADJ_ERR.MAG	not calibrated filter adjustment error amplitude
ADJ_ERR.PHASE	not calibrated filter adjustment error phase
ADJ_ERR.CAL.I	calibrated filter adjustment error inphase
ADJ_ERR.CAL.Q	calibrated filter adjustment error quadrature
ADJ_ERR.CAL.MAG	calibrated filter adjustment error amplitude
ADJ_ERR.CAL.PHASE	calibrated filter adjustment error phase
ADJ_ERR.CAL2.MAG	calibrated filter adjustment error amplitude
ADJ_ERR.CAL2.PHASE	calibrated filter adjustment error phase

Table A.1: Filter adjustment errors

TRAN.I.SPECTRUM	captured transient inphase waveform
TRAN.Q.SPECTRUM	captured transient quadrature waveform
TRAN.MAG.SPECTRUM	captured transient amplitude waveform
TRAN.PHASE.SPECTRUM	captured transient phase waveform
CALC_TRAN.I.SPECTRUM	calculated transient inphase waveform
CALC_TRAN.Q.SPECTRUM	calculated transient quadrature waveform
CALC_TRAN.MAG.SPECTRUM	calculated transient amplitude waveform
CALC_TRAN.PHASE.SPECTRUM	calculated transient phase waveform

Table A.2: Transient waveforms

TRAN.I	transient vector inphase
TRAN.Q	transient vector quadrature
TRAN.MAG	transient vector amplitude
TRAN.PHASE	beam phase
TRAN.I.AVG	average of transient vector inphase
TRAN.Q.AVG	average of transient vector quadrature
TRAN.MAG.AVG	average of transient vector amplitude
TRAN.PHASE.AVG	average of beam phase

Table A.3: Transient measurement results

AGC.BOOL	Automatic gain control on-off
ACT.GAIN	Actual gain
FILT.ADJ.AUTO.BOOL	Automatic filter adjustment on-off
CALIBRATE.BOOL	Filter and amplifier calibration on-off
MOD.CAL.BOOL	IQ modulator calibration on-off

Table A.4: Calibration and automatic control variables

NO_GAIN.PHASE	Phase when att. and gain is off
NO_GAIN.MAG	Attenuation when att. and gain is off
ATT1_5.PHASE	Phase shift of first 5 dB attenuator
ATT1_5.MAG	Attenuation of first 5 dB attenuator
ATT1_10.PHASE	Phase shift of first 10 dB attenuator
ATT1_10.MAG	Attenuation of first 10 dB attenuator
ATT1_20.PHASE	Phase shift of first 20 dB attenuator
ATT1_20.MAG	Attenuation of first 20 dB attenuator
ATT2_5.PHASE	Phase shift of second 5 dB attenuator
ATT2_5.MAG	Attenuation of second 5 dB attenuator
ATT2_10.PHASE	Phase shift of second 10 dB attenuator
ATT2_10.MAG	Attenuation of second 10 dB attenuator
ATT2_20.PHASE	Phase shift of second 20 dB attenuator
ATT2_20.MAG	Attenuation of second 20 dB attenuator
AMP1.PHASE	Phase shift of first amplifier
AMP1.MAG	Attenuation of first amplifier
AMP2.PHASE	Phase shift of second amplifier
AMP2.MAG	Attenuation of second amplifier
FULL.PHASE	Phase shift at full gain
FULL.MAG	Attenuation at full gain
CAL_STEP.COUNT	calibration step number
CAL_MEASUREMENT.COUNT	step measurement number
CAL_MEASUREMENT_QT.COUNT	number of measurements for step

Table A.5: Filter and variable gain amplifier calibration factors

MOD.START.I	temporary I
MOD.START.Q	temporary Q
MOD.IP.I	inphase for I=+5 V, Q=0 V
MOD.IP.Q	quadrature for I=+5 V, Q=0 V
MOD.IN.I	inphase for I=-5 V, Q=0 V
MOD.IN.Q	quadrature for I=-5 V, Q=0 V
MOD.QP.I	inphase for I=0 V, Q=+5 V
MOD.QP.Q	quadrature for I=0 V, Q=+5 V
MOD.QN.I	inphase for I=0 V, Q=-5 V
MOD.QN.Q	quadrature for I=0 V, Q=-5 V
MOD.CAL.STEP	calibration step
MOD.CAL.MEAS	calibration measurement number
MOD.CAL.MEAS.QT	calibration measurement quantity

Table A.6: IQ modulator calibration factors

CAVITY.NR	currently used cavity number
FILTER.ATT	carrier attenuation

Table A.7: Other variables

A.2.2 ipdac08_server

DOOCS variables in ipdac08_server (TTF2.EXP\BITD.DAC\INJECTOR).

Output voltages range $+-10\,V$

CH00	Inphase input of IQ modulator
CH01	Quadrature input of IQ modulator

Table A.8: Filter

A.2.3 ipdigi_server

DOOCS variables in ipdigi_server (TTF2.EXP\BITD.DIO\INJECTOR). All variables are active on 0.

REG_0	Calibration Delay Line
REG_1	Calibration Adjustment Circuitry

Table A.9: Filter

REG_2	First 5 dB attenuator
REG_3	First 10 dB attenuator
REG_4	First 20 dB attenuator
REG_5	First amplifier
REG_6	Second amplifier
REG_7	Second 5 dB attenuator
REG_8	Second 10 dB attenuator
REG_9	Second 20 dB attenuator

Table A.10: Amplifier

REG_10	Calibration

Table A.11: Signal distribution board

A.3 List of parts

The VME crate

1. 1 x Wiener - 6U VME crate type: 6021

The signal distribution board

1. 1 x NAIS - ARD10012 SPDT Microwave Relay
2. 1 x ARRA - 3194-20, 20 dB directional coupler
3. 1 x ULN2804AN - High Voltage, High Current Darlington Transistor Arrays
4. 1 x SN74ALS04BN - Hex Inverters

The RF feedforward comb filter

The Control board

1. 1 x ULN2804AN - High Voltage, High Current Darlington Transistor Arrays
2. 1 x SN74ALS04BN - Hex Inverters
3. 6 x AD8010AN - Low Power, High Current Amplifier

The filter

1. 1 x ARRA - 9426B, variable phase shifter
2. 1 x ARRA - 2-4854-10, variable attenuator
3. 5m Midwest Microwave - cable CSY-SMSM-54-005-MS, delay line
4. 2 x ARRA - 3194-20, 20 dB directional coupler
5. 4 x NAIS - ARD10012 SPDT Microwave Relay
6. 2 x Mini-Circuits - ZAPD-20, splitter
7. 1 x Mini-Circuits - 15542, VAT-10, 10 dB attenuator
8. 1 x Mini-Circuits - 15542, VAT-20, 20 dB attenuator
9. 1 x Hittite Microwave corp. - HMC497LP4 Evaluation board, SiGe Wideband Direct Modulator RFIC, 100 - 4000 MHz

The variable gain amplifier

1. 4 x Teledyne Relays - CCR-33S30-N, SPDT
2. 2 x Mini-Circuits - ZFAT-51020, variable attenuator 10-1000 MHz
3. 2 x AmpliTech - APT3-01000200-0310-D4, low noise amplifier
4. 1 x ULN2804AN - High Voltage, High Current Darlington Transistor Arrays
5. 2 x SN74ALS04BN - Hex Inverters

The downconversion

1. 1 x LeCroy - WaveRunner 6100A oscilloscope, 1 GHz bandwidth, 10 GS/s maximum sampling rate
2. 1 x RLC Electronics - BPF-750-1300-78-4-R, Bandpass filter (center freq. 1.3 GHz, passband 780 MHz)

The control system

1. 1 x THEMIS VME computer - THM 102661 REV C4, microSPARC II processor with Solaris operating system
2. 1 x GreenSpring - 4 slot Industry Pack 6U VME carrier
3. 1 x ACTIS Computer - DAC-08B IndustryPack module, Octal 14-bit Digital to Analog Converter
4. 1 x GreenSpring - IP-UNIDIG-I IndustryPack module, digital IO module

The temperature stabilization

Temperature controlled oven made at DESY by Krzysztof Czuba [35].

A.4 Source files information

Matlab script and rftransient_server source code is available through DOOCS cvs [14]. Matlab script is available in 'source/matlab/rftransient'. rftransient_server is available in 'source/server/ttf/rftransient'.

PUBLICATIONS WITH AUTHOR'S CONTRIBUTION

[1] A. Aghababyan, M. Altarelli, C. Altucci, G. Amatuni, P. Anfinrud, P. Audebert, and et al. The European X-Ray Free-Electron Laser Technical Design Report. Technical report, DESY XFEL Project Group, European XFEL Project Team, Germany, Hamburg, July 2006. Available from: http://xfel.desy.de/tdr/index_eng.html.

[2] P. Pawlik. Metoda dostrajania filtru z linia opozniajaca. *Mikroelektronia i informatyka*, pages 125–129, 2004.

[3] P. Pawlik. Detektor amplitudy i fazy zmian pola wywolanych wiazka elektronow w nadprzewoddzacej komorze rezonansowej w akceleratorze liniowym ttf2. *Mikroelektronia i informatyka*, pages 45–51, 2005.

[4] P. Pawlik, M. Grecki, and S. Simrock. Single bunch transient detection for the beam phase measurement in superconducting accelerators. *Proceedings of DIPAC*, 2005. Available from: http://accelconf.web.cern.ch/AccelConf/d05/PAPERS/POM031.PDF.

[5] P. Pawlik, M. Grecki, and S. Simrock. System for high resolution detection of beam induced transients in RF signals. *12 th International Conference MIXDES*, 2:815–820, June 2005.

[6] P. Pawlik, M. Grecki, and S. Simrock. New method for RF field amplitude and phase calibration in FLASH accelerator. *13 th International Conference MIXDES*, pages 85–88, June 2006.

[7] P. Pawlik, M. Grecki, and S. Simrock. Single bunch induced transient detection. *Proceedings of SPIE*, vol. 6347, October 2006.

[8] P. Pawlik, M. Grecki, S. Simrock, and A. Napieralski. New method for beam induced transient measurement. *submitted to MST IOP*, 2006.

[9] P. Pawlik, S. Simrock, and H.C. Weddig. Simulation and measurement of an RF notch filter for an electron beam single bunch detector. *11 th International Conference MIXDES*, pages 430–434, June 2004.

BIBLIOGRAPHY

[10] About the TESLA Technology Collaboration [online]. Available from: http://tesla-new.desy.de/content/about/index_eng.html.

[11] Cavity design [online]. Available from: http://tesla.desy.de/new_pages/4211_Cavity_design.html.

[12] DESY at a glance [online]. Available from: http://zms.desy.de/about_desy/overview/index_eng.html.

[13] DOOCS [online]. Available from: http://doocs.desy.de/.

[14] DOOCS cvs overview [online]. Available from: http://ttf2svr4.desy.de/doocs/server/DoocsCvs/DoocsCvs.html.

[15] Equipment Name Server (ENS) [online]. Available from: http://tesla.desy.de/doocs/ens/ENS-1.html.

[16] The European X-Ray Laser Project XFEL [online]. Available from: http://xfel.desy.de/xfelhomepage/index_eng.html.

[17] External DOOCS functions for Matlab [online]. Available from: http://tesla.desy.de/doocs/ext_programs/matlab/scriptrwu.html.

[18] FLASH [online]. Available from: http://vuv-fel.desy.de/.

[19] Hamburger Synchrotronstrahlungslabor [online]. Available from: http://www-hasylab.desy.de/.

[20] HERA [online]. Available from: http://www-zeus.desy.de/public/hera.php3.

[21] High performance digital down-converters for FPGAs. Available from: http://www.hunteng.co.uk/pdfs/tech/xcell38_48.pdf.

[22] The International System of Units (SI) [online]. Available from: http://www.bipm.org/en/si/si_brochure/chapter2/2-2/table4.html.

[23] MathWorld [online]. Available from: http://mathworld.wolfram.com/.

[24] Matlab 7.0 help [online]. Available from: http://www.mathworks.com/access/helpdesk/help/techdoc/matlab.shtml.

[25] The theory of digital down conversion. Available from: http://www.hunteng.co.uk/pdfs/tech/ddctheory.pdf.

[26] What is XFEL? [online]. Available from: http://www.xfel.net/XFELpresse/en/hintergrund/was/index.html.

[27] Analog Devices. *Practical Analog Design Techniques*. Available from: http://www.analog.com/UploadedFiles/Associated_Docs/123522623Section4.pdf.

[28] J. Andruszkow, A. Agababyan, A. Ageyev, J. Andruszkow, C. Antoine, V. Aseev, and et al. TESLA Technical Design Report. Technical report, DESY Deutsches Elektronen-Synchrotron, Germany, Hamburg, March 2001. Available from: http://tesla.desy.de/new_pages/TDR_CD/start.html.

[29] B. Aune, R. Bandelmann, D. Bloess, B. Bonin, A. Bosotti, M. Champion, and et al. Superconducting TESLA cavities. *Phys. Rev. ST Accel. Beams*, 3(9):092001–20,21, September 2000. Available from: http://tesla.desy.de/new_pages/TDR_CD/PartII/chapter03/references/rfsys18.pdf.

[30] Valeri Ayvazyan, Stefan Simrock, Stefan Choroba, Alexander Matyushin, Guenter Moeller, Gevorg Petrosyan, Kay Rehlich, and Petr Vetrov. Digital Low Level RF control system for the DESY TTF VUV-FEL linac. October 2005. Workshop on Low Level RF in CERN - LLRF05. Available from: http://indico.cern.ch/contributionDisplay.py?contribId=59&sessionId=29&confId=a050.

[31] J. R. Bogart and et al. A fast and accurate phasing algorithm for the RF accelerating voltages of the SLAC linac. *EPAC'98*, pages 448–450, June 1998. Available from: http://accelconf.web.cern.ch/AccelConf/e98/PAPERS/MOP11H.PDF.

[32] Darren K. Brock, Oleg A. Mukhanov, and Jack Rosa. Superconductor digital RF development for software radio. *IEEE Communications Magazine*, 39:174–179, February 2001. Available from: http://ieeexplore.ieee.org/xpls/abs_all.jsp?arnumber=900649.

[33] Enrico Buracchini. The software radio concept. *IEEE Communications Magazine*, 38:138–143, September 2000. Available from: http://ieeexplore.ieee.org/xpls/abs_all.jsp?arnumber=868153&isnumber=18795.

[34] W. Sayre Cotter. *Complete wireless design*. McGraw-Hill, 2001.

[35] K. Czuba, F. Eints, M. Felber, J. Dobrowolski, and S. Simrock. First generation of optical fiber phase reference distribution system for TESLA. *TESLA Report 2005-08*, 2005. Available from: http://flash.desy.de/sites/site_vuvfel/content/e403/e1644/e1173/e1174/infoboxContent1345/tesla2005-08.pdf.

[36] Pengda Gu, Zheqiao Geng, Guoxi Pei, Shuhong Wang, Mi Hou, and Yanyan Cui. RF phasing system for BEPCII Linac. *Proceedings of APAC*, pages 288–290, March 2004. Available from: http://accelconf.web.cern.ch/AccelConf/a04/PAPERS/TUP11006.PDF.

[37] O. Hensler and K. Rehlich. *DOOCS manual*. 2000. Available from: http://tesla.desy.de/doocs/doocs_manual/DOOCS_MANUAL.pdf.

[38] C. Hovater, M. Chowdhary, J. Karn, M. Tiefenback, J. van Zeijts, and W. Watson. Operational experience with the CEBAF control system*. *Proceedings of the XVIII International Linear Accelerator Conference*, pages 616–620, August 1996. Available from: http://accelconf.web.cern.ch/AccelConf/l96/PAPERS/TH204.PDF.

[39] Harbour Industries. Datasheet SS (Spiral Strip) Coaxial Cable. Available from: http://www.harbourind.com/products/pdf/SS401.pdf.

[40] R. K. Jobe, N. Phinney, and C. Adolphsen. Phasing tools for the klystrons at the SLC. *'Accelerator Science and Technology'., Proceedings*

of the 1989 IEEE (PAC 1989), 3:1984–1986, March 1989. Available from: http://accelconf.web.cern.ch/AccelConf/p89/PDF/PAC1989_1984.PDF.

[41] Jerzy Lech Kacperski. *Opracowywanie danych pomiarowych*. Wydawnictwo Uniwersytetu Lodzkiego, 1997.

[42] J. Kent, M. King, C. Von Zanthier, S. Watson, M. Levi, F. Rouse, and et al. Precision measurements of the SLC beam energy. *PAC*, 1989. Available from: http://accelconf.web.cern.ch/AccelConf/p89/PDF/PAC1989_1550.PDF.

[43] Zygmunt Kusmierek. *Podstawy Metrologii Elektrycznej*. Politechnika Lodzka, 1990.

[44] Massimiliano Laddomada, Fred Daneshgaran, Marina Mondin, and Ronald M. Hickling. A PC-based software receiver using a novel front-end technology. *IEEE Communications Magazine*, 39:136–145, August 2001. Available from: http://ieeexplore.ieee.org/xpls/abs_all.jsp?arnumber=952928.

[45] Marek Lassak. *Matematyka dla studiow technicznych*. WM Sp. z o.o, 2001.

[46] LeCroy Corporation. *Automation Manual*. 2003.

[47] Julian Lipczynski, Mieczyslaw Okolowicz, Stefan Olczak, and Eugeniusz Rybka. *Tablice matematyczne, chemiczne, fizyczne, astronomiczne*. Agencja Poligraficzno-Wydawnicza, 1995.

[48] Midwest Microwave. Standard products catalog [online]. Available from: http://www.midwest-microwave.com/.

[49] Douglas C. Montgomery and George C. Runger. *Applied Statistics and Probability for Engineers*. John Wiley & Sons, Inc., 2003.

[50] Henry W. Ott. *Noise reduction techniques in electronic systems*. John Wiley & Sons, 1988.

[51] J.C. de Paula. Experimental errors and data analysis [online]. Available from: http://www.haverford.edu/chem/302/data.pdf.

[52] T. Schilcher. *Vector Sum Control of Pulsed Accelerating Fields in Lorentz Force Detuned Superconducting Cavities*. PhD thesis, Hamburg University, Hamburg, 1998. Available from: http://flash.desy.de/sites/site_vuvfel/content/e403/e1644/e1377/e1378/infoboxContent1975/TESLA-1998-20.pdf.

[53] S. N. Simrock, R. Kazii, G. A. Krafft, L. Merminga, L. Ninan, and S. Witherspoon. Phasing schemes for the CEBAF cavities*. *Particle Accelerator Conference (PAC)*, 1:599–601, May 1993. Available from: http://accelconf.web.cern.ch/AccelConf/p93/PDF/PAC1993_0599.PDF.

[54] S.N. Simrock. Digital low-level RF controls for future superconducting linear colliders. *Proceedings of 2005 Particle Accelerator Conference*, 2005. Available from: http://msk.desy.de/Publikationen/Reports/PAC2005/FOAA006.PDF.

[55] S.N. Simrock, I. Altmann, K. Rehlich, and T. Schilcher. Design of the digital RF control system for the Tesla Test Facility. 1996. Available from: http://accelconf.web.cern.ch/AccelConf/e96/PAPERS/ORALS/WEO06A.PDF.

[56] S.N. Simrock and T. Schilcher. Transient beam loading based calibration of the vector-sum for the Tesla Test Facility. *Proceedings of the 5th European Particle Accelerator Conference (EPAC 96)*, page 1866, June 1996. Available from: http://accelconf.web.cern.ch/AccelConf/e96/PAPERS/THPL/THP025L.PDF.

[57] Times Microwave Systems. Current innovations in phase stable coaxial cable design [online]. Available from: http://www.timesmicrowave.com/content/pdf/phasearticle.pdf.

[58] M. G. Tiefenback and K. Brown. Beam-based phase monitoring and gradient calibration of Jefferson Laboratory RF systems. *Particle Accelerator Conference*, 2:2271–2273, May 1997. Available from: http://accelconf.web.cern.ch/accelconf/pac97/papers/pdf/8P072.PDF.

[59] ZHOU Xiao-guang and ZHONG Shi-cai. Phasing system for the injector of Beijing Electron Positron Collider BEPC. *Proceedings of the 1987 IEEE Particle Accelerator Conference (PAC 1987)*, pages 800–801, March 1987. Available from: http://accelconf.web.cern.ch/AccelConf/p87/PDF/PAC1987_0800.PDF.